

Energy

**F
O
S
S
I
L**

**TRANSIENT PRESSURE ANALYSIS IN COMPOSITE RESERVOIRS WITH
RECTANGULAR DISCONTINUITIES—SUPRI TR-54**

**By
Edward Y. Teng
H. J. Ramey, Jr.**

August 1986

Work Performed Under Contract No. AC02-81SF11564

**For
U. S. Department of Energy
Bartlesville Project Office
Bartlesville, Oklahoma**

**By
San Francisco Operations Office
Oakland, California**

and

**Stanford University Petroleum Research Institute
Stanford, California**

**Technical Information Center
Office of Scientific and Technical Information
United States Department of Energy**

DISCLAIMER

This report was prepared as an account of work sponsored by an agency of the United States Government. Neither the United States Government nor any agency thereof, nor any of their employees, makes any warranty, express or implied, or assumes any legal liability or responsibility for the accuracy, completeness, or usefulness of any information, apparatus, product, or process disclosed, or represents that its use would not infringe privately owned rights. Reference herein to any specific commercial product, process, or service by trade name, trademark, manufacturer, or otherwise does not necessarily constitute or imply its endorsement, recommendation, or favoring by the United States Government or any agency thereof. The views and opinions of authors expressed herein do not necessarily state or reflect those of the United States Government or any agency thereof.

This report has been reproduced directly from the best available copy.

Available from the National Technical Information Service, U. S. Department of Commerce, Springfield, Virginia 22161.

Price: Printed Copy A07
Microfiche A01

Codes are used for pricing all publications. The code is determined by the number of pages in the publication. Information pertaining to the pricing codes can be found in the current issues of the following publications, which are generally available in most libraries: *Energy Research Abstracts (ERA)*; *Government Reports Announcements and Index (GRA and I)*; *Scientific and Technical Abstract Reports (STAR)*, and publication NTIS-PR-360 available from NTIS at the above address.

DOE/SF/11564-19

(SUPRI-TR-54)

(DE86000289)

Distribution Category UC-92a

**TRANSIENT PRESSURE ANALYSIS IN COMPOSITE RESERVOIRS
WITH RECTANGULAR DISCONTINUITIES — SUPRI TR-54**

By

Edward Y. Teng

H. J. Ramey, Jr.

August 1986

Work Performed Under Contract No. AC03-81SF11564

**Prepared for
U.S. DEPARTMENT OF ENERGY
Assistant Secretary for Fossil Energy**

**H.J. Lechtenberg, Project Manager
San Francisco Operations Office
Fossil Energy Division
1333 Broadway
Oakland, California 94612**

**Stanford University Petroleum Research Institute
Stanford, California 94305**

TABLE OF CONTENTS

	<u>Page</u>
LIST OF TABLES	iii
LIST OF FIGURES	iii
ACKNOWLEDGMENTS	iv
ABSTRACT	v
1. INTRODUCTION	1
2. PREVIOUS WORK	2
2.1 Transient Pressure Behavior of Composite Reservoirs	2
2.2 Transient Pressure Behavior for a Well with a Finite-Conductivity Vertical Fracture	10
3. PROBLEM STATEMENT	18
4. METHOD OF SOLUTION	20
5. RESULTS AND INTERPRETATION	23
6. CONCLUSIONS AND RECOMMENDATIONS	35
NOMENCLATURE	36
REFERENCES	38
APPENDIX A. Two-Dimensional, Areal-Implicit, Single-Phase, Single-Component Numerical Simulator for Slightly Compressible Fluids with Constant Compressibility	40
APPENDIX B. Two-Dimensional, Areal-Implicit, Single-Phase, Single-Component Numerical Simulator for Compressible Gas	61
APPENDIX C. Validation of the Simulator for Slightly Compressible Fluids	70
APPENDIX D. Fluid and Rock Properties Used for Simulation Runs	75
APPENDIX E. Semilog and Cartesian Plots of Pressure vs. Time for all Simulation Runs	76
APPENDIX F. Programs Source Codes	92

LIST OF TABLES

	<u>Page</u>
4.1 List of W/L Ratios Simulated.....	27
5.1 Summary of Results for Semilogarithmic Analysis for Burned Zone.....	28
5.2 Summary of Results for Semilogarithmic Analysis for Outer Zone.....	28
5.3 Summary of Results for Cartesian Analysis for Burned Zone.....	30
5.4 Locations of Tangent Points in Time Which Yield Correct Calculated Burned-Zone Volumes.....	31

LIST OF FIGURES

2.1 Radially Composite Reservoir.....	2
2.2 Van Poolen's Field Fall-Off Curves.....	3
2.3 Kazemi's Fall-Off Curves.....	4
2.4 Carter's Solution (Semilog Plot).....	4
2.5 Carter's Solution (Cartesian Plot).....	4
2.6 Bixel and Van Poolen's Dimensionless Pressure Solution.....	6
2.7 Odeh's Correlation Charts.....	6
2.8 Odeh's Example Drawdown Plot.....	7
2.9 Merrill's Correlation for Dimensionless Intersection Time.....	8
2.10 Eggenschwiler's Simulated Injection Test Response.....	9
2.11 A Cartesian Graph for the Kazemi Data.....	9
2.12 Eggenschwiler's Pseudo Steady State Deviation Factor Chart.....	11
2.13 Well with Finite Conductivity Vertical Fracture in an Infinite Slab Reservoir.....	12
2.14 Cinco's Fracture Flow Model.....	12
2.15 Cinco's Reservoir Flow Model.....	12
2.16 Cinco's Dimensionless Pressure Solution for an Infinite Reservoir with a Finite Conductivity Vertical Fracture (No Storage, No Skin).....	13
2.17 Cinco's Damaged Fracture Model.....	14
2.18 Cinco's Dimensionless Pressure Solution for a Fractured Well with Fracture Skin Damaged.....	15
2.19 Cinco's Dimensionless Pressure Solution for a Fractured Well with Wellbore Storage (No Skin).....	15
2.20 Cinco's Fracture Flow Periods.....	16
2.21 Cinco's Dimensionless Pressure Solution for a Vertically Fractured Well.....	17
3.1 A Vertically Fractured Well in a Finite Reservoir.....	18
3.2 A Rectangular Burned Zone in a Finite Reservoir.....	18
3.3 Pseudoradial Flow Regime.....	19
4.1 Grid Spacing Used in Simulation Runs.....	21
4.2 Dimensions of Square Burned Zone for Simulation Run.....	22
5.1 Semilog Plot of Pressure vs. Time for the Case with the Square Burned Zone (Long Duration).....	23
5.2 Semilog Plot of Pressure vs. Time for the Case with a Square Burned Zone.....	24
5.3 Cartesian Plot of Pressure vs. Time for the Case with a Square Burned Zone.....	25

5.4	Semilog Plot of Dimensionless Pressure Responses for Different W/L Ratios	27
5.5	Error in Calculated Permeability as a Function of W/L Ratio.....	27
5.6	Cartesian Graph of Dimensionless Pressure Responses for Different W/L Ratios	29
5.7	Location of Tangent Points that Yield Correct Calculated Burned-Zone Volume as a Function of W/L Ratios.....	31
5.8	Log-Log Plot of Dimensionless Pressure Responses for Different W/L Ratios	32
5.9	Comparison with Cinco's Type Curve for $W/L = 0.00157$	33
5.10	Comparison of Simulation Results from Liquid and Gas Simulators.....	34
A.1	Control Volume	40
A.2	Block Centered Grid (1-D).....	46
A.3	Block Centered Grid (2-D).....	47
A.4	Nomenclature for Grid Construction	47
A.5	Well Block Representation (2-D)	54
C.1	Well in the Center of a Closed Square Reservoir.....	70
C.2	Physical Dimensions of Well in the Center of a Closed Square Reservoir.....	72
C.3	Dimensionless Pressure Solution for a Well in a Closed, Square Reservoir (Full Reservoir Simulation).....	73
C.4	Dimensionless Pressure Solution for a Well in a Closed, Square Reservoir (Quarter Reservoir Simulation).....	74

ACKNOWLEDGMENTS

Financial support was provided by Stanford University Petroleum Research Institute under the DOE contract DEACO381SF11564.

ABSTRACT

Numerical simulation was used to determine if the pseudosteady-state method presented by Eggenchwiler *et al.* (1980) can be applied to a long and narrow, rectangular swept-zone geometry.

Two simulators were developed to generate transient pressure responses for a reservoir with a rectangular discontinuity. Cases with different width to length ratio (W/L) for the inner-zone were simulated for a mobility ratio of 200. The reservoir has a square geometry with closed outer boundaries. Sufficiently large distance was provided between the well and reservoir boundaries to prevent boundary effects during the time of interest. Results were analyzed with the pseudosteady-state method to find inner zone volumes.

Results from the analysis indicate that pseudosteady-state flow does not exist for the inner zone for low W/L ratio cases. The curvature of the Cartesian plot of the pressure responses increases as W/L ratio decreases. For cases with W/L ratio below 0.4, the curvature becomes significant and many straight lines can be drawn through segments of the data. For cases with W/L ratio below 0.1, there is clearly no pseudosteady-state flow, and the Cartesian plot of pressure versus time is a continuous curve.

It was found that swept-zone volume calculations are extremely sensitive to the slope of the pseudosteady-state straight line, if one exists. If the distance between the burning front and the well is not approximately equal in all directions, the slope will usually be too flat, and the volume calculated will be too large.

A comparison between Cinco's type curve for a finite conductivity fracture and a case with an extremely low W/L ratio was also performed. The results show a favorable match. However, for a rectangular burned zone to behave like a fracture at early time, the dimensions of the burned zone must be similar to that of a fracture.

1. INTRODUCTION

Economic incentives prior to the recent changes in oil prices have accelerated the development of thermal oil recovery processes such as *in-situ* combustion and steam injection. Knowledge of the volume swept at intermediate stages yields critical information and makes economic evaluation of the project possible. The determination of the swept volume in a composite reservoir has traditionally been obtained by coring and/or temperature surveys made at wells during passage of the displacement front. This process is costly and time consuming.

Numerous researchers have presented methods to estimate the swept volume by means of pressure transient data. Van Poolen (1965) utilized the radius of drainage concept to estimate the swept zone radius. Kazemi (1966) used a thermal simulator and calculated the distance to the burning front by solving a pressure falloff test model numerically. Merrill *et al.* (1974) proposed a method to calculate the distance to the radial discontinuity. Their method uses the intersection point of the two semilog straight lines for the swept and unswept zones. Eggenschwiler *et al.* (1980) analytically determined the pressure response of a radial composite reservoir and found a simple method to estimate the volume of the swept zone. They discovered that there is a pseudosteady-state flow period for the swept zone immediately following the first infinite-acting period. This method is suitable for high mobility ratio situations and is powerful, yet simple to use.

All methods mentioned were developed for composite reservoirs of radial geometry, and are suitable for use in analyzing a normal injection well situation. However, recent field data suggest that there are thermal injection wells which are intercepted by a natural vertical fracture. In such cases, the displacement front will move in a direction which is normal to the plane of the fracture at early time. The swept region at early times can be idealized as a low width to length ratio rectangle. As time goes on, the front moves outward and the width to length ratio of the rectangle will increase.

It is suspected that the pseudosteady-state method presented by Eggenschwiler *et al.* can not be applied at early times for a system when the rectangular swept zone is very narrow and long. At the initial condition, the pressure transient response of an injection well, intersected by a vertical fracture, can be described by the type curves for vertically fractured wells presented by Cinco *et al.* (1978) There will be no pseudosteady-state flow period at this time since there is no swept region. However, as the front propagates and the size of the rectangular swept region increases, the behavior of the system will begin to depart from Cinco's type curves. Eventually, there will be a time when the system will exhibit a pseudosteady-state flow period for the swept region and the Eggenschwiler *et al.* method can be applied.

The purpose of this study was to generate transient pressure responses of an injectivity test for a rectangular composite reservoir via numerical simulation, and to determine the necessary width of the rectangular burned zone before the pseudosteady-state method can be applied to such systems.

In this study, a high mobility ratio case is considered and the fluid properties are typical of those found in an *in-situ* combustion operation. The mobility ratio used in this study is 200.

2. PREVIOUS WORK

Two areas of research directly related to this study are the analyses of composite reservoirs and a well intercepted by a vertical fracture with finite conductivity. Previous work related to these two areas will be discussed in this section.

2.1. TRANSIENT PRESSURE BEHAVIOR OF COMPOSITE RESERVOIRS

A number of studies have analyzed transient pressure data from thermal injection wells in order to define a composite reservoir. A radially composite reservoir is usually created by an *in-situ* combustion or steam injection process. The physical system can be described as shown in Fig. 2.1 (Eggenschwiler *et al.*, 1980).

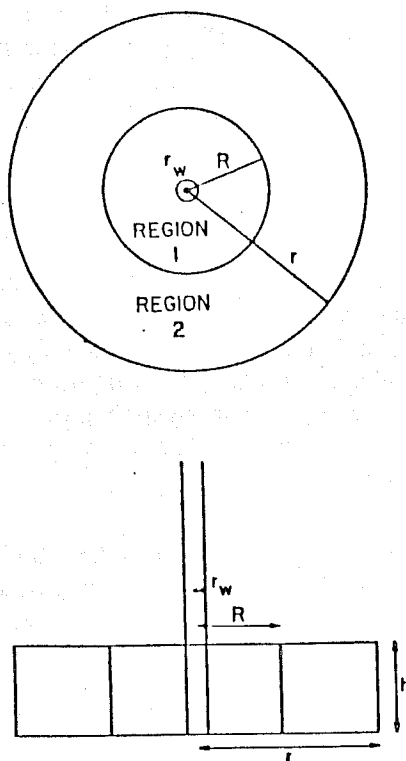


Fig. 2.1 Radially Composite Reservoir

For an injection test performed on such a system, the pressure response usually consists of four different stages on a semilog plot of pressure versus time. There is an initial period where wellbore-storage effects dominate followed by a semilog straight line whose slope is related to the permeability-thickness product of the swept zone. The semilog straight line is then followed by a transition period. Finally, a second semilog straight line appears which characterizes the permeability-thickness product of the unswept region.

The parameter one would try to determine in analyzing a composite reservoir is the swept volume or the swept-zone radius. There have been several major publications in this area.

Van Poolen (1965) presented a method to calculate the radius to the discontinuity by using the radius-of-drainage concept. He presented a series of actual field fall-off curves of an

in-situ combustion project as shown in Fig. 2.2 to illustrate how fall-off curves change with time.

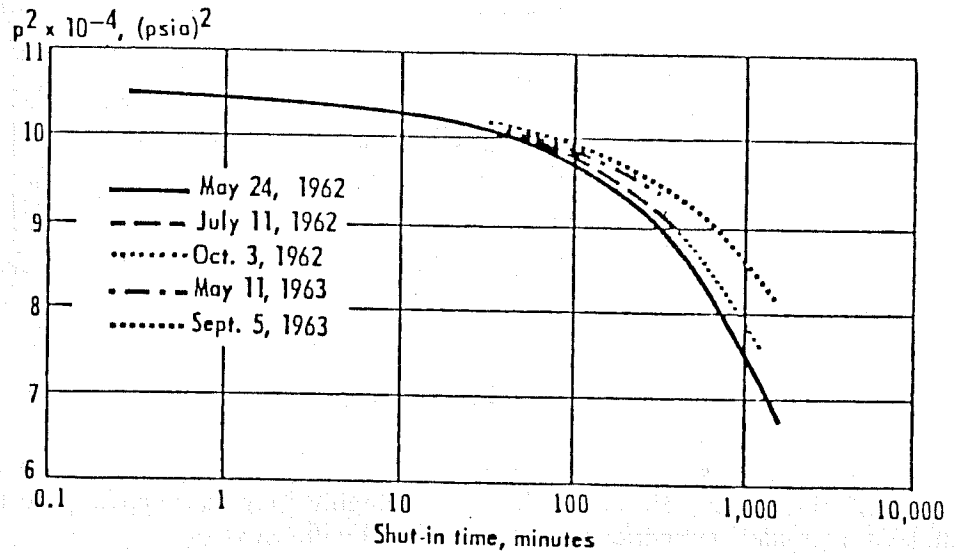


Fig. 2.2 Field Fall-Off Curves

Van Poolen suggested that the permeability of the burned zone can be calculated from the slope of the first semilog straight line by :

$$k = \frac{1637q_{11}ZT}{mh} \quad (2.1)$$

The radius to the discontinuity can then be estimated by :

$$R = \sqrt{\frac{k_1 t}{\phi_1 \mu_1 c_1}} \quad (2.2)$$

where t is the time when the curve starts to deviate from the first semilog straight line.

The idea of Van Poolen's method is theoretically correct. However, in practice, the swept volume does not have a constant thickness, and the transition region following the initial semilog straight line is usually long. Because the point of deviation from the semilog straight line is not always clearly defined, it is difficult to pick a single point where deviation starts. Also, wellbore storage and boundary effects may affect the shape of the curve, making it difficult to base an entire calculation on a single point.

Kazemi (1966) presented a method that utilized a numerical model in the determination of the burning-front location. He calculated the effective permeability of the burned zone from the first semilog straight line, then a trial and error method was used to calculate the radius of discontinuity. Several burned-zone radii were first assumed, then the temperature distribution was determined by using a model developed by Chu (1963). A numerical radial model was used to determine the pressure distribution in the reservoir and that result was compared with the actual field falloff data. The radius that produced the closest match with the field data is taken to be the radius to the discontinuity.

This process was tested by Kazemi with a field case which is shown in Fig. 2.3. He concluded that the average distance to the front for this case is 150 feet.

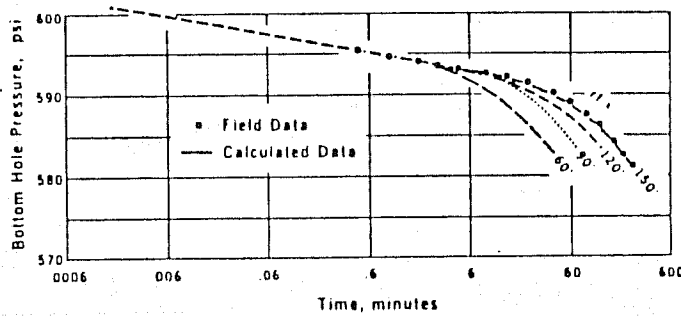


Fig. 2.3 Fall-Off Curves

Kazemi also presented a discussion of probable causes of error in the interpretation of field data in his paper. He emphasized that a highly irregular shape of the burning front as compared to an ideal cylindrical front will cause significant error.

Carter (1966) presented an analytical solution for a composite reservoir with a closed outer boundary. His results for an example case are shown in Figs. 2.4 and 2.5. Carter concluded that the properties of the swept zone can be determined from the initial semilog straight line. However, the transition to the second semilog straight line is quite long and boundary effects will prevent the forming of the second semilog straight line. Therefore, a reliable kh value for the outer zone cannot be calculated.

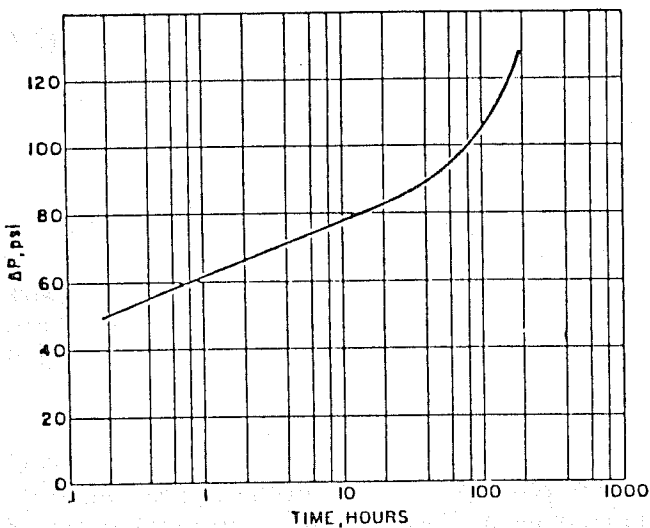


Fig. 2.4 Solution
(Semilog plot)

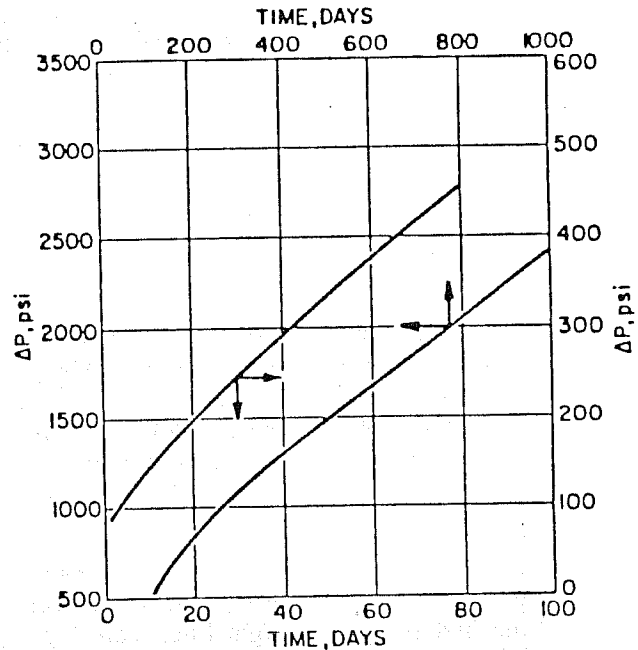


Fig. 2.5 Solution
(Cartesian plot)

He also concluded that there is a period during which the data form nearly a straight line when plotted on Cartesian coordinate graph. He calculated a volume somewhat greater than the volume of the inner zone using this Cartesian straight line. He did not continue to investigate this straight line portion and seems to have overlooked the importance of this Cartesian straight line.

What Carter found is remarkably supportive of the pseudosteady-state method developed by Eggenchwiler *et al.* (1980), at a later date. This method utilized the Cartesian straight line, and results have some similarity to Carter's findings.

Bixel and van Poolen (1967) solved the problem by using a one-dimensional radial single-phase numerical simulator. They reported correlation charts for the interpretation of flow tests for a wide range of mobility and storage capacity ratios. A curve-matching technique was used for analyzing field data. They provided dimensionless pressure solutions in graphical form for mobility ratios ranging from 0.001 to 100, and storativity ratio from 0.001 to 1000. An example of their solution is shown in Fig. 2.6. The mobility ratio and the storativity ratios used in their study are defined as follows:

$$\text{Storativity Ratio} = \frac{(\phi c)_{\text{zone2}}}{(\phi c)_{\text{zone1}}} \quad (2.3)$$

$$\text{Mobility Ratio} = \frac{(k/\mu)_{\text{zone2}}}{(k/\mu)_{\text{zone1}}} \quad (2.4)$$

Bixel and van Poolen proposed to analyze field data by a curve matching technique. The field data are first made dimensionless by the following equation:

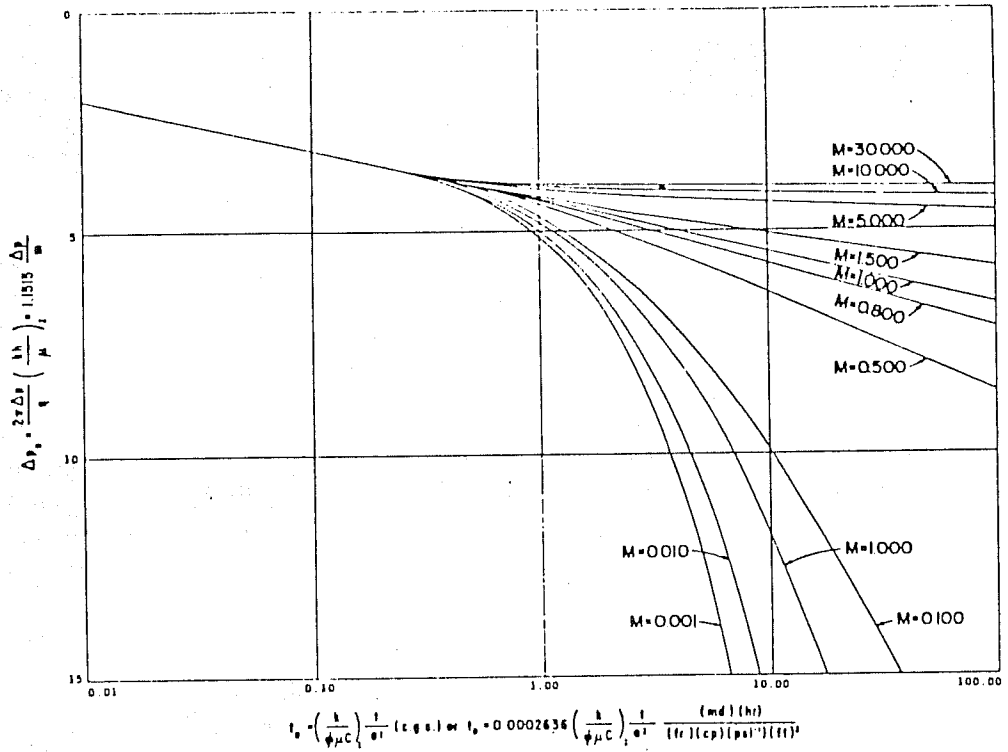
$$P_D = 1.151 \frac{\Delta p}{m} \quad (2.5)$$

where m is the slope from the initial semilog straight line. The dimensionless field data are then plotted against the log of time and matched against his curves. When a match is found, the distance to the discontinuity can be found by the following equation:

$$R = \sqrt{\frac{0.000264 k_1 t}{t_D \phi_1 \mu_1 c_1}} \quad (2.6)$$

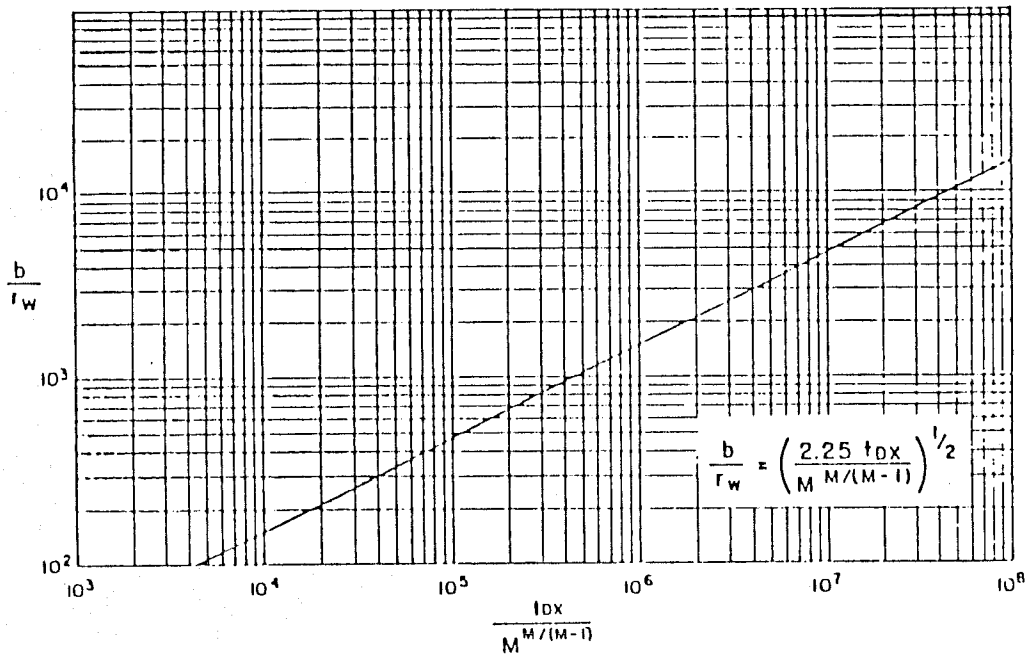
When examining Bixel and van Poolen's dimensionless pressure solution, one can notice that quite a few curves have the same shape. Therefore, it is possible that a unique match is difficult to find when both the mobility and storativity of both zones are unknowns.

Odeh (1969) presented an analytical solution for the same formulation, assumptions and boundary conditions as in Carter's study. He reported the same findings as in Carter's paper, but proposed a different method to calculate the distance to the discontinuity. He proposed to use the point of intersection between the two semilog straight lines in calculating the front radius. Odeh developed a set of charts for correlation between the intersection point of the two semilog straight lines and the dimensionless front radius. An example is shown in Fig. 2.7.



SOLUTION FOR STORAGE CAPACITY RATIO OF 1.0.

Fig. 2.6 Dimensionless Pressure Solution



Radial discontinuity distance-time relation.

Fig. 2.7 Correlation Chart

The calculation procedures for locating the burning front involves the graphing of field data as shown in Fig. 2.8. The dimensionless time at the point of intersection of the two semilog straight lines is then determined. From the radial discontinuity distance versus time chart (Fig. 2.7), the dimensionless radius of discontinuity is found. Figures like 2.7 are then used to determine the end of the first semilog straight line and the start of the second semilog straight line. If these values disagree with the values determined from the field data plot, the process is repeated. A trial and error method is employed to find the burning-front radius.

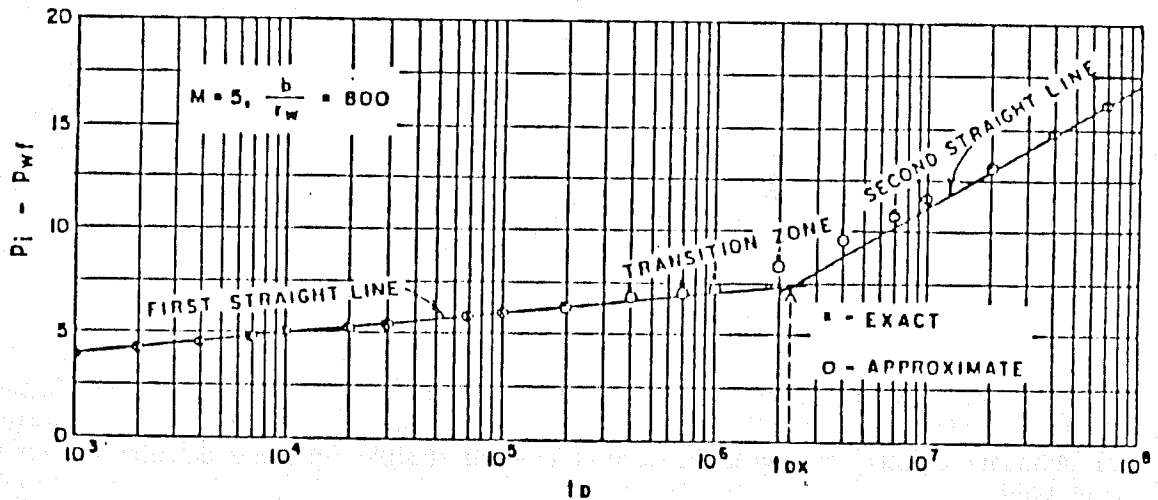


Fig. 2.8 Example Draw-down Plot

The weakness of this method is that it requires the presence of both semilog straight lines in order to calculate the front radius. As Odeh reported in his paper, the transition zone between the two semilog straight lines is very long, and boundary effects will mask the second semilog straight line. In practice, it is difficult to obtain field data that gives a second semilog straight line. Therefore, this method is of limited use.

A method based on the time of deviation from the first semilog straight line was presented by Merrill *et al.* (1974). Their idea was similar to that of van Poolen. Merrill *et al.* solved the problem with an implicit finite-difference method, and made test runs with different mobility ratios and storage ratios. From the data generated by the finite-difference model, they developed a correlation between the slope ratio of the two semilog straight lines and the dimensionless time at intersection. This correlation is shown in Fig. 2.9.

To analyze field data, the slope ratio of the two semilog straight lines is found from a semilog plot of the falloff data. The dimensionless intersection time Δt_{Dfs} is then determined from Fig. 2.9. The front radius is then calculated by using the following equation:

$$R_{f1} = \sqrt{\frac{0.0002637k\Delta t_{f1}}{\phi\mu c_t\Delta t_{Df1}}} \quad (2.7)$$

where Δt_{f1} is the intersection point in the semilog plot of the falloff data.

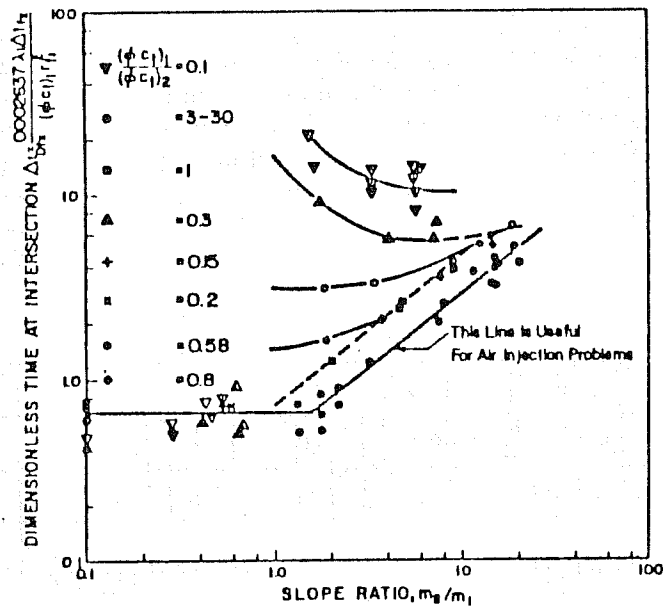


Fig. 2.9 Correlation for Dimensionless Intersection Time

The weak point of Merrill *et al.*'s method is the same as in Odeh's method. Both require the second semilog straight line, and the storativity of the second zone. A long transition zone or boundary effects will mask the second semilog straight line, and calculation will become impossible.

The latest publication in analysis of composite reservoirs is by Eggenschwiler *et al.* (1980). They solved the problem analytically, and discovered a new and powerful method to determine the swept-zone volume.

The problem was formulated for a swept region in an infinite reservoir and solved, using Laplace Transformation followed by numerical inversion. In order to study the important zonal effects, the gas in the reservoir was considered to be a liquid of slight and constant compressibility. The simulated result for an example *in-situ* combustion injection test is shown in Fig. 2.10.

It was discovered that for cases with a high mobility ratio, the discontinuity behaves like an impermeable boundary for several hours. This is evident by the existence of a Cartesian straight line for the period immediately following the initial semilog straight line in a pressure versus time graph. This Cartesian straight line is the key element which enables the estimation of the swept volume. The following two equations are employed in the calculation of the swept-zone volume and radius to the discontinuity if a Cartesian straight line is evident.

$$V_1 = \frac{qB5.615}{mc_{11}} \quad (2.8)$$

$$V_1 = \pi R_f^2 h \phi_1 \quad (2.9)$$

Eggenschwiler *et al.* also substantiated findings by plotting the data presented by Kazemi (1966) in Cartesian coordinates and found a straight line following the infinite-acting period. This Cartesian graph is shown in Fig. 2.11.

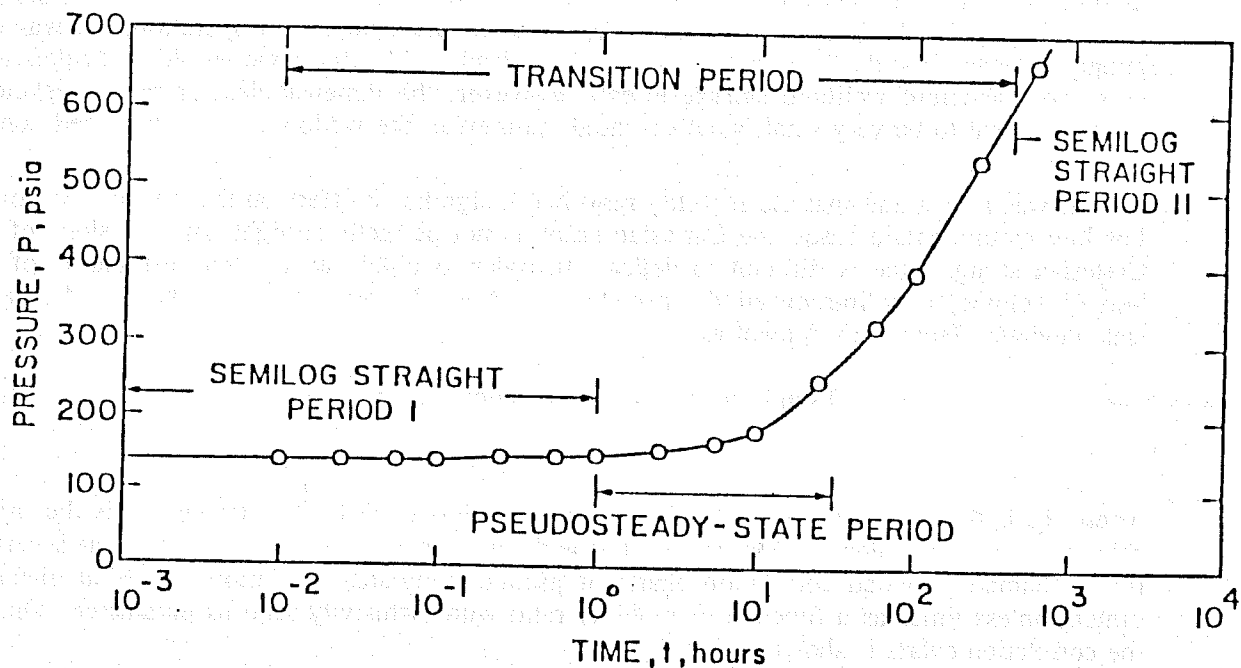


Fig. 2.10 Simulated Injection Test Response

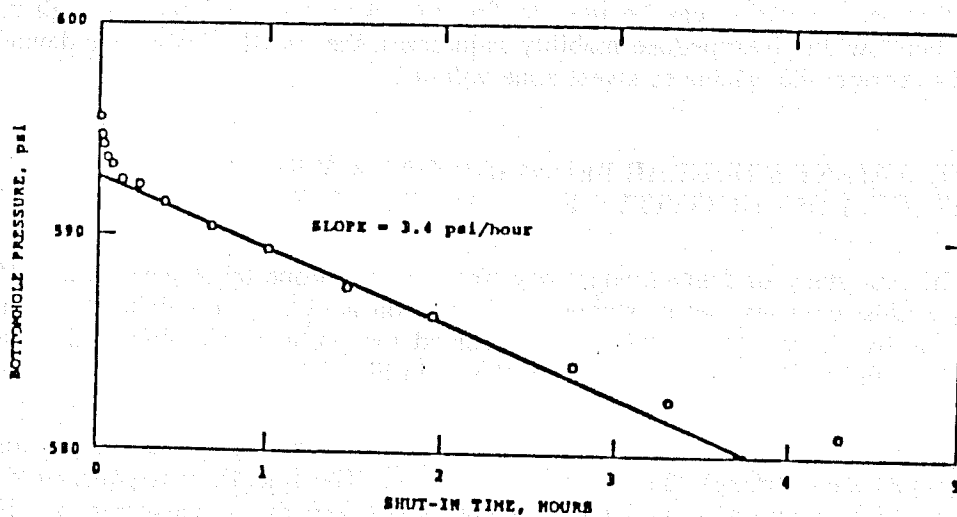


Fig. 2.11 A Cartesian Graph of the Kazemi Data

In a later study, Satman *et al.* (1980) investigated the effects of wellbore storage and mobility ratio on the pressure response of a radially composite system. The wellbore storage effect dies rapidly for injection conditions typical of *in-situ* combustion operations. It was originally expected that the large pore volume of the displaced burned zone would be evident as a very large apparent wellbore storage effect. However, the dimensionless storage coefficient, C_D , was found to be very small whether based upon either the wellbore or the displaced zone.

It was also found that the mobility ratio had a significant effect on the pressure response. For low mobility ratio cases, the Cartesian graph is not perfectly straight, and the slope of the Cartesian straight line is difficult to define. In order to obtain an accurate estimation of the burned volume, they introduced the pseudosteady-state deviation factor. The pseudosteady-state deviation factor was defined as:

$$\text{Pseudosteady-State Deviation Factor} = \frac{R_D}{R_D^*} \quad (2.10)$$

where R_D is the correct value of the dimensionless radius of discontinuity and R_D^* is the radius calculated from the slope of the apparent straight line on a graph of p_w vs. time at a certain time. Satman provided correlation charts of pseudosteady-state deviation factors at different dimensionless times as a function of mobility ratio with diffusivity ratio as parameter. One of the correlation charts is shown in Fig. 2.12.

To calculate the radius to the discontinuity, the slope of the apparent Cartesian straight line immediately following the initial semilog straight line is used to find R_D^* . An appropriate correlation chart is then used to find the pseudosteady-state deviation factor. This factor is directly applicable to correct the R_D^* to find the radius to the discontinuity. Strictly speaking, it would have been better to work in terms of the displaced volume.

Several conclusions were made in this study. The duration of wellbore storage is usually very short, and the properties of the swept zone can be calculated from the first semilog straight line. It was also concluded that the Cartesian straight line immediately following the first infinite-acting period can be used to find the swept-zone volume for high mobility ratio cases. For low and intermediate mobility ratio cases, the pseudosteady-state deviation factor is needed to correct the calculated swept-zone volume.

2.2. TRANSIENT PRESSURE BEHAVIOR FOR A WELL WITH A FINITE-CONDUCTIVITY VERTICAL FRACTURE

The first study of finite-conductivity fractures was done by Arihara *et al.* (1977). However, the most complete set of studies performed on a well with a finite-conductivity vertical fracture is by Cinco *et al.* (1978). They solved the problem semifinite slab reservoir intercepted by a finite-conductivity fracture as shown in Fig. 2.13.

Cinco *et al.* formulated the problem for the flow in the fracture and in the reservoir, and then coupled them through the continuity condition. The fracture was considered as a homogeneous, finite, slab porous medium of height, h , half length, x_f and width, w . Fluid entered the fracture at a rate $q(x,t)$ per unit of fracture length; and flow across the edge of this porous medium was negligible. The assumption of a no-flow boundary at the fracture tip allows the flow in the fracture to be linear, and the well production is simulated by a uniform flux plane source of dimensions h and w . This fracture flow model is shown in Fig. 2.14.

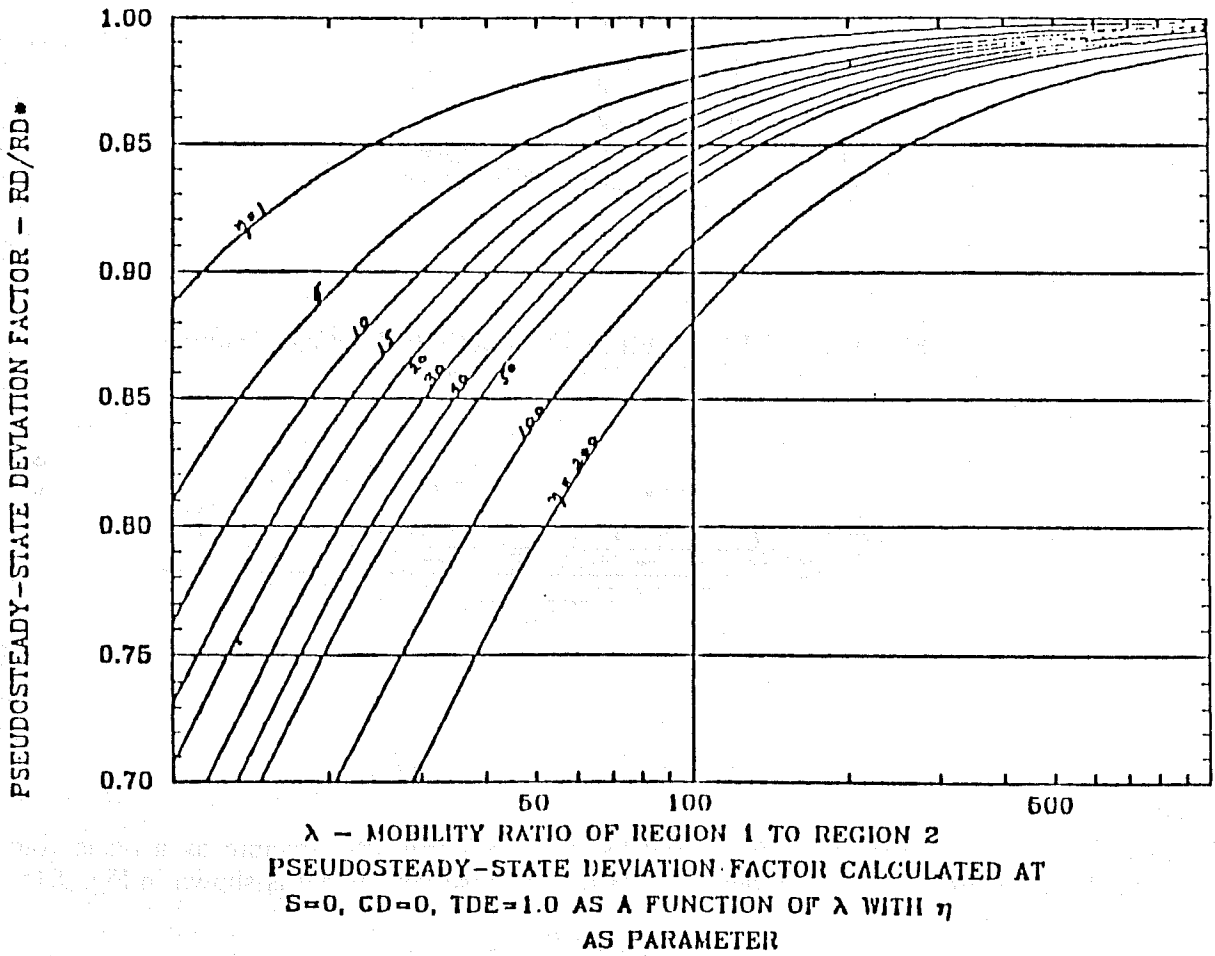


Fig. 2.12 Pseudosteady-State Deviation Factor Chart

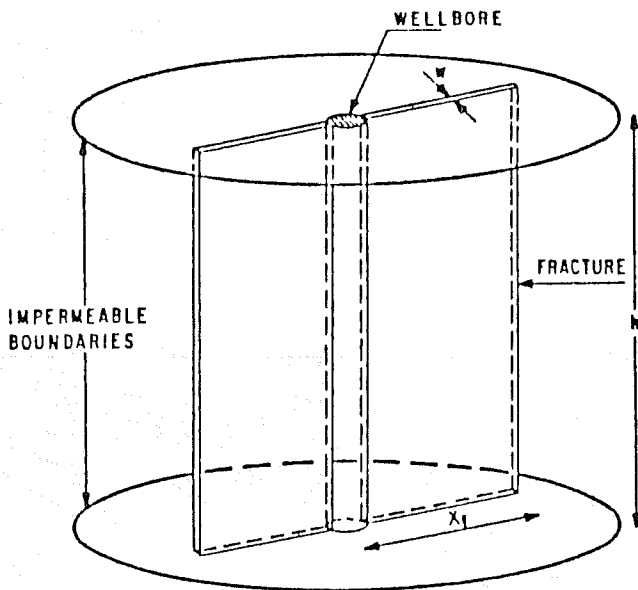


Fig. 2.13 Well with Finite Conductivity Vertical Fracture in an Infinite Slab Reservoir

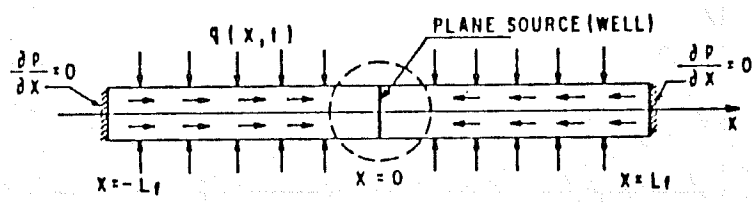


Fig. 2.14 Fracture Flow Model

The flow in the reservoir is modeled by considering the fracture as a plane source of height, h , length, $2x_f$, and flux density $q_f(x,t)$. The reservoir model is shown in Fig. 2.15.

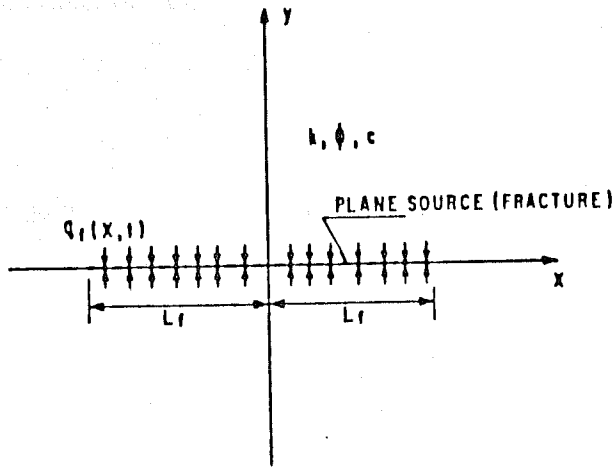


Fig. 2.15 Reservoir Flow Model

The two models were then coupled using the continuity condition. The dimensionless pressure drop and flux density in the fracture model must equal that on the plane source of the reservoir model.

They found that the dimensionless pressure solution could be correlated by one parameter, namely, the dimensionless fracture conductivity. This parameter is defined as:

$$K_{fd}W_{fd} = \frac{k_{fv}}{\pi k x_f} \quad (2.11)$$

where :

- k_{fd} = relative fracture permeability
- W_{fd} = dimensionless fracture width
- k_f = fracture permeability
- w = fracture width
- k = formation permeability
- x_f = fracture half length

Large values for the product ($k_{fd}W_{fd}$) represent highly conductive fractures, and small values represent fractures of low conductivity. Small values of the product may be caused either by low fracture permeability or large fracture length. The results were presented in a graphical form as shown in Fig. 2.16.

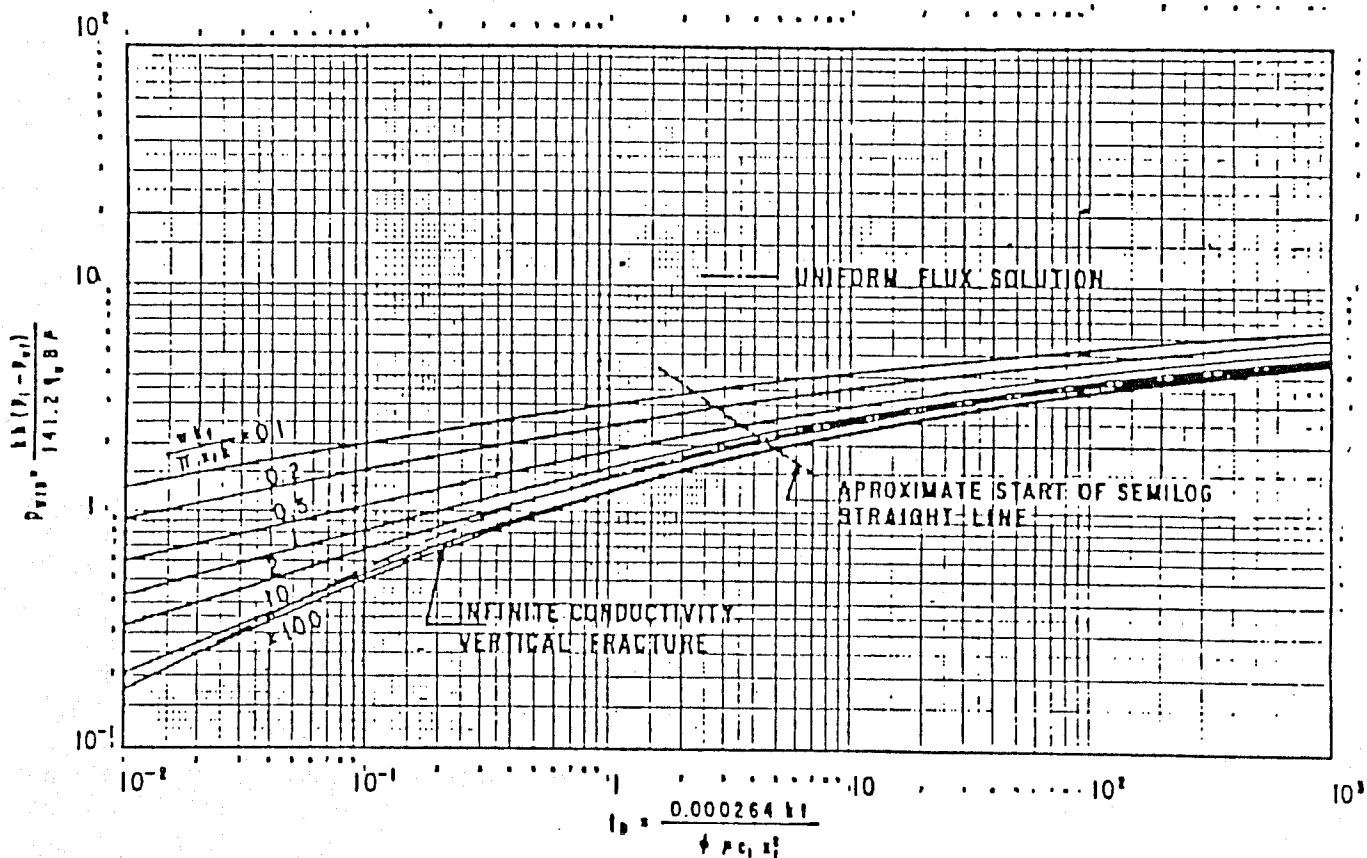


Fig. 2.16 Dimensionless Pressure Solution for an Infinite Reservoir with a Finite Conductivity Vertical Fracture (No Storage, No Skin)

It can be seen from Fig. 2.16 that as the value of $k_{fd}W_{fd}$ increases, the dimensionless wellbore pressure drop for a fixed time decreases. For $k_{fd}W_{fd}$ values greater than 300, the solution is essentially equal to the infinite-conductivity solution of Gringarten *et al.*. For large times, all curves in Fig. 2.16 approach a straight line of slope 1.151, characteristic of the semi-logarithmic methods of pressure analysis. However, for finite reservoirs, boundary effects will affect this straight line, and the semilogarithmic technique is not applicable.

At small values of dimensionless time, the curves have a distinct form for different values of dimensionless fracture conductivity. This feature of the solution can be used to analyze field data by a type-curve matching technique. However, early time data must be available before a type-curve matching technique can be used. Otherwise, a uniqueness problem will arise since all the curves in Fig. 2.16 have similar shapes at late times; therefore, care and diligence are needed if type-curve matching is attempted.

The dimensionless pressure solution presented in Fig. 2.16 did not include the effects of wellbore storage and skin. Cinco and Samaniego investigated the effects of these two parameters in a second paper presented in 1977. They found that both skin and wellbore storage have significant effects on the pressure response.

Cinco modeled the skin as a zone of reduced permeability caused by fluid loss around the fracture. This model is illustrated in Fig. 2.17.

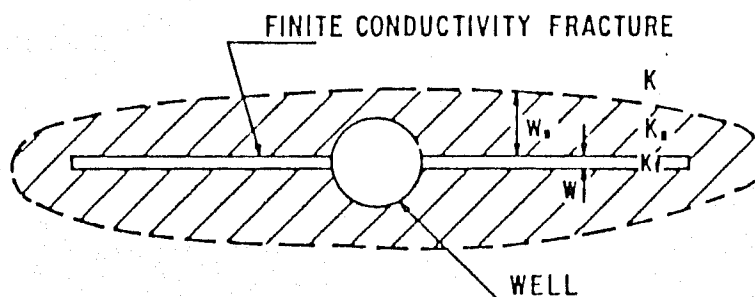


Fig. 2.17 Damaged Fracture Model

They found that when the pressure response is graphed as a function of $\log p_{wD}$ versus $\log t_D$ for early times, results show flat, almost horizontal lines, that later become concave upward curves asymptotically approaching the curve for undamaged fractures. This is shown in Fig. 2.18.

Because the log-log curves for an undamaged fracture shown in Fig. 2.16 never have a slope less than one-fourth at small values of time, they suggested that a fracture that is skin damaged may be detected when the slope of the log-log curve of pressure data, at small values of time, is less than one-fourth. However, if early time pressure data are not available, erroneous conclusions may be reached because a finite-conductivity fracture may be taken as an infinite conductivity fracture with a skin damage.

The effect of wellbore storage on the transient behavior of a fractured well with no skin is shown in Fig. 2.19. This graph indicates that wellbore storage greatly affects the transient pressure behavior of fractured wells. For short times, there is a wellbore storage dominated

flow period characterized by straight lines of slope one. There is a transition period after the unit slope straight line, whose duration depends on the $(k_f w/kx_f)$ value and C_{Df} values. Later in time, the pressure behavior is not affected by wellbore storage and approaches the curves for no skin and no storage cases.

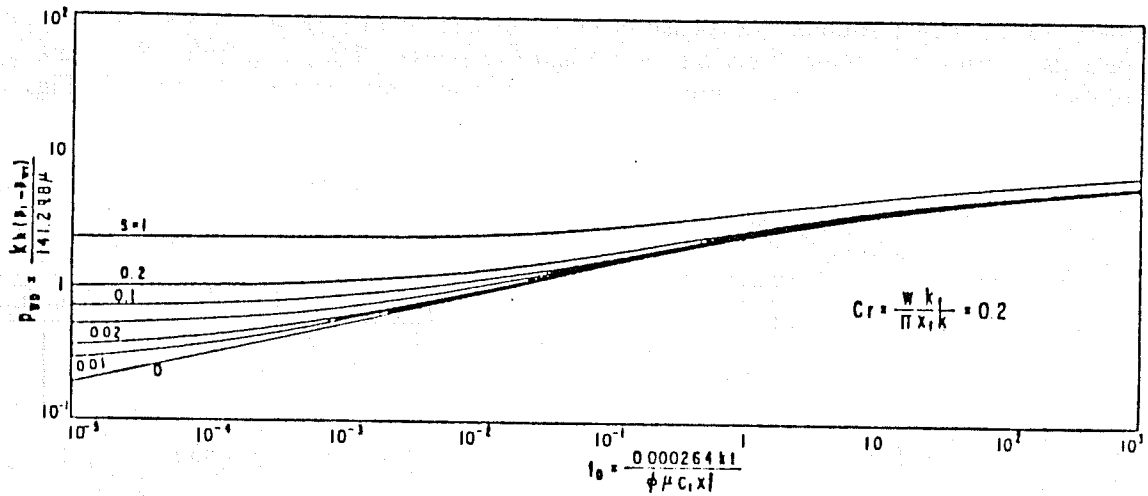


Fig. 2.18 Dimensionless Pressure Solution for a Fractured Well with Fracture Skin Damaged

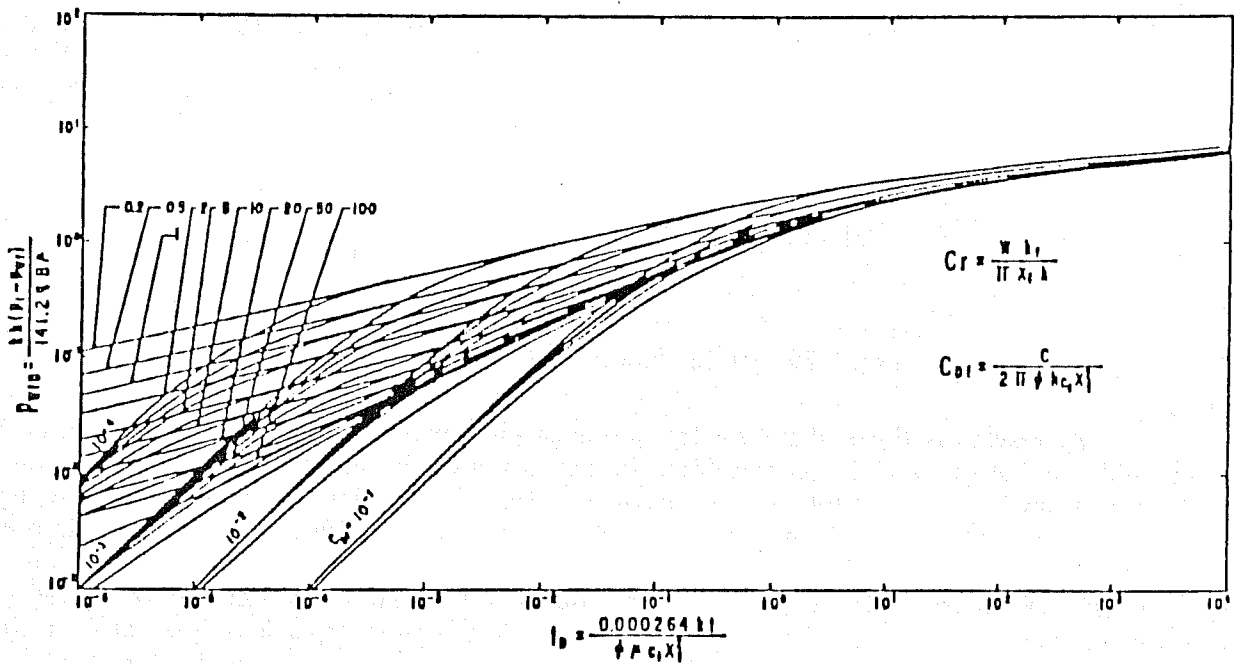


Fig. 2.19 Dimensionless Pressure Solution for a Fractured Well with Wellbore Storage (No Skin)

In general, the curves in Fig. 2.19 have different slopes, and a type curve matching technique can be used to analyze field data. However, problems of characterization may arise when insufficient pressure data match the type curve in the region of lines of one-fourth slope. Therefore, the use of the type curve matching technique becomes practical only when a large span of pressure data are available.

Cinco and Samaniego reported further investigations of the subject in two papers in 1978 and 1981. They presented the possible flow periods in the fracture system during different periods of time, and their effect on the pressure response. They concluded that there are four possible flow regimes for a fractured system. These four regimes are illustrated in Fig. 2.20.

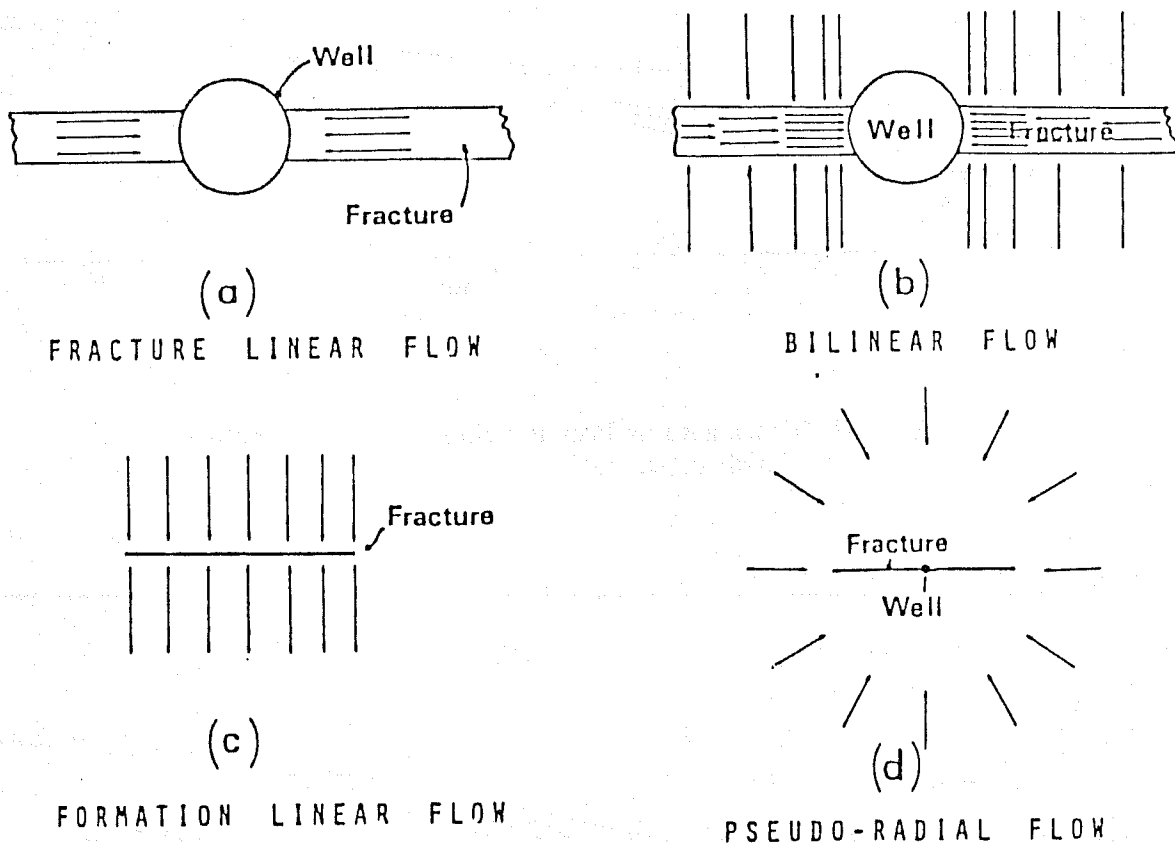


Fig. 2.20 Finite Conductivity Fracture Flow Periods

At very early times, there is a fracture linear-flow period. During this period, most of the fluid entering the wellbore comes from the expansion of the fluid within the fracture, and the flow behavior is essentially linear on a log-log graph with a slope of one-half. Following the fracture linear-flow period, there is a bilinear-flow period. During this period, there is a linear incompressible flow within the fracture and a linear compressible flow in the formation. The pressure behavior exhibits a straight line whose slope is equal to one-fourth on a log-log graph of p_{wD} versus t_{Dxf} . The existence of this bilinear-flow regime depends on the value of dimensionless fracture conductivity and dimensionless storage coefficient. Following the bilinear-flow period, there is a formation linear-flow period for cases where the dimensionless fracture conductivity has a value greater than fifty. The pressure behavior during this period exhibits a half-slope straight line on a log-log plot of pressure versus time. After the formation linear flow period, the pressure behavior of a fractured well will eventually reach pseudoradial flow

conditions, regardless of the fracture conductivity value, provided boundary effects are not present. During this period, a graph of p_{wD} versus the log of t_{Dxf} gives a straight line of slope equal to 1.151, no matter what the fracture conductivity. The conventional semilog analysis technique can be applied for this period.

In a later study, Cinco and Samaniego (1981) presented a new type curve that has great utility for practical applications. As mentioned before, the type curve shown in Fig. 2.16 has a problem of application because all the curves have a similar shape. Cinco and Samaniego showed that in practice the problem can be overcome by plotting $p_{wD}(K_{fD}W_{fD})$ versus $t_{Dxf}(K_{fD}W_{fD})^2$. This type curve is shown in Fig. 2.21.

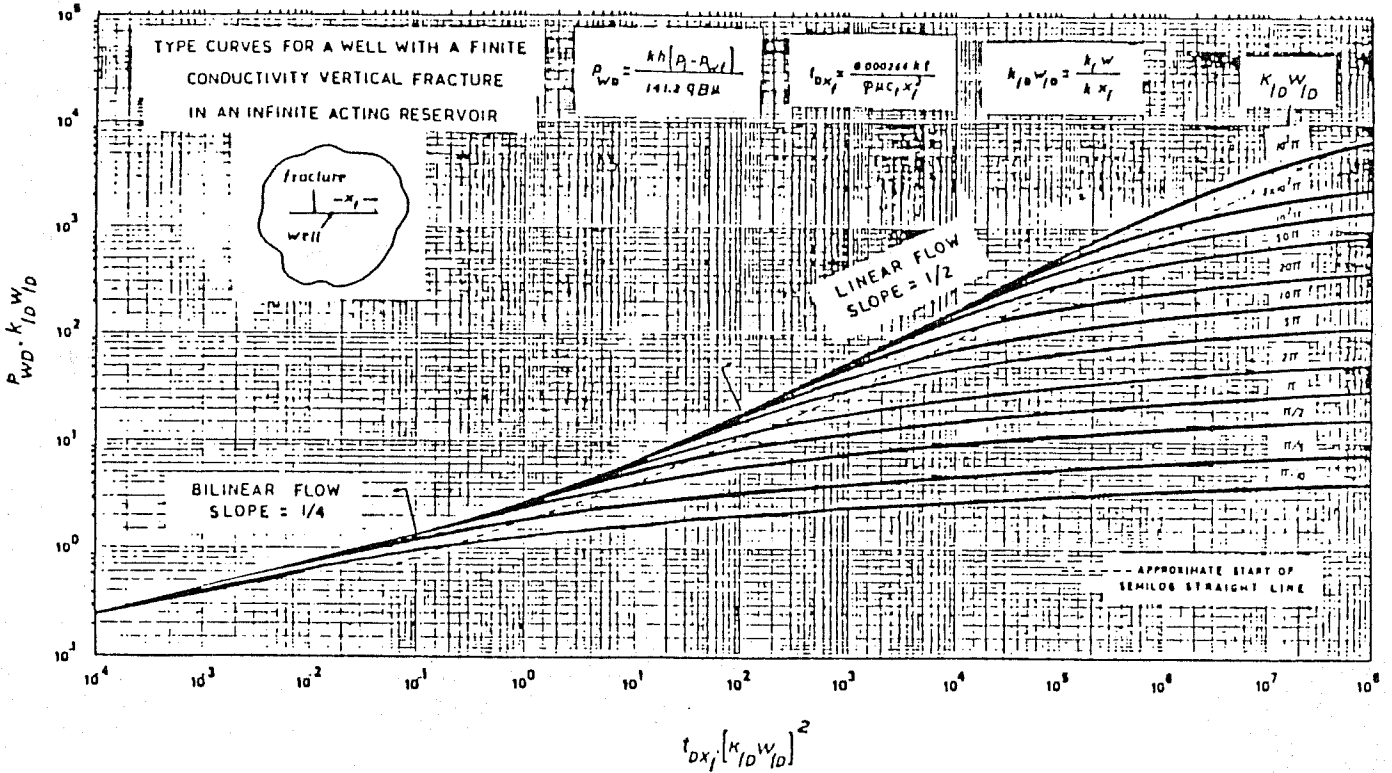


Fig. 2.21 Dimensionless Pressure Solution for a Vertically Fractured Well

3. PROBLEM STATEMENT

A horizontal finite square slab reservoir with a centrally located well intercepted by a vertical fracture is shown in Fig. 3.1.

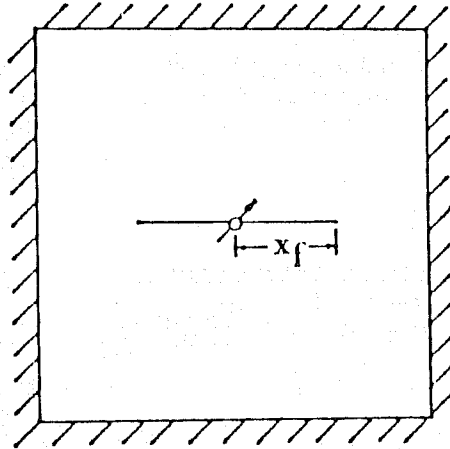


Fig. 3.1 A Vertically Fractured Well in a Finite Reservoir

If an *in-situ* combustion project is to be commenced with this well as an air injector, the burned zone will propagate in a direction normal to the plane of the fracture at early times as shown in Fig. 3.2.

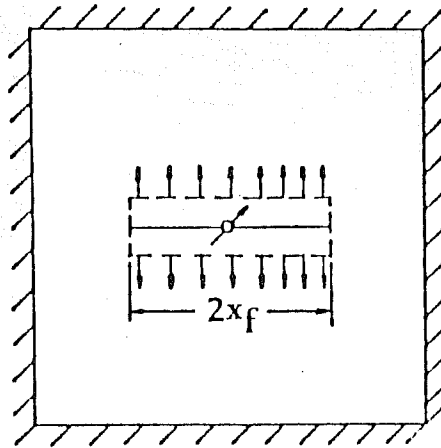


Fig. 3.2 A Rectangular Burned Zone in a Finite Reservoir

This burned zone can be idealized as a rectangular region of length, $2x_f$, and width, w , with properties different from those in the unburned region. As time goes on, the rectangular burned zone volume will increase. If boundary effects are not present, the burning front will eventually achieve a radial geometry and can be approximated by a radial discontinuity. This is shown in Fig. 3.3.

As explained in the previous section, Eggenschwiler *et al.* presented a pseudosteady-state method for finding the swept-zone volume for a radial, composite reservoir. The method can be applied to a composite system with an injection well intercepted by a vertical fracture if the burning front has already achieved a nearly cylindrical shape. However, during the early stage

of the operation, the burned zone resembles a long and narrow rectangle as shown in Fig. 3.2. Therefore, it is of interest to know if the pseudosteady-state method can be applied to such a rectangular burned region geometry.

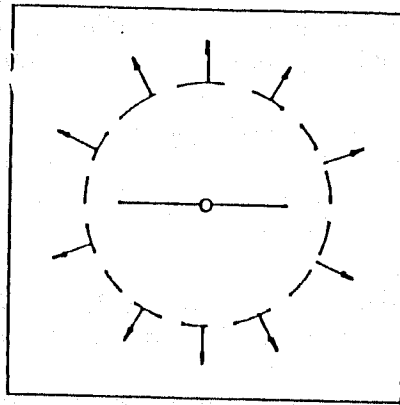


Fig. 3.3 Pseudoradial Flow Regime

Eggenschwiler *et al.* concluded that pseudosteady-state involves only a material balance depletion of a closed volume of any shape. Therefore, the detection of the burned volume is not dependent on burned volume geometry. However, the method is based on the similarity between the closed and the composite radial system. As a result, it is of importance to know if the concept can be applied when the system in consideration has a geometry substantially different from that of the composite radial system.

The purpose of this study was to determine the necessary width of the rectangular burned zone before the pseudosteady-state method may be applied.

4. METHOD OF SOLUTION

Two numerical simulators were developed to generate the necessary pressure responses for an injection test for this study. Both simulators are isothermal, two-dimensional, single-phase simulators in a Cartesian coordinate system. One was formulated for a slightly compressible fluid with a constant compressibility and the other was for a compressible gas. A detailed description of simulators is provided in Appendix A and Appendix B.

In an *in-situ* combustion operation, the region behind the front contains mostly air, while the region ahead of the front contains hydrocarbon, water and gas. However, the mobility of the gas in the swept zone is so much greater than that of the liquid phase ahead of the burning front, only gas flow will be considered.

In order to study the most important effects, the fluid in the reservoir was treated as a liquid with slight and constant compressibility rather than as a gas. Handling the fluid as a liquid permitted the investigation of the effects of certain important parameters. However, the pressure gradient in the reservoir is small; therefore, treating the gas as a liquid with constant compressibility is acceptable. This will be shown with the results obtained by utilizing the compressible gas simulator, as compared to those obtained using a slightly compressible fluid.

Other assumptions implicit in this study are listed as follows:

- (1) The formation is horizontal, of uniform thickness, and homogeneous.
- (2) The front is considered stationary throughout the testing period.
- (3) The front is of infinitesimal thickness.
- (4) Gravity and capillary effects are negligible.
- (5) Darcy's law applies.

A complication in the system being simulated, however, is that the temperature is not uniform throughout the reservoir. It would be expected that the temperature of the burning front would be around 1000°F (540°C) while the rest of the reservoir is at a much lower temperature. However, in order to study the most important effects, it is assumed that the reservoir exists at some mean temperature. The mean temperature used in this study is 500°F (260°C).

In this study, only a high mobility ratio case is considered. A mobility ratio of 200 and a diffusivity ratio of 12 are used in all simulation runs. The definitions of these two quantities are:

$$\lambda = \frac{(k/\mu)_{zone1}}{(k/\mu)_{zone2}} \quad (4.1)$$

$$\eta = \frac{(k/\phi\mu C_t)_{zone1}}{(k/\phi\mu C_t)_{zone2}} \quad (4.2)$$

Fluid and rock properties used in this study are typical of those found in an *in-situ* combustion operation. They can be found in Appendix D.

The viscosity and system compressibility were held constant in this study. Therefore, permeability and porosity of the two zones were adjusted to achieve the desired values for mobility ratio and diffusivity ratio.

Due to the symmetry of the problem, all simulation runs were performed for one quarter of the reservoir, with a grid of 21x21 blocks. Fine grid spacing was used near the well for all runs. However, when a simulation run is performed for a burned zone which is very long and narrow, similar to a fracture, fine grid spacing was also used at the tip of the rectangular zone. This is illustrated in Fig. 4.1.

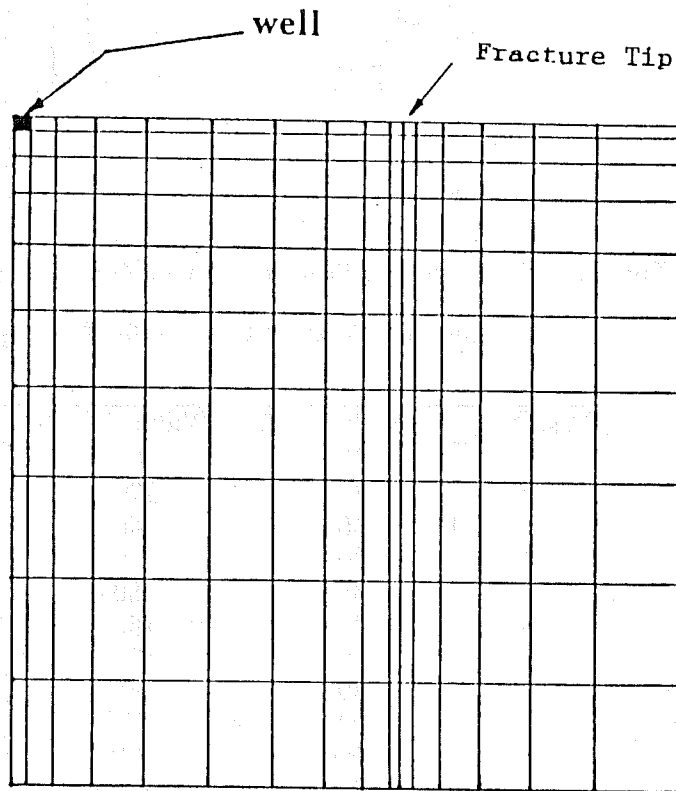


Fig. 4.1 Grid Spacing Used in Simulation Runs

Drainage boundaries were chosen far enough from the well and the burned zone so that the pressure response would be unaffected by their presence during times of interest. The drainage area used for this study is a square 7500 feet per side.

A series of simulation runs were performed for different width to length ratios (W/L) of the rectangular burned zone. Starting from a square burned zone of 300 ft. (100 m) per side as shown in Fig. 4.2, the width of the burned zone was then reduced successively to yield width-to-length ratios from 0.9 to 0.00157. Since the length of the burned zone is a constant of 300 ft. (100 m), which is the total length of the fracture, therefore, $2x_f = 300$ ft. (100 m) and $x_f = 150$ ft. (50 m). Table 4.1 presents the width-to-length ratios for all the simulation runs performed in this study.

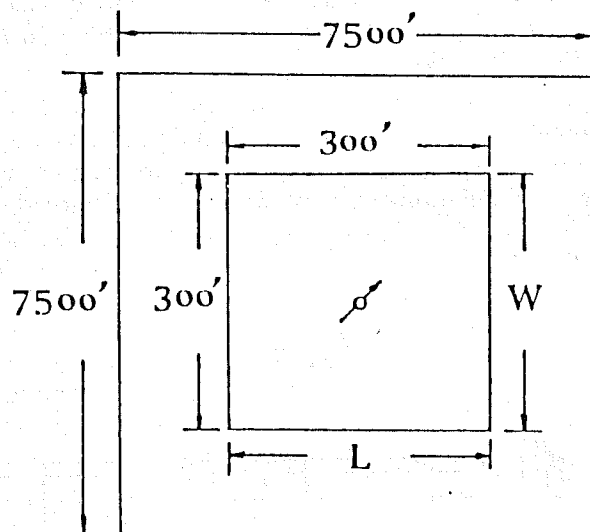


Fig. 4.2 Dimensions of Square Burned Zone for Simulation Runs

Table 4.1 List of W/L Ratios Simulated

Case No.	Length (L) ft	Width (W) ft	W/L
1	300	300.0	1.0
2	300	270.0	0.9
3	300	240.0	0.8
4	300	210.0	0.7
5	300	180.0	0.6
6	300	150.0	0.5
7	300	120.0	0.4
8	300	90.0	0.3
9	300	60.0	0.2
10	300	30.0	0.1
11	300	23.5617	0.078539
12	300	11.7809	0.039269
13	300	4.7121	0.015707
14	300	2.3561	0.007853
15	300	1.1780	0.003926
16	300	0.4712	0.001570

5. RESULTS AND INTERPRETATIONS

In this section, we will present the pressure responses in both dimensionless form and in the form of pressure (psia). Pressure responses presented in dimensionless form are used to show general trends. However, pressure versus time graphs are used to illustrate the calculations involved in semilogarithmic analysis and in the determination of the burned-zone volumes. For the sake of brevity, semilog and Cartesian plots of the pressure responses are shown for selected cases only. Pressure versus time graphs for all cases can be found in Appendix E.

We will start by presenting the pressure analysis of the case with the square burned zone. Then proceed to present the pressure responses in dimensionless form for various width-to-length ratios. Geometrically, the square burned zone is not a great departure from a radial-burned region. Therefore, the pseudosteady-state method should predict a correct burned-zone volume. In order to illustrate the pressure response of the system from very early times to late times, a simulation run of very long duration was performed for this case.

Figure 5.1 is a semilog plot of the pressure response for this run. There is a short initial period where the storage effect of the inner zone dominates. Then there is a semilog straight line, characterizing the inner zone conductivity, followed by a long transition when the discontinuity is felt. It is in this transition period where the pseudosteady-state flow period exists. The second semilog straight line began to form after the transition period, however, boundary effects prevented the completion of the second semilog straight line, and the pressure response began another transition. The entire reservoir eventually enters pseudosteady-state flow.

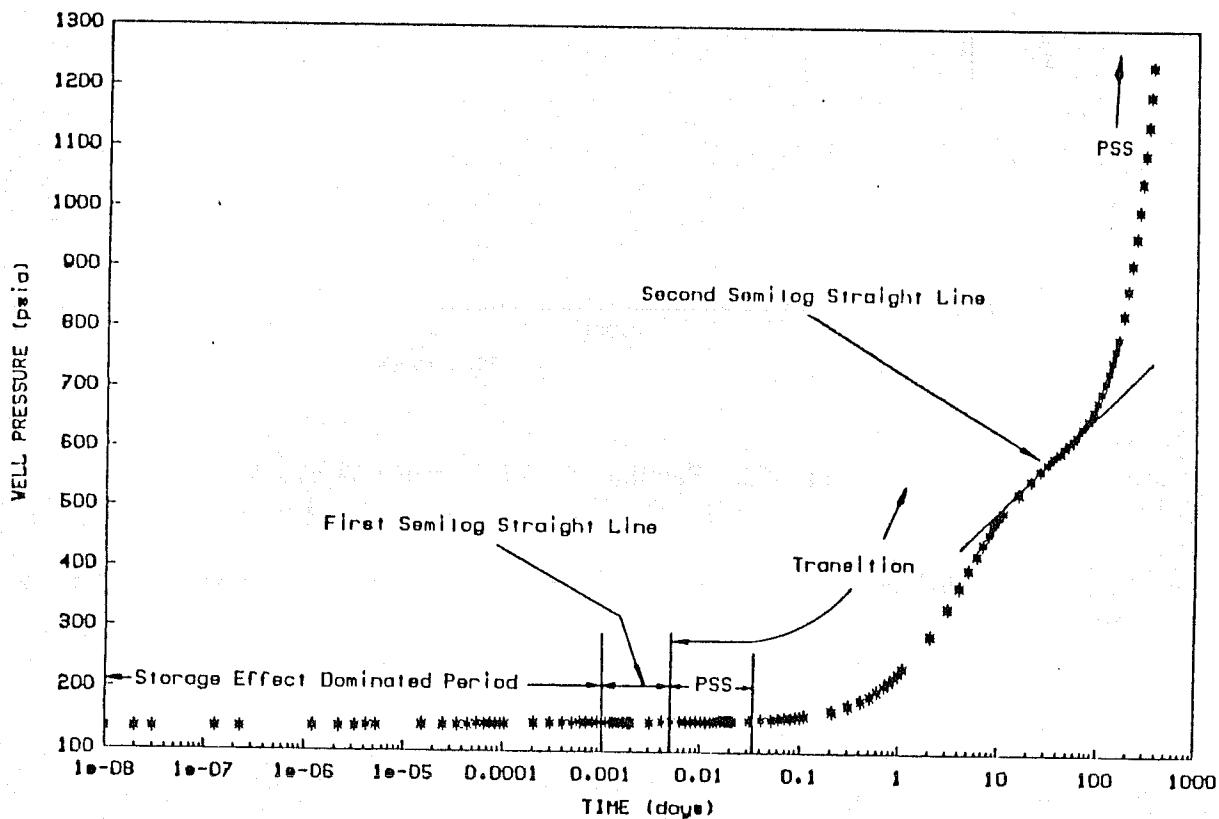


Fig. 5.1 Semilog Plot of Pressure Versus Time for the Case with the Square Burned Zone (long duration run)

We will now consider a realistic time frame. Figure 5.2 is a semilog plot of the same case from 0.0001 day to 0.1 day. As expected, the storage effect diminished rapidly, and was followed by a semilog straight line. From the slope of this straight line, the permeability of the swept zone could be calculated from :

$$k = \frac{162.6qB_{g_s}\mu}{mh} \quad (5.1)$$

where B_{g_s} is the gas formation volume factor at the average pressure where the semilog straight line exists.

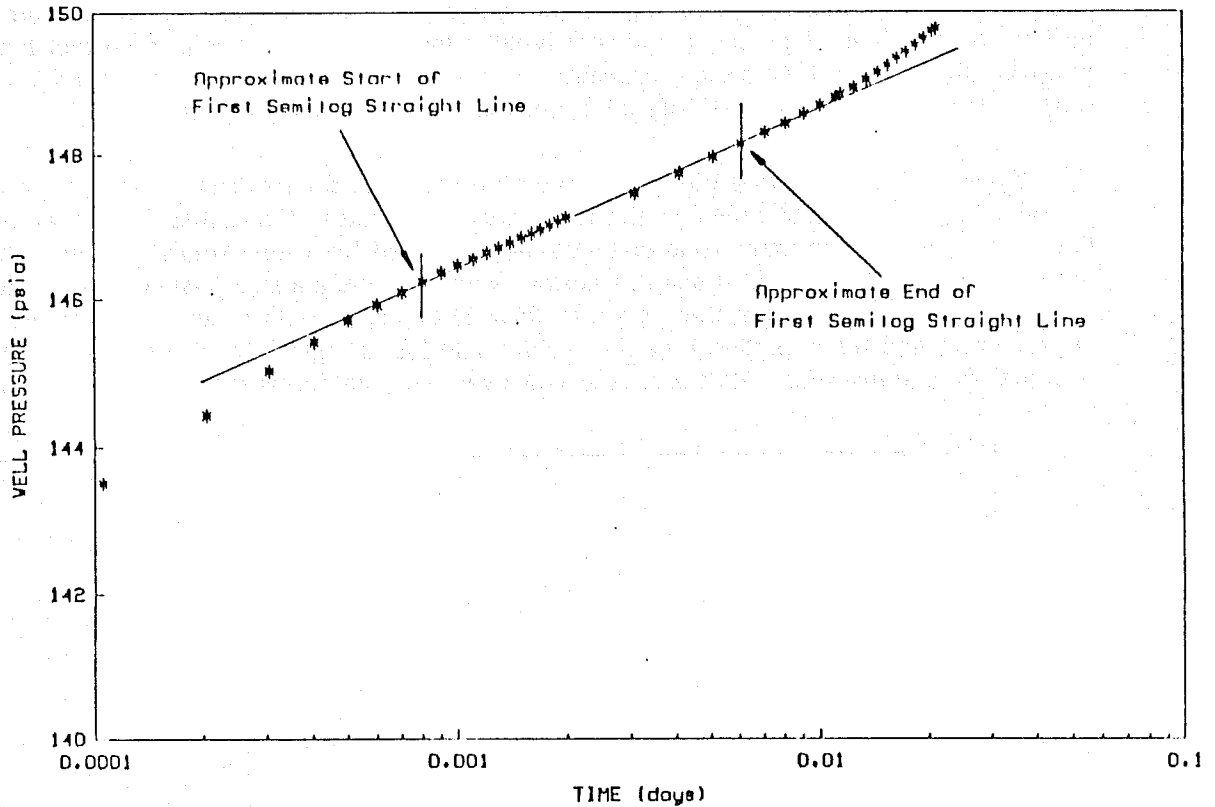


Fig. 5.2 Semilog Plot of Pressure Versus Time for the Case with the Square Burned Zone

The following calculation was performed to calculate the permeability for the burned zone:

$$\begin{aligned} \text{Slope} &= m = 2.2491 \text{ psi/day} \\ p_{avg_s} &= 147.17 \text{ psia} \\ B_{g_s} &= \frac{ZRT}{380.69p_{avg_s}} = 0.1837 \text{ RV/STV} \\ k &= 7913.7 \text{ md} \end{aligned}$$

The computed value of the permeability of the burned zone agrees favorably with the input value of 8000 md. The end of the semilog straight line is at 0.006 days which corresponds to a t_{DA_1} of 0.1053. This value compares favorably with an analytical value of 0.1.

When the data are graphed on a Cartesian coordinate graph as shown in Fig. 5.3, we can see an apparent straight line form almost immediately following the end of the first semilog straight line. The word "apparent" is used because the data did not form a perfect straight line. This is not a true pseudosteady-state straight line. The pressure response actually had a slight curvature and continually bent downward. This is also evident in the data presented by Eggenchwiler *et al.* (1980). However, for a short period of time immediately after the end of the first semilog straight line, the data almost forms a Cartesian straight line. Therefore, it is essential to have an initial semilog straight line to locate the Cartesian straight line. The straightness and duration of the Cartesian line depends largely on the plotting scale of p_w v.s. t . This is not a new finding. The same dilemma occurs in the classic case of determining when pseudosteady-state starts for a closed square reservoir. In this study, scales that are similar to those found in a realistic field pressure analysis are used.

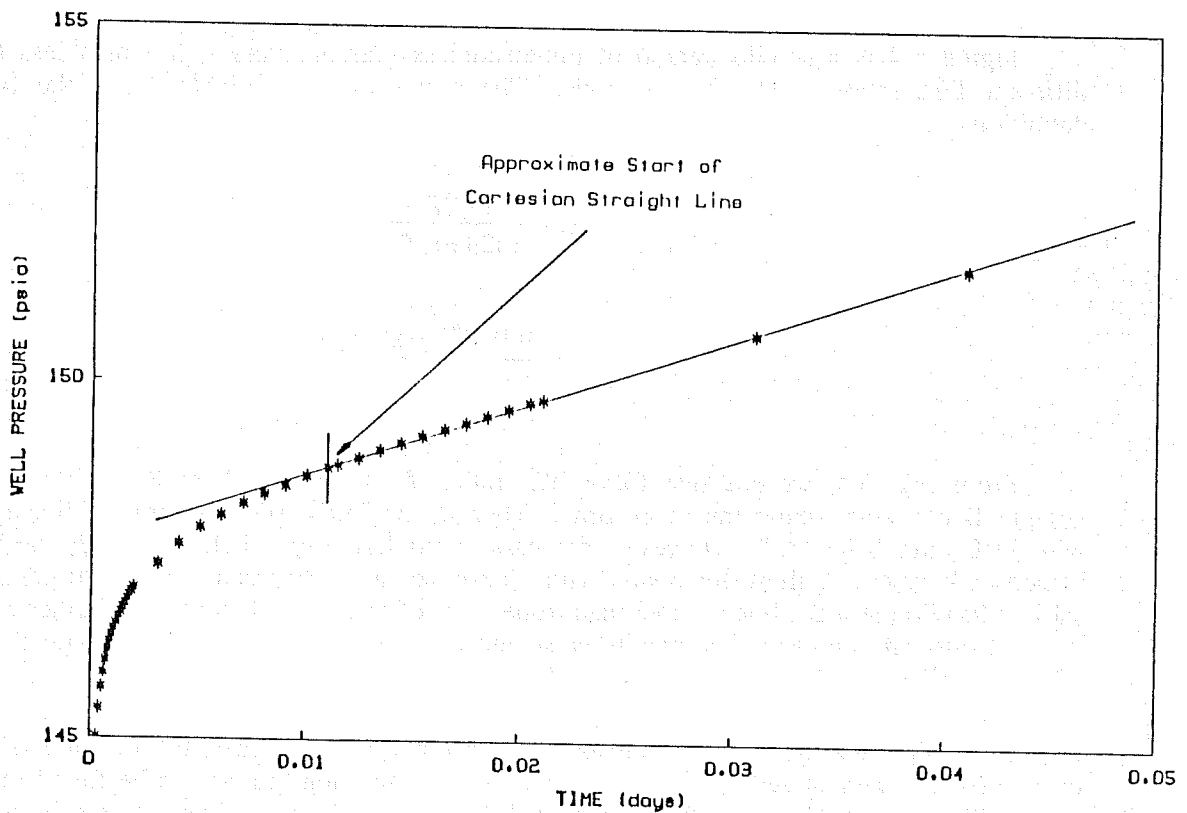


Fig. 5.3 Cartesian Plot of Pressure Versus Time for the Case with the Square Burned Zone

The slope of the pseudosteady-state straight line for this case is $m = 104.46$ psi/day. The burned-zone volume is related to this slope as follows:

$$V_1 = \frac{qB_{gc}5.615}{c_{l,avg}m} \quad (5.2)$$

The quantity B_{gc} is the gas formation volume factor at the average pressure where the Cartesian straight line begins.

Using Eq. (5.2), the burned-zone volume was calculated to be 944,670 ft^3 . This value compares favorably with the correct value of 945,000 ft^3 with an error of 0.03 %.

As mentioned before, the second semilog straight line is affected by the outer closed boundaries, therefore, the slope of the second semilog straight line should be too high, and should yield a low value of permeability for the outer zone. The slope of the second semilog straight line obtained from Fig. 5.1 is $m = 165.49$ psi/day. Using Eq. (5.1), the computed permeability for the outer zone is 27.1 md. As expected, this value is too low when compared with the true value of 40 md. The second line on Fig. 5.1 would have continued to bend down had the outer boundary not caused a pseudosteady state.

From this analysis, we can see the pseudosteady-state method yields favorable results for the case with the square-burned zone. We will now show the effects of reduction of the burned zone width on pressure responses.

Figure 5.4 is a semilog graph of dimensionless pressure versus dimensionless time for different W/L ratios of the burned zone. The dimensionless variables have the following definitions:

$$p_{wD} = \frac{k_1 h \Delta(p^2)}{1424 q \mu_1 Z T} \quad (5.3)$$

$$t_{Dxf} = \frac{0.000264 k_1 t}{\phi_1 \mu_1 c_{f1} x_f^2} \quad (5.4)$$

From Fig. 5.4, we see that for a W/L ratio of 1.0 to 0.2, there is an initial semilog straight line characterizing the inner zone. There is no initial semilog straight line for cases with W/L ratio below 0.2. However, for cases with W/L ratios below 0.0157, the pressure responses behave like those for a well with a finite-conductivity fracture in late times and then show a semilog straight line for the outer zone. It is of interest to determine whether the simulation results are similar to the results presented by Cinco *et al.* for the case with the lowest W/L ratio. This will be discussed later in this section.

A detailed semilogarithmic analysis was performed for each case. For the sake of brevity, the results are summarized in Tables 5.1 and 5.2. All semilog graphs can be found in Appendix E. Table 5.1 summarizes the results of the semilogarithmic analysis for the burned zone, whereas Table 5.2 is for the outer zone. Semilogarithmic analysis for the outer zone was only performed for cases with W/L ratio that are less than unity.

The results shown in Table 5.1 indicate that there is no semilog straight line for the burned region for cases with W/L ratio that is below 0.2. However, for cases with W/L ratio below 0.5, the duration of the semilog straight line is short, and yields excessive error in permeability calculations. This is illustrated with a graph of W/L ratio versus % error in permeability calculations as shown in Fig. 5.5.

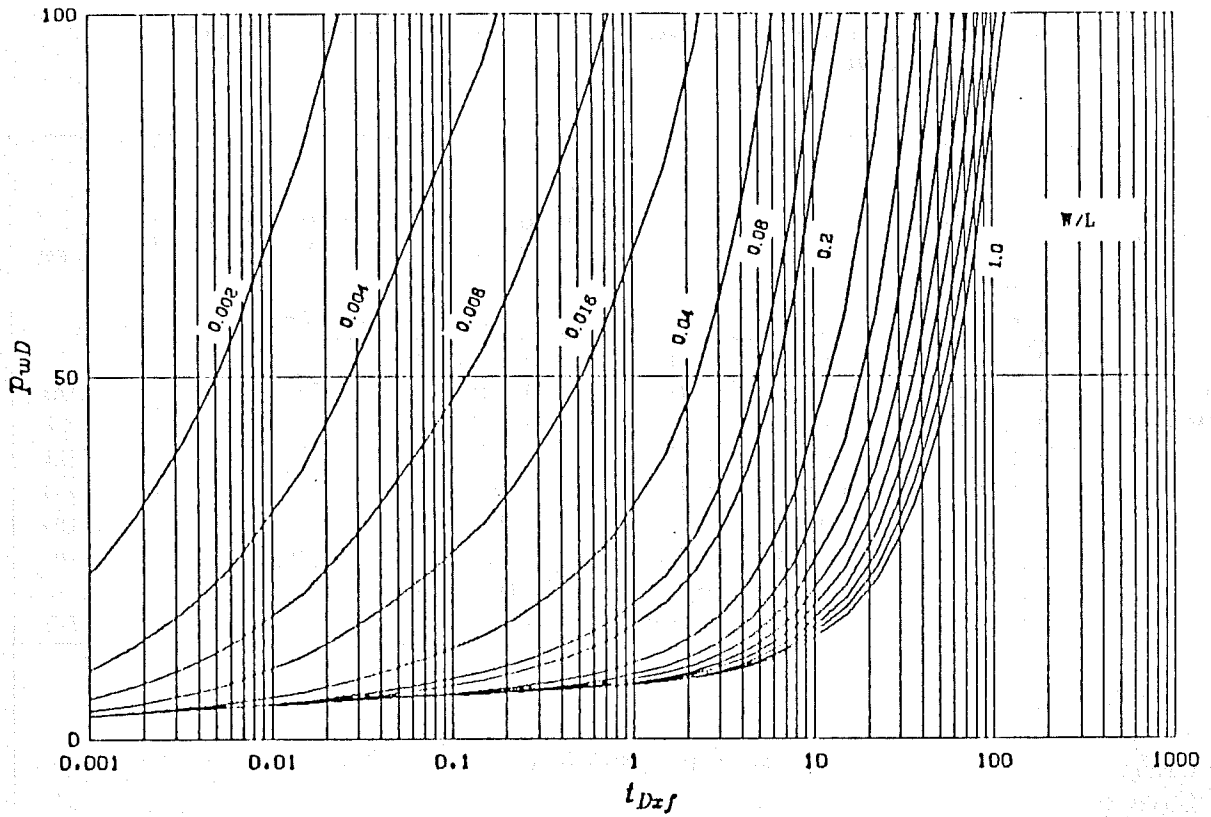


Fig. 5.4 Semilog Graph of Dimensionless Pressure Responses for Different W/L Ratio

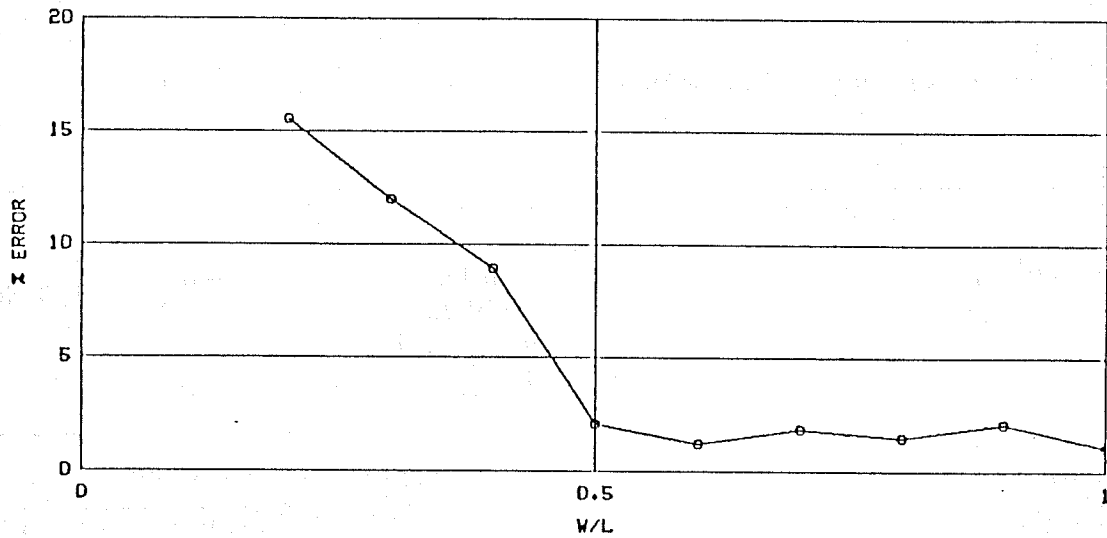


Fig. 5.5 Error in Calculated Permeability as a Function of W/L Ratio

Table 5.1 Summary of Results for Semilogarithmic Analysis for Burned Zone

W/L	Approximate Start of Semilog Straight Line		Approximate End of Semilog Straight Line		Permeability Calculated (md)	% Error
	(days)	t_{Def}	(days)	t_{Def}		
1.0	0.0008	0.056179	0.006	0.421344	7913.8	1.08
0.9	0.0008	0.056179	0.0055	0.386232	7832.5	2.09
0.8	0.0008	0.056179	0.005	0.351120	7882.0	1.47
0.7	0.0008	0.056179	0.005	0.351120	7852.8	1.84
0.6	0.0007	0.049156	0.004	0.280896	7904.2	1.20
0.5	0.0007	0.049156	0.0033	0.231739	7833.4	2.08
0.4	0.0006	0.042134	0.0031	0.217694	7284.0	8.95
0.3	0.0005	0.035112	0.0014	0.098313	7042.4	11.97
0.2	0.000105	0.007387	0.000305	0.021432	6755.9	15.55
0.1 0.078539 0.039269 0.015707 0.007853 0.003926 0.001570	No Initial Semilog Straight Line					

Table 5.2 Summary of Results for Semilogarithmic Analysis for Outer Zone

W/L	$\frac{k_1 W}{k_2 x_f}$	Approximate Start of Semilog Straight Line (days)	Approximate Start of Semilog Straight Line Presented by Cinco (days)	Permeability Calculated (md)	% Error
0.078539 0.039269	10π 5π	No Semilog Straight Line for Outer Zone			
0.015707 0.007853 0.003926 0.001570	2π π $\pi/2$ $\pi/5$	0.8 0.7 0.6 0.5	0.75 0.65 0.6 0.43	38.3 38.6 39.0 39.2	4.25 3.5 2.5 2.0

From Table 5.2, it appears that there is a semilog straight line for the outer zone for cases with W/L ratio below 0.0157. The permeabilities calculated for the outer zone from these straight lines agree favorably with the input values. These results indicate that at a low W/L ratio, the burned zone behaves more like a fracture and will have no semilog straight line for the swept region.

We will now discuss the main objective of this study. From the semilogarithmic analysis, we can see that as the width of the burned zone is reduced, the duration of the semilog straight line shortens and eventually vanishes. We would expect the same would be true for the pseudosteady-state straight line for the inner zone. Below a certain W/L ratio, there probably will no longer be a Cartesian straight line for the burned zone.

Figure 5.6 is a Cartesian graph of the dimensionless pressure response.

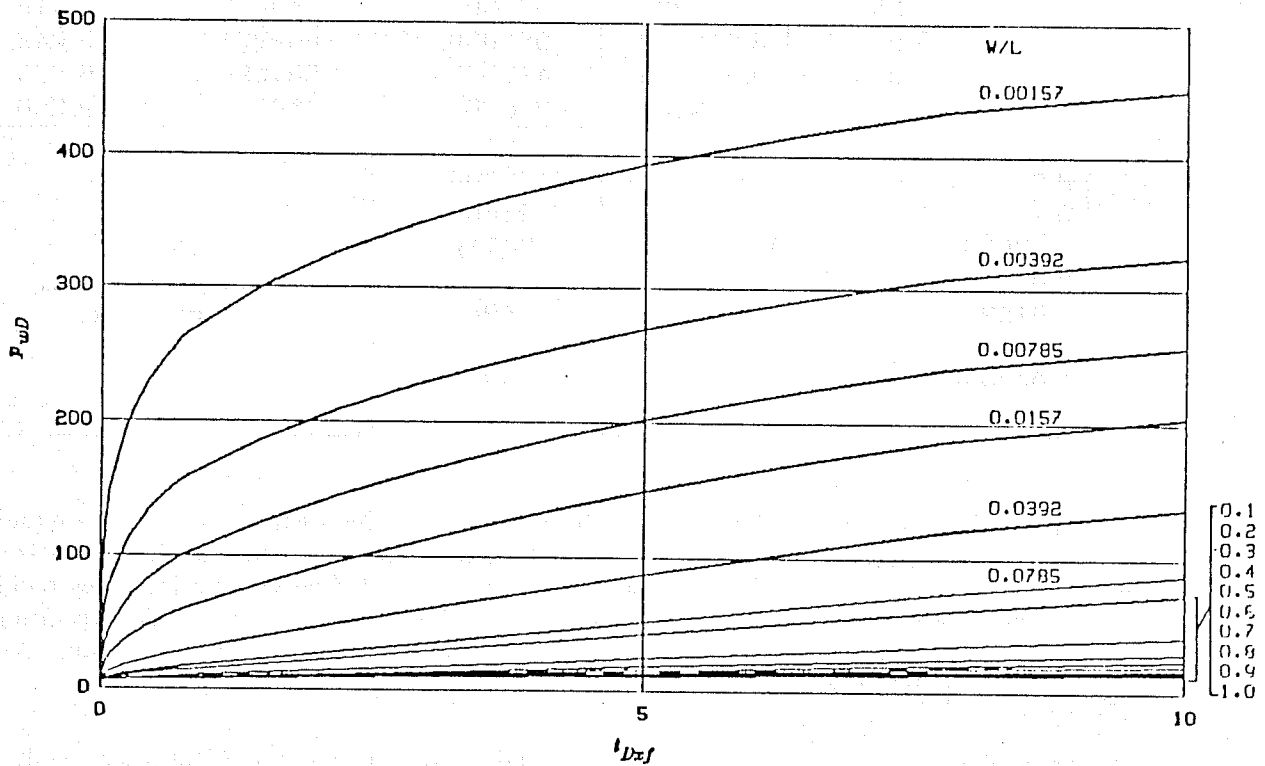


Fig. 5.6 Cartesian Plot of Dimensionless Pressure Responses for Different W/L Ratio

From Fig. 5.6 for W/L ratios below 0.1, there is no pseudosteady-state Cartesian straight line. However, due to the coarseness of the scale, the curvature for the lines of W/L ratio above 0.1 might have been masked. A detailed Cartesian analysis was performed for each case to calculate the burned-zone volume. The result is summarized in Table 5.3.

From the Cartesian analysis, the results indicate that for W/L ratio below 0.4, the curvature of the pressure response becomes significant and many apparent straight lines can be drawn through segments of the data. For cases with W/L ratio at 0.1 or below, no Cartesian straight line exists.

Table 5.3 Summary of Results for Cartesian Analysis for Burned Zone

W/L	Approximate Start of Cartesian Straight Line		True Burned-Zone Volume ft^3	Calculated Burned-Zone Volume ft^3	% Error
	(days)	t_{Dxf}			
1.0	0.0111	0.779488	945000.0	944669.7	0.035
0.9	0.0145	1.0182503	850500.0	931201.9	9.488
0.8	0.017	1.193810	756000.0	837412.3	10.768
0.7	0.024	1.685379	661500.0	743635.0	12.416
0.6	0.043	3.019639	567000.0	652291.2	15.042
0.5	0.05	3.511208	472500.0	551094.2	16.630
0.4	0.059	4.143225	378000.0	450768.6	19.250
0.3	No Cartesian Straight Line		283500.0	No Cartesian Straight Line	
0.2			189000.0		
0.1			94500.0		
0.078539			74219.3		
0.039269			37100.7		
0.015707			14843.1		
0.007853			7421.0		
0.003926			3710.0		
0.001570	1484.3				

The results also confirm Kazemi's conclusion that when the distance to the discontinuity is not equal in all directions, significant error will result in the calculation of the burned-zone volume. Table 5.3 shows that the % error in calculated burned-zone volume increases rapidly when the W/L ratio is decreased even slightly. As the burned-zone geometry departs from a perfect square, the correct straight line that will yield a correct burned-zone volume may be a tangent at some point of the pressure response.

An analysis was performed to find the locations of tangent points for cases with no Cartesian straight line. The result is summarized in Table 5.4. The results presented in Table 5.4 have error of less than 2% in calculated burned-zone volumes.

Table 5.4 presents some interesting results. For cases with W/L ratio larger than 0.1, the tangent point which yields a correct calculated burned-zone volume stays approximately where the pseudosteady-state straight line starts for the case with the square burned zone. However, for cases with W/L ratio at or below 0.1, the tangent point moves backward and locates at a much earlier time.

Figure 5.7 is a graph of the location of these tangent points versus the corresponding W/L ratio. From Fig. 5.7, as W/L ratio decreases, the tangent point moves to earlier times. However, for W/L ratio above 0.1, the tangent point remains approximately at 0.01 days ($t_{Dxf} = 0.702$) which is where the pseudosteady-state straight line starts for the case with the square burned zone.

Table 5.4 Locations of Tangent Points which Yield Correct Burned-Zone Volumes

W/L	Locations in Time of Tangent Point Which Yields Correct Burned-Zone Volume		
	(days)	t_{DEF}	t_{DA_1}
1.0	0.0111	0.779488	0.194872
0.9	0.0111	0.779488	0.216524
0.8	0.0111	0.779488	0.243590
0.7	0.0105	0.737353	0.263340
0.6	0.01	0.702241	0.292800
0.5	0.01	0.702241	0.351120
0.4	0.009	0.632017	0.395010
0.3	0.009	0.632017	0.526681
0.2	0.009	0.632017	0.790021
0.1	0.0075	0.526681	1.316703
0.078539	0.007	0.491569	1.564729
0.039269	0.0055	0.386232	2.459455
0.015707	0.0035	0.245784	3.912022
0.007853	0.0015	0.105336	3.353375
0.003926	0.0011	0.077246	4.918911
0.001570	0.0006	0.042134	6.706324

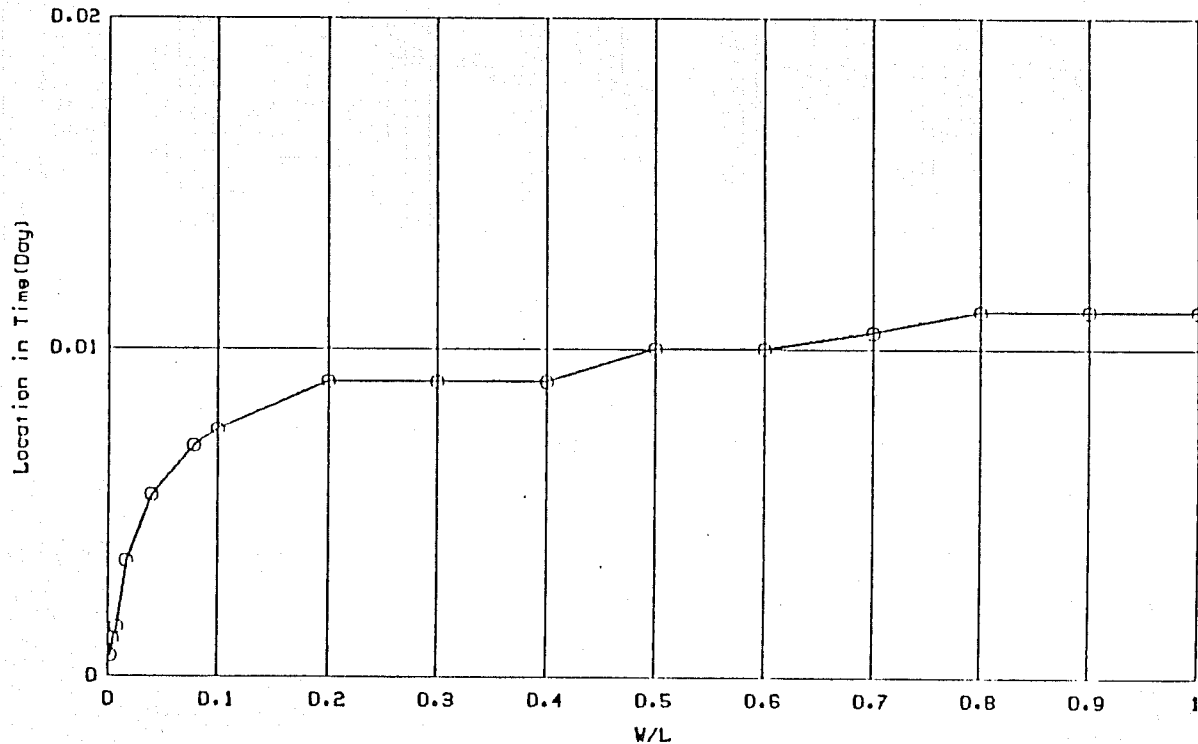


Fig. 5.7 Locations of Tangent Points that Yield Correct Calculated Burned-Zone Volume as a Function of W/L Ratio

From the Cartesian analysis, we conclude that as the burned-zone width is decreased, the error involved in calculated burned-zone volume increases. For W/L ratio below 0.4, the curvature of the Cartesian plot become significant, and many straight lines can be drawn through segments of the data. For W/L ratios at or below 0.1, there is clearly no pseudosteady-state flow period for the burned zone.

Since the semilog graph of the dimensionless pressure response has different shapes for different W/L ratios, we suspect a log-log plot of the dimensionless pressure response could be used for a type-curve matching purpose. Figure 5.8 is a log-log plot of the dimensionless pressure response.

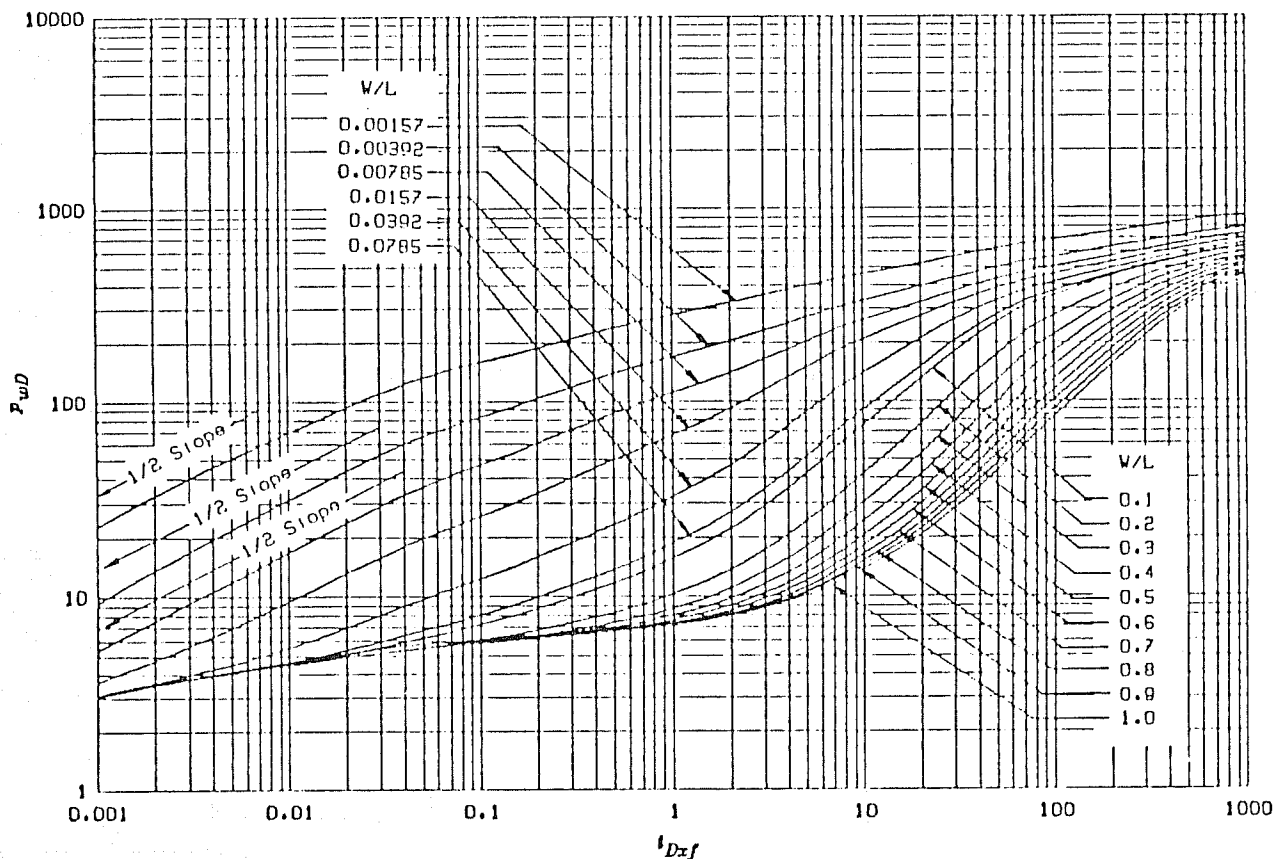


Fig. 5.8 Log-Log Plot of Dimensionless Pressure Responses for Different W/L Ratio

From Fig. 5.8, the curves do have different shapes for different W/L ratio. Therefore, a type-curve matching technique may be used to find burned-zone properties. However, in practical terms, Fig. 5.8 might not have value in realistic field data analysis. Most of the curves have similar shapes over a range of dimensionless times. A uniqueness problem may arise in the process of type curve matching. Therefore, type curve matching techniques will be practical only if a long range of data are available. Recently, pressure-time derivative type curves have been shown to have great details for some cases. Perhaps an analysis of this possibility will be useful.

The log-log plot does illustrate some general trends. For W/L ratio below 0.0157, the curves show half slopes at early times. This indicates a formation linear flow, and is a behavior of wells with a vertical fracture. At late times, all curves approach each other. This is expected, because the system should achieve pseudoradial-flow after a long time, regardless of the burned-zone geometry.

It is of interest to find out how the simulation result would compare with the Cinco *et al.* type curves for the case with the lowest W/L ratio, which is the case that has the smallest width and is most similar to a fracture. We would not expect the result to agree with the type curve at early times because the two models are fundamentally different. Cinco *et al.* assumed a fracture model which has a length much larger than the width and no flow at the tip. The model simulated here has a significant width, and flow is allowed at the burned-zone tip. Also, the burned zones simulated in this study have significant volume, and will generate a storage effect. The combination of these three factors will produce a pressure response lower than that reported by Cinco *et al.* at early times. However, we would expect the pressure response to match Cinco *et al.*'s type curve after the pressure influence has passed the burned zone. The burned zone or fracture dimension and storage effect play no role in the pressure response after the pressure influence has passed the fracture and propagated into the reservoir.

Figure 5.9 is a log-log graph of the dimensionless pressure solution and Cinco *et al.*'s type curve. The curve is for a W/L ratio of 0.001570. This curve corresponds to a dimensionless fracture conductivity of $\pi/5$.

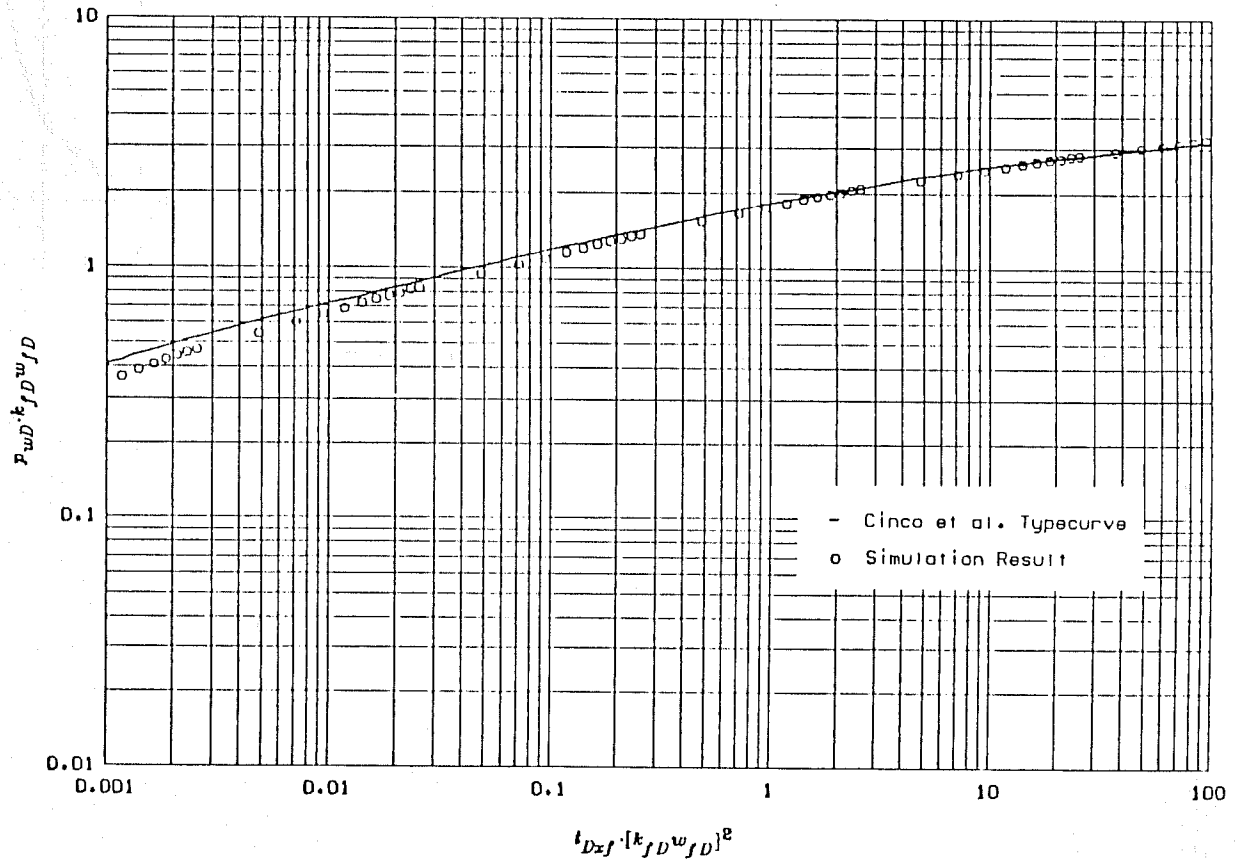


Fig. 5.9 Comparison with Cinco's Type Curve for W/L Ratio of 0.001570

From Fig. 5.9, the simulation results do show a lower pressure drop response than Cinco *et al.*'s type curve at early times. However, the simulation result shows a favorable match with the Cinco *et al.*'s type-curve at later times. The dimensionless time that the curves begin to show good match is $t_{Dxf} = 3$. This time agrees reasonably well with the time of 2.7 reported by Cinco *et al.* for start of the semilog straight line for the reservoir.

As mentioned before, the fluid in the reservoir is handled as a constant compressibility liquid, instead of gas. To show that this is reasonable we simulated the case with the square burned zone utilizing a gas flow simulator. Figure 5.10 is a semilog graph of the pressure response of both runs. The figure shows an excellent match between the results obtained from the gas simulator and the liquid simulator. The results show a better match at early times than at late times. This is expected, since the pressure gradient is higher at later times, and the assumption of constant compressibility is poor. However, for the purpose of this study, the assumption of constant compressibility is acceptable.

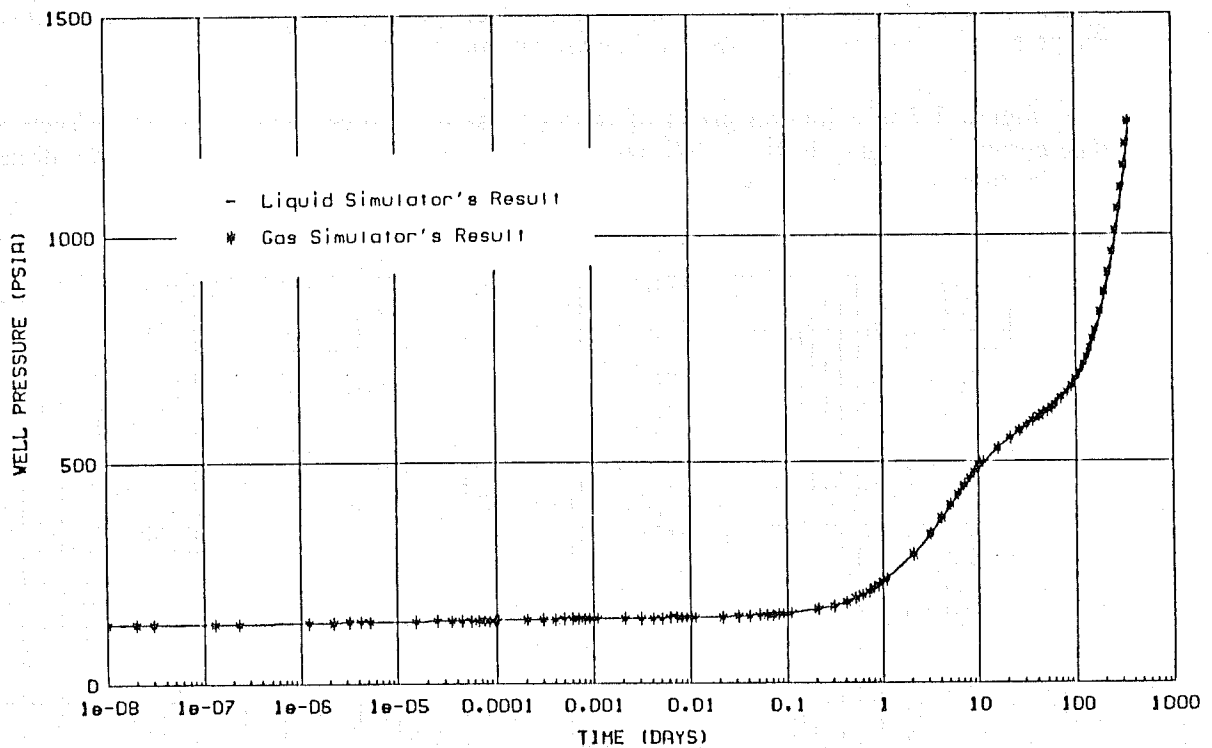


Fig. 5.10 Comparison of Simulation Results From Liquid and Gas Simulators

6. CONCLUSIONS AND RECOMMENDATIONS

The following conclusions and recommendations can be drawn from this study :

6.1. CONCLUSIONS:

1. It can be concluded that pseudosteady-state flow does not exist for the inner zone for low W/L ratio cases. The curvature of the Cartesian plot of the pressure responses increases as W/L ratio decreases. For cases with W/L ratio below 0.4, the curvature becomes significant, and many straight lines can be drawn through segments of the data. For cases with W/L ratio below 0.1, there is clearly no pseudosteady-state flow, and the Cartesian plot of pressure versus time is a curve.
2. Burned zone volume calculation is sensitive to the slope of the pseudosteady-state Cartesian straight line but less sensitive to the average pressure when the Cartesian straight line exists.
3. The calculated burned-zone volume will have significant error if the distance from the well to the burning front is not similar in all directions. The volume calculated will usually be too large when an uneven burning front distance exists. However, trial and error corrections may be possible if W/L can be established.
4. There is a semilog straight line characterizing the burned zone for cases with a W/L ratio higher than 0.2. However, for cases with W/L ratio below 0.4, the semilog straight line becomes short, and results in significant error in the calculated permeability for the burned zone.
5. It is of advantage to have a semilog straight line for the burned zone to locate the Cartesian straight line, if one exists. However, the existence of a semilog straight line does not guarantee a pseudosteady-state Cartesian straight line that will yield a correct burned-zone volume.
6. Using the type-curve matching technique to find burned-zone properties is possible. However, it is practical only when data that spans a long time is available. Otherwise, a uniqueness problem might arise.
7. For a rectangular burned zone to behave like a fracture at early times, the dimensions of the burned zone must be similar to those of a fracture, or the rectangular burned zone will not behave as a fracture.

6.2. RECOMMENDATIONS:

1. It is of interest to determine if pressure-time differential type-curve matching has more practical value in finding burned-zone properties.
2. Finite-difference modeling might not have enough accuracy to permit analysis of early time data. A theoretical approach may yield more quantitative results.

NOMENCLATURE

A	= cross-sectional area (ft ²)
A^n	= accumulation matrix at time level n
B	= fluid formation volume factor (RV/STV)
B_{g_c}	= gas formation volume factor at p_{avg_c} (RV/STV)
B_{g_s}	= gas formation volume factor at p_{avg_s} (RV/STV)
B_{STC}	= fluid formation volume factor at standard conditions (RV/STV)
c_g	= well geometric factor
c_f	= fluid compressibility (psi ⁻¹)
c_R	= rock compressibility (psi ⁻¹)
c_t	= total compressibility (psi ⁻¹)
c_{t_1}	= total compressibility in burned zone (psi ⁻¹)
$c_{t_{avg_c}}$	= total compressibility at p_{avg_c} (psi ⁻¹)
C_D	= dimensionless storage coefficient
C_{D_f}	= dimensionless fracture storage coefficient
f	= fraction of well associated with the well block
h	= thickness of reservoir (ft)
k	= formation permeability (md)
k_1	= permeability of burned zone (md)
k_2	= permeability of unburned region (md)
k_f	= permeability of fracture (md)
k_{fD}	= relative fracture permeability
$k_{fD}W_{fD}$	= dimensionless fracture conductivity
m	= slope of semilog or Cartesian straight line (psi/day)
M	= molecular weight of gas
p_{wD}	= dimensionless well pressure
p_{avg_c}	= pressure at which the apparent Cartesian straight line starts
p_{avg_s}	= arithmetic averaged pressure where the semilog straight line exists
p_i	= initial reservoir pressure (psia)
p_o	= calculated well block pressure (psia)
p_{STC}	= standard pressure (psia)
p_w	= bottom hole pressure (psia)
p_{wf}	= flowing bottom hole pressure (psia)
q	= flow rate (STB/D or MSCF/D)
\bar{q}	= production (mass per unit volume per unit time)
r_o	= equivalent well block radius (ft)
r_w	= wellbore radius (ft)
R	= radius to discontinuity (ft)
R_D	= dimensionless radius of discontinuity

R_D^*	= apparent dimensionless radius of discontinuity calculated from the Cartesian straight line
t	= time (hrs)
T	= temperature °R
t_{DA1}	= dimensionless time based on burned-zone area
t_{Df}	= dimensionless time based on fracture half-length
Δt_{Df1}	= dimensionless time of deviation
Δt_{Df_s}	= dimensionless intersection time
Δt_{f1}	= intersection point of first and second semilog straight line
V_1	= bulk volume of burned zone (ft ³)
ΔV	= control volume (length ³)
w	= fracture width (ft)
W/L	= width to length ratio of burned zone
W_{fd}	= dimensionless fracture width
x_f	= fracture half length (ft)
Δx	= block length in the x direction (ft)
Z	= Standing-Katz gas compressibility factor

Greek symbols:

μ	= fluid viscosity (cp)
μ_1	= fluid viscosity in the burned zone (cp)
μ_2	= fluid viscosity in the unburned region (cp)
ϕ	= formation porosity (fraction)
ϕ_1	= porosity in burned zone (fraction)
ϕ_2	= porosity in unburned region (fraction)
ρ	= fluid density (lbm/ft ³)
ρ_{STC}	= density of fluid at standard conditions (lbm/ft ³)
γ_g	= specific gravity of gas
η	= diffusivity ratio
λ	= mobility ratio

Subscripts:

i	= block number
-----	----------------

Superscripts:

n	= time level
-----	--------------

REFERENCES

1. Abou-Kassem, J.H. and Aziz, K.: "Analytical Well Models for Reservoir Simulation," SPE 11719, presented at the 1983 California Regional Meeting of SPE of AIME, Ventura, March 23-25, 1983.
2. Agarwal, R.G., Carter, R.D., and Pollock, C.B.: "Evaluation and Performance Prediction of Low-Permeability Gas Wells Stimulated by Massive Hydraulic Fracturing," *J. of Pet. Tech.*, (March 1979) 362.
3. Arihara, N., Barker, B., Ramey, H.J. Jr., Mao, M.L., and Marques, J.K.: "Pressure Transient Testing of Hydraulically Fractured Wells," paper presented at American Society Topical Meeting, Golden (April 12-14, 1977).
4. Aziz, K., and Settari, A.: Petroleum Reservoir Simulation, Applied Science Publishers LTD, London (1979).
5. Bixel, H.C., van Poolen, H.K.: "Pressure Drawdown and Buildup in the Presence of Radial Discontinuities," *Soc. Pet. Eng. J.* (September 1967) 301.
6. Carter, R.D.: "Pressure Behavior of a Limited Circular Composite Reservoir," *Soc. Pet. Eng. J.* (December 1966) 328.
7. Cinco-Ley, H., and Samaniego, F.V.: "Effect of Wellbore Storage and Damage on the Transient Pressure Behavior of Vertically Fractured Wells," SPE 6752, presented at the 52nd Annual Fall Technical Conference of SPE of AIME, Denver, Oct. 9-12, 1977.
8. Cinco-Ley, H., and Samaniego, F.V.: "Transient Pressure Analysis for Fractured Wells," SPE 7490, presented at the 53rd Annual Fall Technical Conference of SPE of AIME, Houston, Oct. 1-3, 1978; also *J. of Pet. Tech.* (Sept. 1981), 1749.
9. Cinco-Ley, H., Samaniego, F.V., and Dominguez, N.A.: "Transient Pressure Behavior for a Well with a Finite Conductivity Vertical Fracture," *Soc. Pet. Eng. J.* (Aug. 1978), 253.
10. Chu, C.: "Two Dimensional Analysis of a Radial Heat Wave," *J. Pet. Tech.* (Oct. 1963) 1137.
11. Earlougher, R.C., Jr., Ramey, H.J. Jr., Miller, F.G., and Mueller, T.D.: "Pressure Distributions in Rectangular Reservoirs," *J. Pet. Tech.* (Feb. 1968) 199-208; *Trans. AIME* 243.
12. Eggenschwiler, M., Satman, A., and Ramey, H.J., Jr.: "Interpretation of Injection Well Pressure Transient Data in Thermal Oil Recovery," SPE 8908, presented at the 50th Annual California Regional Meeting of SPE of AIME, Los Angeles, April 9-11, 1980.
13. Kazemi, H.: "Locating a Burning Front by Pressure Transient Measurements," *J. Pet. Tech.* (Feb. 1966) 227.
14. Kazemi, H., Merrill, L.S., and Jargon, J.R.: "Problems in Interpretation of Pressure Fall-Off Tests in Reservoirs with and without Fluid Banks," *J. Pet. Tech.* (Sept. 1972) 1147.

15. Merrill, L.S., Jr., Kazemi, H., and Gogarty, W.B.: "Pressure Falloff Analysis in Reservoirs with Fluid Banks," *J. Pet. Tech.* (July 1974) 809.
16. Odeh, A.S.: "Flow Test Analysis for a Well with Radial Discontinuity," *J. Pet. Tech.* (Feb. 1969) 207.
17. Peaceman, D.W.: "Interpretation of Well-Block Pressure in Numerical Reservoir Simulation," *Soc. Pet. Eng. J.* (June 1978) 183.
18. Satman, A., Eggenschwiler, M., Tang, W-K., and Ramey, H.J., Jr.: "An Analytical Study of Transient Flow in System with Radial Discontinuities," SPE 9399, presented at the 55th Annual Fall Technical Conference of SPE of AIME, Dallas, Sept. 21-24, 1980.
19. Theory and Practice of the Testing of Gas Wells, Third Edition, Pub. ECRB-75-34, Energy Resources and Conservation Board, Calgary, Alta., (1975).
20. Van Poolen, H.K.: "Radius of Drainage and Stabilization-Time Equation," *Oil and Gas Jour.* (Sept. 14, 1964) 138.
21. Van Poolen, H.K.: "Transient Tests Find Fire Front in an *In-Situ* Combustion Project," *Oil and Gas Jour.*, (Feb. 1, 1965) 78.
22. Walsh, J.W., Jr., Ramey, H.J., Jr., and Brigham, W.E.: "Thermal Injection Well Falloff Testing," SPE 10227, presented at the 56th Annual Fall Technical Conference of SPE of AIME, San Antonio, Oct. 5-7, 1981.

APPENDIX A

TWO-DIMENSIONAL, AREAL-IMPLICIT SINGLE-PHASE, SINGLE-COMPONENT NUMERICAL SIMULATOR FOR SLIGHTLY COMPRESSIBLE FLUIDS WITH CONSTANT COMPRESSIBILITY

This appendix contains a description of the captioned simulator and the associated user instructions. Since the theory behind the simulator is standard and well established, only a brief description is included here. Detailed theoretical development can be found in references by Abou-Kassem and Aziz (1983), Aziz and Settari (1979), and Peaceman (1978).

A.1. DERIVATION OF GOVERNING EQUATIONS

The governing equations for fluid flow in porous media are derived from a material balance for a control volume based on the fundamental laws of conservation of mass, momentum and some empirical relations concerning transport laws and PVT behavior of the fluids.

A control volume is constructed based on the continuum approach. The actual porous medium is replaced by a fictitious continuum at any point of which variables and parameters may be assigned. Continuous functions of the space and time coordinates can be assigned as variables and parameters.

In this section, the governing equation for one-dimensional flow in Cartesian coordinates of a single fluid, modeled as a slightly compressible fluid is derived. The derivation is then expanded to two-dimensional flow.

For one-dimensional flow in Cartesian coordinates, the control volume is constructed as illustrated in Fig. A.1.

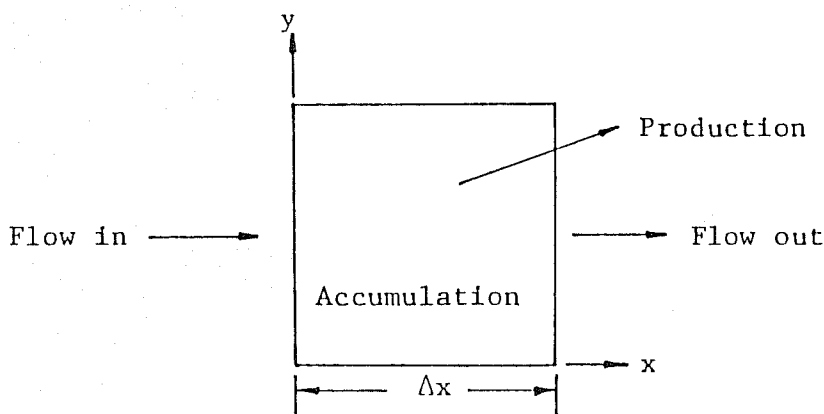


Fig. A.1 Control Volume

In the control volume, a material balance will result in the following equation:

$$\text{Flow in} - \text{Flow out} = \text{Accumulation} + \text{Production} \quad (\text{A.1})$$

Several terms are defined as follows:

- A = cross-sectional area
- Δx = control volume thickness in the x direction
- $+ \bar{q}$ = production (mass per unit volume per unit time)
- $\dot{m}_x|_x$ = mass flux vector (mass flow per unit area per unit time in the x direction at x)
- Δt = time elapsed
- ρ = density of fluid
- ϕ = porosity of medium
- $\Delta V = \Delta x A$

Then :

$$\text{Flow In} = \dot{m}_x|_x A \Delta t$$

$$\text{Flow Out} = \dot{m}_x|_{x+\Delta x} A \Delta t$$

$$\text{Accumulation} = \frac{\partial}{\partial t} (\rho \phi \Delta V) \Delta t$$

$$\text{Production} = \bar{q} \Delta V \Delta t$$

Substitute in Eq. (A.1):

$$\dot{m}_x|_x (A \Delta t) - \dot{m}_x|_{x+\Delta x} (A \Delta t) = \frac{\partial}{\partial t} (\rho \phi \Delta V) \Delta t + \bar{q} \Delta V \Delta t$$

Divided by $\Delta V \Delta t$:

$$(\dot{m}_x|_x - \dot{m}_x|_{x+\Delta x}) \frac{A}{\Delta V} = \frac{\partial}{\partial t} (\rho \phi) + \bar{q}$$

Substitute $\Delta V = \Delta x A$:

$$\frac{\dot{m}_x|_x - \dot{m}_x|_{x+\Delta x}}{\Delta x} = \frac{\partial}{\partial t} (\rho \phi) + \bar{q}$$

Take limit as $\Delta x \rightarrow 0$:

$$\frac{-\partial \dot{m}_x}{\partial x} = \frac{\partial}{\partial t} (\rho \phi) + \bar{q}$$

Substitute $\dot{m}_x = \rho u_x$ (u_x is the fluid velocity in x direction) results in the following equation:

$$\frac{-\partial(\rho u_x)}{\partial x} = \frac{\partial(\rho\phi)}{\partial t} + \bar{q} \quad (\text{A.2})$$

This equation is for flow in one spacial variable, namely, in the x direction. In general, Eq. (A.2) can be written for any spacial coordinate system by using the Laplace operator. In general Eq. (A.2) can be written as :

$$-\nabla \cdot (\rho u) = \frac{\partial(\rho\phi)}{\partial t} + \bar{q} \quad (\text{A.3})$$

Darcy's law for one-dimension in x is:

$$u_x = -\frac{k}{\mu} \left[\frac{\partial p}{\partial x} + \rho \frac{g}{g_c} \frac{\partial z}{\partial x} \right]$$

In general, Darcy's law can be written as:

$$u = -\frac{k}{\mu} (\nabla p - \gamma \nabla z)$$

where :

$$\gamma = -\rho \frac{g}{g_c}$$

Substitute Darcy's law in Eq. (A.3):

$$\nabla \cdot \left[\frac{\rho k}{\mu} (\nabla p - \gamma \nabla z) \right] = \frac{\partial(\rho\phi)}{\partial t} + \bar{q} \quad (\text{A.4})$$

Recall that the formation volume factor is defined as :

$$B = \frac{V_{RC}}{V_{STC}} = \frac{\rho_{STC}}{\rho_{RC}} \quad (\text{A.5})$$

where:

- V_{RC} = volume of fluid at reservoir conditions
- V_{STC} = volume of fluid at stock tank conditions
- ρ_{RC} = density of fluid at reservoir conditions
- ρ_{STC} = density of fluid at stock tank conditions

Divide Eq. (A.4) by ρ_{STC} , and substitute Eq. (A.5) into (A.4):

$$\nabla \cdot \left[\frac{k}{\mu B} (\nabla p - \gamma \nabla z) \right] = \frac{\partial}{\partial t} \left[\frac{\phi}{B} \right] + q \quad (\text{A.6})$$

where:

$$q = \frac{\bar{q}}{\rho_{STC}}$$

Define $\lambda = k/\mu B$ and substitute into Eq. (A.6):

$$\nabla \cdot [\lambda(\nabla p - \gamma \nabla z)] = \frac{\partial}{\partial t} \left[\frac{\phi}{B} \right] + q \quad (\text{A.7})$$

Recall that isothermal fluid compressibility is defined as:

$$c_f = - \frac{1}{V} \frac{\partial V}{\partial P} \Big|_T = \frac{1}{\rho} \frac{\partial \rho}{\partial p} \Big|_T$$

If constant compressibility is assumed, the preceding equation becomes an ordinary differential equation:

$$c_f dP = \frac{d\rho}{\rho}$$

Integrating from p to p_{STC} and ρ to ρ_{STC} :

$$c_f(p - p_{STC}) = \ln \frac{\rho}{\rho_{STC}} \quad (\text{A.8a})$$

$$e^{c_f(p - p_{STC})} = \frac{\rho}{\rho_{STC}} \quad (\text{A.8b})$$

From Eq. (A.5) and (A.8), the relationship between formation volume factor and pressure can be written as :

$$\frac{B_{STC}}{B} = \frac{\rho}{\rho_{STC}} = e^{c_f(p - p_{STC})} \quad (\text{A.9})$$

The right-hand side of Eq. (A.9) can be expanded with an infinite series, resulting in the following equation:

$$e^{c_f(p - p_{STC})} = 1 + c_f(p - p_{STC}) + \frac{1}{2} c_f^2(p - p_{STC})^2 + \dots \quad (\text{A.10})$$

Since the fluid being modeled has a constant and small compressibility, the third and following terms on the right hand side of Eq. (A.10) are much smaller than unity. Therefore, Eq. (A.10) can be written in an approximate form by retaining only the first two terms of the expansion. The resulting equation is:

$$\frac{B_{STC}}{B} = \frac{\rho}{\rho_{STC}} = 1 + c_f(p - p_{STC}) \quad (A.11)$$

Similarly, the change in pore volume with respect to pressure in a medium with constant and small matrix compressibility can be represented by :

$$\frac{\phi}{\phi_{STC}} = 1 + c_R(p - p_{STC}) \quad (A.12)$$

The time derivative in Eq. (A.7) can be written as :

$$\frac{\partial \left[\frac{\phi}{B} \right]}{\partial t} = \frac{\partial \left[\frac{\phi}{B} \right]}{\partial p} \frac{\partial p}{\partial t} \quad (A.13)$$

Substituting Eqs. (A.11) and (A.12) into Eq. (A.7), and expanding the time derivative as shown in Eq. (A.13) results in the following equation:

$$\nabla \cdot [\lambda(\nabla p - \gamma \nabla z)] = \left[\phi \frac{c_f}{B_{STC}} + \phi_{STC} \frac{c_R}{B} \right] \frac{\partial p}{\partial t} + q \quad (A.14)$$

Equation (A.14) is the equation for flow of a single-phase, single-component fluid with a constant and slight compressibility.

If the system being modeled is at a low pressure, the matrix can be considered to have zero compressibility. Therefore, the term that involves matrix compressibility can be neglected, and resulted in the following equation:

$$\nabla \cdot [\lambda(\nabla p - \gamma \nabla z)] = \phi \frac{c_f}{B_{STC}} \frac{\partial p}{\partial t} + q \quad (A.15)$$

Since flow in the areal sense is considered in this development, the gravity term can be neglected. This results in the final equation for simulating horizontal flow of a fluid with slight and constant compressibility.

$$\nabla \cdot (\lambda \nabla p) = \phi \frac{c_f}{B_{STC}} \frac{\partial p}{\partial t} + q \quad (A.16)$$

A.2. COORDINATE SYSTEM

Since this study involves simulation of fluid flow in a square, closed-boundary system, the Cartesian coordinate system was chosen. In a two-dimensional Cartesian coordinate system, the Laplace operator in Eq. (A.16) can be expanded in the following manner:

$$\frac{\partial}{\partial x} (\lambda \nabla p) + \frac{\partial}{\partial y} (\lambda \nabla p) = \phi \frac{c_f}{B_{SIC}} \frac{\partial p}{\partial t} + q$$

$$\frac{\partial}{\partial x} \left[\frac{k}{\mu B} \frac{\partial p}{\partial x} \right] + \frac{\partial}{\partial y} \left[\frac{k}{\mu B} \frac{\partial p}{\partial y} \right] = \phi \frac{c_f}{B_{SIC}} \frac{\partial p}{\partial t} + q \quad (\text{A.17})$$

When K ; μ and B in Eq. (A.17) are functions of pressure, the equation has no closed form solution to this date, and can be solved only by one of the many available numerical methods.

A.3. FINITE-DIFFERENCE SCHEME

The classical implicit method of Central Difference in space, and Backward Difference in time was chosen for this development.

A.3.a. Discretization in Space

Central Difference is used for spacial discretization. The Central-Difference approximation for first derivatives is obtained in the following manner:

$$\frac{du_i}{dx} = \frac{u_{i+1} - u_{i-1}}{x_{i+1} - x_{i-1}} \quad (\text{A.18})$$

The nomenclature for the discretization process can be found in the next section.

A.3.b. Discretization in Time

Backward Difference is used for time discretization. This is the classical implicit method and the approximation for first derivatives is obtained as follows :

$$\left[\frac{du_i}{dt} \right]^{n+1} = \frac{u_i^{n+1} - u_i^n}{\Delta t} \quad (\text{A.19})$$

The left-hand side of Eq. (A.16) may be written at the time level $n + 1$:

$$\nabla \cdot (\lambda \nabla p)_i^{n+1} = \phi \frac{c_f}{B_{src}} \left[\frac{p_i^{n+1} - p_i^n}{\Delta t} \right] + q_i \quad (\text{A.20})$$

$$i = 1, 2, 3, \dots, N$$

$$n = 0, 1, 2, \dots$$

All p_i^{n+1} are unknowns, therefore, Eq. (A.20) will result in N algebraic equations for a given time level n and must be solved simultaneously.

A.4. GRID SYSTEM AND NOMENCLATURE FOR DISCRETIZATION

The popular "Block Centered" grid system is used for this study. This grid system is constructed by dividing the length L_x into M blocks and then locating grid points in the centers of these blocks. This process is illustrated in Fig. (A.2).

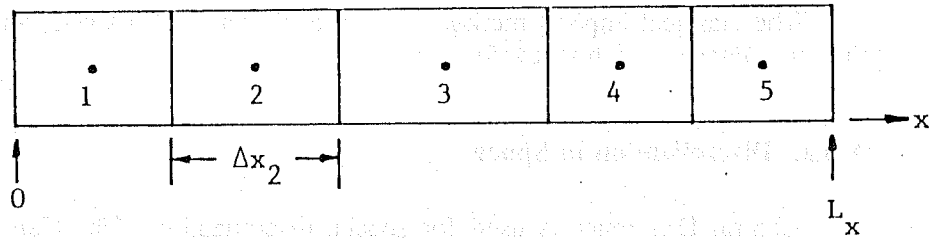


Fig. A.2 Block Centered Grid(1-D)

In two dimensions, the length L_x and L_y are divided into M and N blocks and then grid points are located in the centers of these blocks. This process is illustrated in Fig. A.3.

In Fig. A.3, $M = 4$ and $N = 5$, notice the block size is not necessarily a constant. The consequence of this irregular grid, and the treatment of variable coefficients will be discussed in later sections.

The nomenclature used for discretization will be described by showing an arbitrary point (i, j) and the four neighboring points as shown in Fig. A.4.

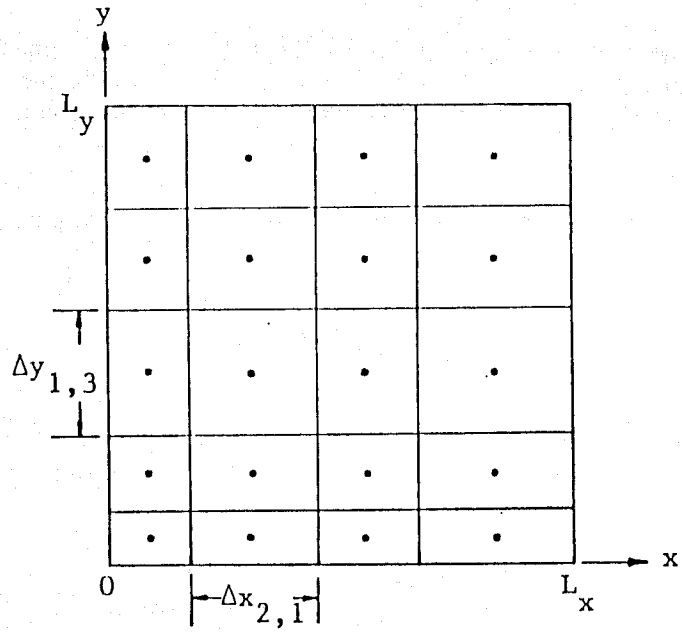


Fig. A.3 Block Centered Grid(2-D)

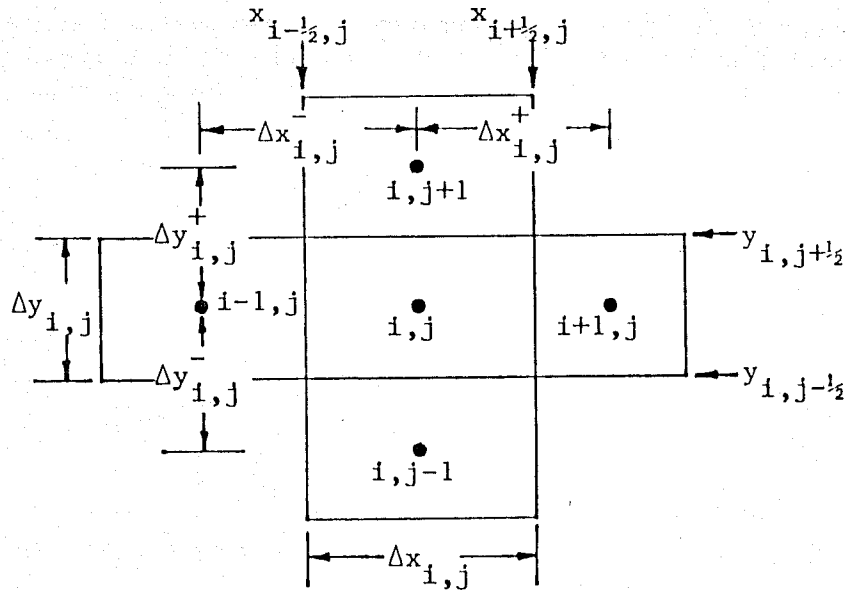


Fig. A.4 Nomenclature for Grid Construction

A.5. TREATMENT OF VARIABLE COEFFICIENTS

The transmissivity λ in Eq. (A.20) is located at block boundaries, $i + 1/2$ and $i - 1/2$ locations after discretization. This will be shown clearly in the next section. However, the transmissivities are known only at grid points but not at block boundaries. Therefore, some manipulation must be done to obtain the values $\lambda_{i+1/2}$ and $\lambda_{i-1/2}$.

In this development, the transmissivity is considered in two parts, as shown in the following equation:

$$\lambda = \frac{k}{\mu B} = k \left[\frac{1}{\mu B} \right] \quad (\text{A.21})$$

Therefore, after discretization, Eq. (A.21) will have the form:

$$\lambda_{i+1/2} = k_{i+1/2} \left[\frac{1}{\mu B} \right]_{i+1/2} \quad (\text{A.22.a})$$

$$\lambda_{i-1/2} = k_{i-1/2} \left[\frac{1}{\mu B} \right]_{i-1/2} \quad (\text{A.22.b})$$

In this study, the pressure gradients are small and the pressures are expected to be in a low range. The fluid viscosity and fluid formation volume factors are functions of pressure. Therefore, if pressure gradients are small, the nonlinearities of μ and B are weak, and a simple arithmetic average may be used to find the values of μ and B at block boundaries. Therefore, the term $1/\mu B$ in Eq. (A.22) may be calculated in the following manner:

$$\left[\frac{1}{\mu B} \right]_{i+1/2} = \frac{\left[\frac{1}{\mu B} \right]_{i+1} + \left[\frac{1}{\mu B} \right]_i}{2} \quad (\text{A.23.a})$$

$$\left[\frac{1}{\mu B} \right]_{i-1/2} = \frac{\left[\frac{1}{\mu B} \right]_i + \left[\frac{1}{\mu B} \right]_{i-1}}{2} \quad (\text{A.23.b})$$

In fact, in this study, the fluid viscosity will be kept constant. Therefore, Eq. (A.23) will yield an adequate approximation.

The permeability in Eq. (A.22) will be a step function with respect to spacial variables in this study, and therefore cannot be averaged by arithmetic means. Rather, the permeability at block boundaries are calculated by using harmonic mean shown as follows:

$$k_{i+1/2} = \frac{\frac{\Delta x_i + \Delta x_{i+1}}{2}}{\frac{\frac{\Delta x_i}{2}}{k_i} + \frac{\frac{\Delta x_{i+1}}{2}}{k_{i+1}}} \quad (\text{A.24.a})$$

$$k_{i-1/2} = \frac{\frac{\Delta x_i + \Delta x_{i-1}}{2}}{\frac{\frac{\Delta x_i}{2}}{k_i} + \frac{\frac{\Delta x_{i-1}}{2}}{k_{i-1}}} \quad (\text{A.24.b})$$

A.6. DISCRETIZATION

Recall that $q = \bar{q}/\rho_{STC}$ and Eq. (A.17):

$$\frac{\partial}{\partial x} \left[\frac{k}{\mu B} \frac{\partial p}{\partial x} \right] + \frac{\partial}{\partial y} \left[\frac{k}{\mu B} \frac{\partial p}{\partial y} \right] = \phi \frac{c_f}{B_{STC}} \frac{\partial p}{\partial t} + \frac{\bar{q}}{\rho_{STC}} \quad (\text{A.25})$$

Using the nomenclature demonstrated in Fig. A.3, and carrying out the discretization process:

$$\begin{aligned} & \frac{\left(\frac{k}{\mu B} \right)_{i+1/2,j}^{n+1} \left(\frac{p_{i+1,j} - p_{i,j}}{x_{i+1,j} - x_{i,j}} \right)^{n+1} - \left(\frac{k}{\mu B} \right)_{i-1/2,j}^{n+1} \left(\frac{p_{i,j} - p_{i-1,j}}{x_{i,j} - x_{i-1,j}} \right)^{n+1}}{x_{i+1/2,j} - x_{i-1/2,j}} \\ & + \frac{\left(\frac{k}{\mu B} \right)_{i,j+1/2}^{n+1} \left(\frac{p_{i,j+1} - p_{i,j}}{y_{i,j+1} - y_{i,j}} \right)^{n+1} - \left(\frac{k}{\mu B} \right)_{i,j-1/2}^{n+1} \left(\frac{p_{i,j} - p_{i,j-1}}{y_{i,j} - y_{i,j-1}} \right)^{n+1}}{y_{i,j+1/2} - y_{i,j-1/2}} \\ & = \frac{\phi_{i,j} c_{f_{i,j}}}{B_{STC,i,j} \Delta t} p_{i,j}^{n+1} - \frac{\phi_{i,j} c_{f_{i,j}}}{B_{STC,i,j} \Delta t} p_{i,j}^n + \frac{\bar{q}_{i,j}}{\rho_{STC}} \end{aligned} \quad (\text{A.26})$$

Break up the transmissivity as shown in Fig. A.23, and collect terms:

$$\begin{aligned}
 & \frac{k_{i-1/2,j}^{n+1} \left[\left[\frac{1}{\mu B} \right]_{i-1,j} + \left[\frac{1}{\mu B} \right]_{i,j} \right]^{n+1}}{2(x_{i,j} - x_{i-1,j})(x_{i+1/2,j} - x_{i-1/2,j})} p_{i-1,j}^{n+1} \\
 & - \left[\frac{k_{i-1/2,j}^{n+1} \left[\left[\frac{1}{\mu B} \right]_{i-1,j} + \left[\frac{1}{\mu B} \right]_{i,j} \right]^{n+1}}{2(x_{i,j} - x_{i-1,j})(x_{i+1/2,j} - x_{i-1/2,j})} + \frac{k_{i+1/2,j}^{n+1} \left[\left[\frac{1}{\mu B} \right]_{i+1,j} + \left[\frac{1}{\mu B} \right]_{i,j} \right]^{n+1}}{2(x_{i+1,j} - x_{i,j})(x_{i+1/2,j} - x_{i-1/2,j})} \right. \\
 & + \frac{k_{i,j-1/2}^{n+1} \left[\left[\frac{1}{\mu B} \right]_{i,j-1} + \left[\frac{1}{\mu B} \right]_{i,j} \right]^{n+1}}{2(y_{i,j+1/2} - y_{i,j-1/2})(y_{i,j} - y_{i,j-1})} + \frac{k_{i,j+1/2}^{n+1} \left[\left[\frac{1}{\mu B} \right]_{i,j+1} + \left[\frac{1}{\mu B} \right]_{i,j} \right]^{n+1}}{2(y_{i,j+1} - y_{i,j})(y_{i,j+1/2} - y_{i,j-1/2})} \\
 & \left. + \frac{\phi_{i,j} \mathcal{C}_{f_{i,j}}}{B_{STC_{i,j}} \Delta t} \right] p_{i,j}^{n+1} \\
 & + \frac{k_{i+1/2,j}^{n+1} \left[\left[\frac{1}{\mu B} \right]_{i+1,j} + \left[\frac{1}{\mu B} \right]_{i,j} \right]^{n+1}}{2(x_{i+1,j} - x_{i,j})(x_{i+1/2,j} - x_{i-1/2,j})} p_{i+1,j}^{n+1} + \frac{k_{i,j-1/2}^{n+1} \left[\left[\frac{1}{\mu B} \right]_{i,j-1} + \left[\frac{1}{\mu B} \right]_{i,j} \right]^{n+1}}{2(y_{i,j+1/2} - y_{i,j-1/2})(y_{i,j} - y_{i,j-1})} p_{i,j-1}^{n+1} \\
 & + \frac{k_{i,j+1/2}^{n+1} \left[\left[\frac{1}{\mu B} \right]_{i,j+1} + \left[\frac{1}{\mu B} \right]_{i,j} \right]^{n+1}}{2(y_{i,j+1} - y_{i,j})(y_{i,j+1/2} - y_{i,j-1/2})} p_{i,j+1}^{n+1} \\
 & = \frac{-\phi_{i,j} \mathcal{C}_{f_{i,j}}}{B_{STC_{i,j}} \Delta t} p_{i,j}^n + \frac{\bar{q}_{i,j}}{\rho_{STC}} \tag{A.27}
 \end{aligned}$$

Apply the conversion factor associated with permeability and the appropriate units for each term as shown in the following :

conversion factors associated with $k = 7.3243814 \times 10^{-5}$:

$$\begin{aligned}
 \Delta t &= \text{second} & p &= \text{psia} & q &= \text{lbm/sec.} \\
 \rho_{STC} &= \text{lbm/ft}^3 & \Delta x &= \text{ft} & \Delta y &= \text{ft} \\
 \mu &= \text{cp} & h &= \text{ft} & k &= \text{Darcy} \\
 B &= \text{RB/STB}
 \end{aligned}$$

The final discretized equation is shown as follows:

$$\begin{aligned}
 & \frac{k_{i-1/2,j_x}^{n+1} \left[\left[\frac{1}{\mu B} \right]_{i-1,j} + \left[\frac{1}{\mu B} \right]_{i,j} \right]^{n+1}}{\Delta x_{i,j} \Delta x_{i,j}^-} p_{i-1,j}^{n+1} \\
 & - \left[\frac{k_{i-1/2,j_x}^{n+1} \left[\left[\frac{1}{\mu B} \right]_{i-1,j} + \left[\frac{1}{\mu B} \right]_{i,j} \right]^{n+1}}{\Delta x_{i,j} \Delta x_{i,j}^-} + \frac{k_{i+1/2,j_x}^{n+1} \left[\left[\frac{1}{\mu B} \right]_{i+1,j} + \left[\frac{1}{\mu B} \right]_{i,j} \right]^{n+1}}{\Delta x_{i,j} \Delta x_{i,j}^+} \right. \\
 & + \frac{k_{i,j-1/2,y}^{n+1} \left[\left[\frac{1}{\mu B} \right]_{i,j-1} + \left[\frac{1}{\mu B} \right]_{i,j} \right]^{n+1}}{\Delta y_{i,j} \Delta y_{i,j}^-} + \frac{k_{i,j+1/2,y}^{n+1} \left[\left[\frac{1}{\mu B} \right]_{i,j+1} + \left[\frac{1}{\mu B} \right]_{i,j} \right]^{n+1}}{\Delta y_{i,j} \Delta y_{i,j}^+} \\
 & \left. + \frac{27306.06 \phi_{i,j} c_{f,i,j}}{B_{SFC,i,j} \Delta t} \right] p_{i,j}^{n+1} \\
 & + \frac{k_{i+1/2,j_x}^{n+1} \left[\left[\frac{1}{\mu B} \right]_{i+1,j} + \left[\frac{1}{\mu B} \right]_{i,j} \right]^{n+1}}{\Delta x_{i,j} \Delta x_{i,j}^+} p_{i+1,j}^{n+1} + \frac{k_{i,j-1/2,y}^{n+1} \left[\left[\frac{1}{\mu B} \right]_{i,j-1} + \left[\frac{1}{\mu B} \right]_{i,j} \right]^{n+1}}{\Delta y_{i,j} \Delta y_{i,j}^-} p_{i,j-1}^{n+1} \\
 & + \frac{k_{i,j+1/2,y}^{n+1} \left[\left[\frac{1}{\mu B} \right]_{i,j+1} + \left[\frac{1}{\mu B} \right]_{i,j} \right]^{n+1}}{\Delta y_{i,j} \Delta y_{i,j}^+} p_{i,j+1}^{n+1} \\
 & = \frac{-27306.06 \phi_{i,j} c_{f,i,j}}{B_{SFC,i,j} \Delta t} p_{i,j}^n + \frac{27306.06 q_{i,j}}{\rho_{SFC} h \Delta x_{i,j} \Delta y_{i,j}} \tag{A.28}
 \end{aligned}$$

A.7. BOUNDARY CONDITIONS

In this study, the boundaries of the reservoir are modeled as closed boundaries. Therefore, all boundaries which are normal to the x-direction will be described by the following:

$$\frac{k_x}{\mu} \left[\frac{\partial p}{\partial x} - \gamma \nabla z \right] = 0 \tag{A.29}$$

and for all boundaries which are normal to the y direction:

$$\frac{k_y}{\mu} \left[\frac{\partial p}{\partial y} - \gamma \nabla_z \right] = 0 \quad (\text{A.30})$$

In this study, Eq. (A.29), and (A.30) are satisfied by setting the transmissivities of the boundary blocks equal to zero. In the simulator, the transmissivities of the boundary blocks are set to zero by setting the $k_{i+1/2}$ and $k_{i-1/2}$ of the boundary blocks equal to zero. Therefore, the elements in the coefficient matrix for the boundary blocks will be zero.

A.8. INITIAL CONDITION

Since this is a simulation of single-phase, single-component fluid flow, any given initial pressure distribution can be simulated. The initial pressure distribution will be used as the first guess in the iteration scheme to obtain the pressure distribution at the end of the time step.

In this study, a constant initial pressure throughout the reservoir is used.

A.9. METHOD OF LINEARIZATION

Equation (A.28) can be written in the form:

$$T^{n+1} p^{n+1} = A^n \quad (\text{A.31})$$

where T^{n+1} is the coefficient matrix which consists of the transmissivities of the blocks. Equation (A.31) is nonlinear because the transmissivities are functions of the dependent variable p^{n+1} . Since this study involves single-phase flow, the nonlinearities are weak. Therefore, a simple successive iteration scheme was used to solve the set of nonlinear equations.

The simple iteration scheme can be expressed by the following equation:

$$T^{(v)} p^{(v+1)} = A^n \quad (\text{A.32})$$

where v is the counter for the iteration level. The original pressure distribution is used for the first guess for the first iteration. The iteration is continued until convergence is obtained. For this simple, single-phase flow problem, the iteration process converges quite rapidly.

A.10. SOLUTION OF MATRIX EQUATIONS

It can be seen from Eqs. (A.28) and (A.31) that the coefficient matrix T is a banded matrix with five nonzero diagonals. In this study, this system of algebraic equations is solved by a band-elimination routine based on a band solve algorithm developed by Graska and Poliak [See Aziz and Settari (1979)]. In this study, a grid of 21 by 21 blocks was used, and this direct-matrix solution scheme was more efficient than iterative methods, such as LSOR.

A.11. INTERPRETATION OF WELL-BLOCK PRESSURES

The pressure calculated for a block that contains a well is different from the flowing bottomhole pressure of the well. Usually some kind of well model is included in a simulator to calculate the flowing bottomhole pressure of a well from the block pressures.

In this study, a well model was not included in the simulator. The flowing bottomhole pressure was obtained by giving the well block dimensions which could simulate a given wellbore radius. The interpretation method proposed by Peaceman (1978) was used to obtain the well-block dimensions.

Through a series of numerical experiments, Peaceman reached the conclusion that for single phase flow, the well-block pressure is essentially equal to the actual flowing pressure at a radius of $0.2\Delta x$. If we use the equation for steady-state radial flow, it allows calculation of the flowing bottomhole pressure. In this study, the well-block dimensions are set so that the block pressure is equal to the flowing bottomhole pressure for a given well bore radius. Combining the equation proposed by Peaceman and the steady-state radial flow equation, the relationship between flowing bottomhole pressure and the well-block pressure can be expressed by the following equation:

$$p_{wf} = p_o + \frac{qB}{2\pi kh} \ln \frac{r_w}{0.2 \Delta x} \quad (A.33)$$

where p_{wf} is the flowing bottomhole pressure, and p_o is the well-block pressure. It can be seen from Eq. (A.33) that if Δx is set so that $0.2\Delta x = r_w$, then the bottomhole flowing pressure can be approximated by the unaltered well-block pressure.

The preceding method is valid only for a square well block that is an interior block, i.e., none of the well-block boundaries coincide with the reservoir boundaries. Furthermore, the well is located in the middle of the well block. However, due to symmetry, a lot of reservoir geometry can be simulated in symmetrical parts to obtain the responses of the reservoir as a whole by proper modification of the data. The most obvious example is the quarter of a five spot injection. In this study, the two-zone reservoir can be simulated by the same quarter of the system in order to obtain a detailed pressure map. In such a case, the well block is not an internal block, and the well is no longer located in the middle of the well block. The system simulated has the well block at one corner, and one quarter of the well located at a corner of the well block. The system simulated is illustrated in Fig. A.5.

In such a case, the approximation proposed by Peaceman no longer applies, and proper modification must be applied. Abou-Kassem and Aziz (1983) proposed the following equation for calculation of the equivalent well-block radius:

$$c_g = \frac{r_o}{\left[\frac{A}{\pi f} \right]^{1/2}} \quad (A.34)$$

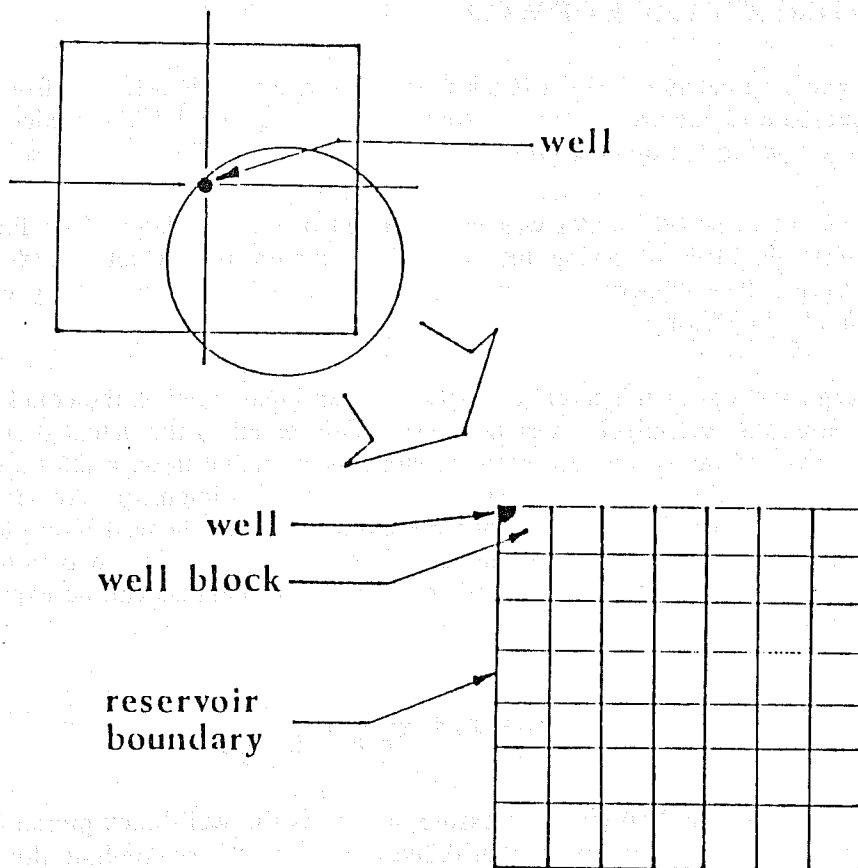


Fig. A.5 Well-Block Representation (2-D)

where:

- c_g = well geometric factor
- f = fraction of well associated with the well block
- A = area of the well block

The well geometric factor can be calculated by the following equation:

$$c_g = \left(\frac{\pi f}{A} \right)^{1/2} \frac{1}{a} [\exp(-4\pi f) \pi_i (R_i)^{T_i b/2}] \quad (\text{A.35})$$

The definition of the terms in Eq. (A.35) is lengthy, and can be found in Abou-Kassem and Aziz (1983).

In this study, Eq. (A.35) was not used to calculate the well-block dimensions due to the fact that there are two unknowns in Eq. (A.35), namely, c_g and A . The well-block dimensions are calculated by using Eq. (A.34), which still contains the two unknown c_g and A . However, according to Abou-Kassem and Aziz, a typical c_g value for a corner well block with a five-point discretization scheme is 0.63888. This c_g value is then used to find the well block dimensions, and then adjustment to the well block dimensions was performed until the calculated pressure values for the full well block and the quarter well block differed less than 0.2%.

A.12. MATERIAL BALANCE ERROR CALCULATIONS

The simulator calculates material balance error for every time step in order to check the quality of the calculated pressures. Original fluid in place is calculated at the onset of each simulation run. Two material balance error values were calculated at each time step; an incremental material balance error, and a cumulative material balance error.

The incremental material balance error is calculated by comparing the theoretical mass of fluid produced for that time step to the calculated mass of fluid produced for that time step. The calculated mass of fluid produced is obtained by subtracting the calculated mass in place of the current time step from that of the previous time step. The mass in place of each time step is calculated based on the pressure distribution of the current time step. The cumulative material balance error is obtained by comparing the theoretical mass in place to the calculated mass in place. Therefore, the cumulative material balance error will only increase, whereas the incremental material balance error may increase, decrease, or stay constant. However, if the simulator is functioning correctly, the incremental material balance error should stay relatively small and constant.

In theory, this is not the best indication of the quality of the calculated pressures, since a wrong pressure distribution could give a correct material balance value. However, in a single-phase flow situation, the material balance error calculation presented here is an adequate indication of the quality of the calculated pressures.

A.13. USER INSTRUCTIONS AND INPUT FORMAT

The simulator described in the preceding is written in FORTRAN WATFIV for the purpose of maximum portability. However, this version is designed to run under FORTRAN 77. The only command that is nonstandard WATFIV is the OPEN statement on line 51, and the WRITE statement on line 914, and 915. These two statements perform the automatic output of the well-block pressure as explained in the following paragraph. Deletion of these two lines will return the program to standard FORTRAN WATFIV, and the program can be run with any machine with a FORTRAN 66 compiler. Deletion of these two lines will also remove the automatic well-block pressure output capability.

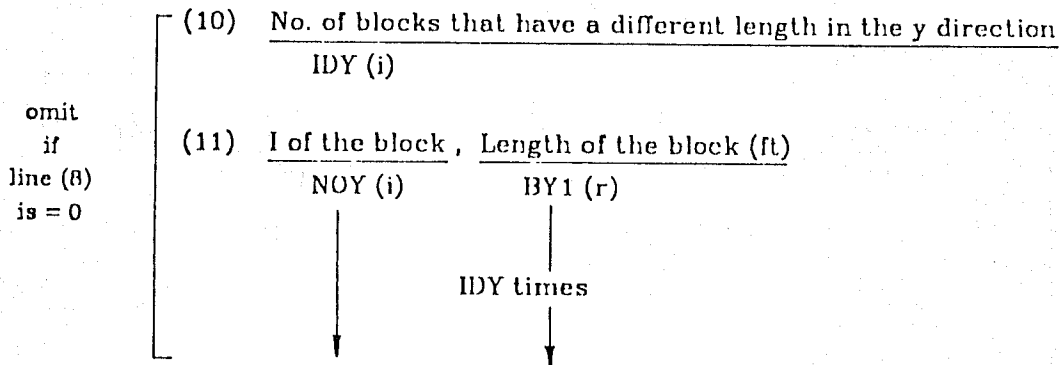
This program will automatically output the calculated block pressure of one chosen block to a file named PWOUT. The file PWOUT must exist in the same directory where the program is located in order for the program to function. This option is designed so that the well-block pressure can be recorded in a file for immediate plotting as soon as the simulation run is finished. The *I* and *J* coordinates of the chosen block is to be supplied in the input data file.

The current version of this simulator is written for the purpose of this study. Therefore, it lacks some features that could be found in a general simulator. This program does not have the capability of a restart mechanism, and must use a grid of 21 by 21 blocks. However, both of these features can be added to the program without a large effort. The program is currently set to perform calculations for up to 500 time steps. To increase or decrease this capability, the dimensions of the variables TIME and IPRINT will need to be changed accordingly.

Since this study involves the simulation of gas as a fluid with slight and constant compressibility, the material balance calculations in the simulator must be capable of gas material balance calculations. In this version, both liquid and gas material balance calculations are included. However, this current version has an active liquid material balance routine and

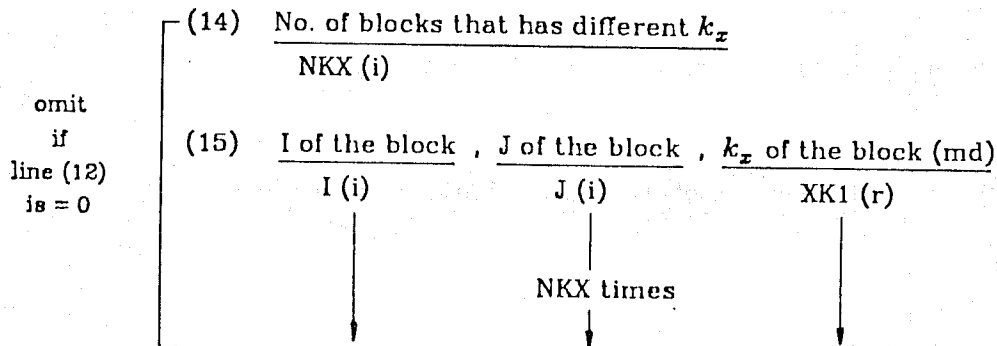
(8) Uniform block length indicator for the y direction (0 for yes, 1 for no)
IY (i)

(9) Base length for blocks in the y direction (ft)
BY (r)



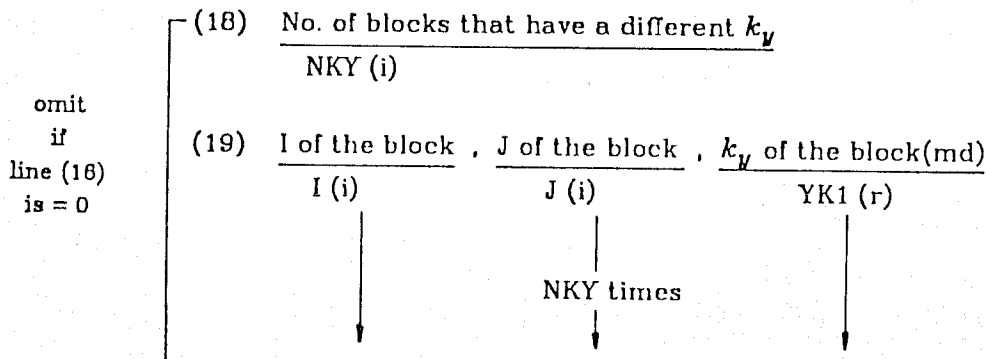
(12) Uniform k_x indicator (0 for yes, 1 for no)
KXI (i)

(13) k_x base value (md)
BKX (r)



(16) Uniform k_y indicator (0 for yes, 1 for no)
KYI (i)

(17) k_y base value (md)
BKY (r)

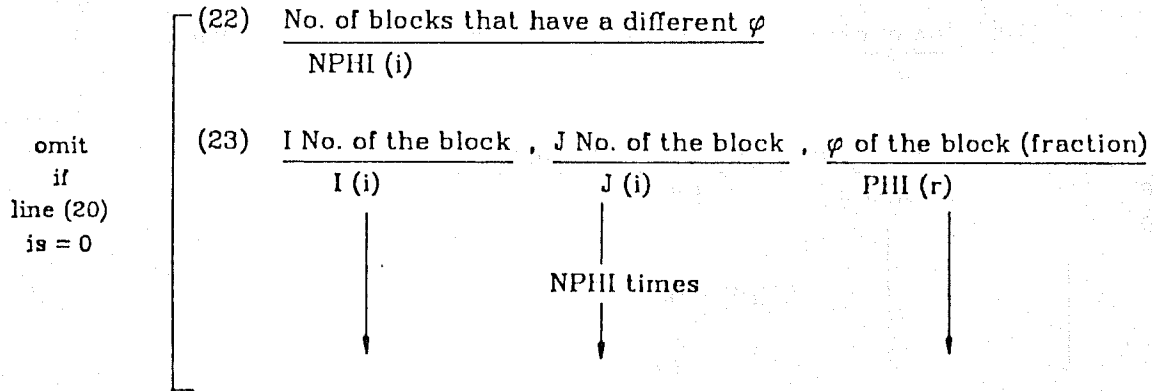


(20) Uniform ϕ indicator (0 for yes, 1 for no)

IPHI (i)

(21) ϕ base value (fraction)

BPHI (r)

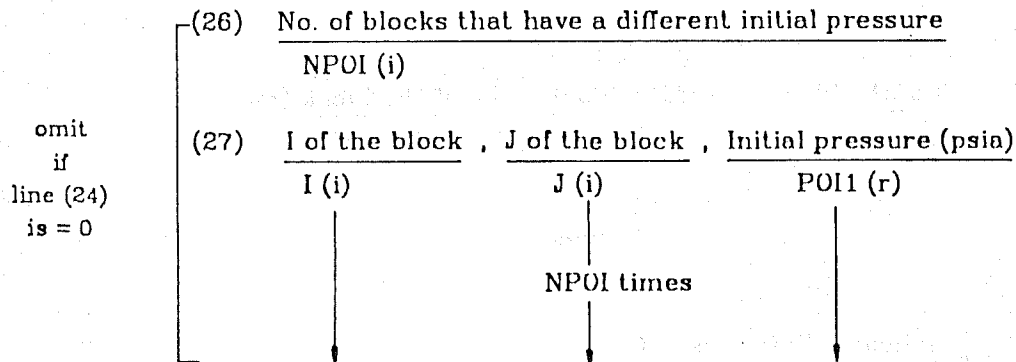


(24) Uniform initial pressure indicator (0 for yes, 1 for no)

IPOI (i)

(25) Initial pressure base value (psia)

BPOI (r)



(28) Density of fluid at STC (lbm / ft^3)

ROOW (r)

(29) Compressibility of fluid at STC (psi^{-1})

CFL (r)

(30) Formation volume factor of fluid at STC (RB/STB)

BSTD (r)

(31) Reservoir temperature ($^{\circ}F$)

TEMP (r)

(32) No. of PVT entries (maximum 50)

NPVT (i)

(46) Convergence criteria (psia)

CONVER (r)

(47) Force iteration indicator (0 for no, 1 for yes)

IFORCE (i)

omit

if

line (47)

is = 0

(48) No. of iteration forced to perform
NFORIT (i)

(49) No. of time steps to be printed (enter 0 if all is to be printed)

NPRINT (i)

omit

if

line (49)

is = 0

(50) The corresponding numbers of the time steps to be printed

NOPRT (i)

NPRINT times

(51) Omit pressure map indicator (0 for not omit, 1 for omit)

ISKIPP (i)

omit

if

line (51)

is = 0

(52) I of the block to be printed , J of the block to be printed

IBLPR (i)

JBLPR (i)

(53) I of the block , J of the block (to be output to file PWOUT)

IBLPR2 (i)

JBLPR2 (i)

APPENDIX B

TWO-DIMENSIONAL, AREAL-IMPLICIT, SINGLE PHASE, SINGLE COMPONENT
NUMERICAL SIMULATOR FOR A REAL GAS

This appendix contains a description of the captioned simulator and the associated user instructions. This appendix contains only a brief description for the same reason stated in Appendix A. Detailed theoretical development can be found in Ref. by Abou-Kassem and Aziz (1983), Aziz & Settari (1979), and Peaceman (1978).

B.1. DERIVATION OF GOVERNING EQUATIONS

The derivation of the governing equation for gas flow in a porous medium follows the same procedure as in the derivation for slightly compressible fluid illustrated in Appendix A.

Start with a material balance for the control volume, and substitute Darcy's law to produce the general partial differential equation:

$$\nabla \cdot \left[\frac{\rho k}{\mu} (\nabla p - \gamma \nabla z) \right] = \frac{\partial(\rho\phi)}{\partial t} + \tilde{q} \quad (\text{B.1})$$

For gas flow, the assumptions of constant and slight compressibility are usually not valid. However, gravitational force can be neglected, since the effect of gravity on gas is relatively small.

An equation of state is used to replace the density term. Recall the equation of state for a real gas:

$$\rho = \frac{pM}{ZRT} \quad (\text{B.2})$$

where :

- M = molecular weight for gas
- Z = real gas compressibility factor
- T = temperature in $^{\circ}R$
- R = constant of 10.72 for English units
- p = pressure in psia

Assuming k is independent of pressure, and substituting the equation of state in to Eq. (B.1):

$$\nabla \cdot \left[\frac{kp}{\mu z} (\nabla p - \gamma \nabla z) \right] = \frac{\partial}{\partial t} \left[\frac{\phi p}{Z} \right] + \frac{RT}{M} \tilde{q} \quad (\text{B.3})$$

If the gravity term is neglected, the equation becomes:

$$\nabla \cdot \left[\frac{Kp}{\mu Z} \nabla p \right] = \frac{\partial}{\partial t} \left[\frac{\phi p}{Z} \right] + \frac{RT}{M} \bar{q} \quad (\text{B.4})$$

B.2. FINITE-DIFFERENCE METHOD AND COORDINATE SYSTEM

The finite-difference method and coordinate system used are the same as for the slightly compressible model.

B.3. TREATMENT OF VARIABLE COEFFICIENT

The averaging technique used to find the quantity $kp/\mu Z$ at block boundaries is the same as described in Section 5 in Appendix A.

The transmissivity is broken into two parts:

$$\frac{kp}{\mu Z} |_{i+1/2} = k|_{i+1/2} \frac{p}{\mu Z} |_{i+1/2} \quad (\text{B.5.a})$$

$$\frac{kp}{\mu Z} |_{i-1/2} = k|_{i-1/2} \frac{p}{\mu Z} |_{i-1/2} \quad (\text{B.5.b})$$

The permeability in Eq. (B.5) is at the block boundaries, and is found by weighted harmonic average as shown in Appendix A.

There is no unique way of finding $p/\mu Z$ at block boundaries. However, since μZ is not a direct function of distance, it should not be averaged by harmonic mean. An arithmetic average is used in this study. There are two ways to determine the quantity $p/\mu Z$ at block boundaries. It can be determined by averaging $p_i + 1$ and p_i to determine $p_i + 1/2$, then determine $p/\mu Z$ at $i + 1/2$ from $p_i + 1/2$. Another way to determine $p/\mu Z$ at $i + 1/2$ is to average $p/\mu Z$ at i and $p/\mu Z$ at $i + 1$. The difference between the two methods is usually small however, the quantity $p/\mu Z$ is usually less non-linear than μ or Z as a function of pressure. Therefore, the method of averaging $p/\mu Z$ at i and $i + 1$ to obtain $p/\mu Z$ at $i + 1/2$ is used in this study.

B.4. DISCRETIZATION

Recall Eq. (B.4) and expand the Laplace operator in a Cartesian coordinate system:

$$\frac{\partial}{\partial x} \left[\frac{kp}{\mu Z} \frac{\partial p}{\partial x} \right] + \frac{\partial}{\partial y} \left[\frac{kp}{\mu Z} \frac{\partial p}{\partial y} \right] = \frac{\partial}{\partial t} \left[\frac{\phi p}{Z} \right] + \frac{RT}{M} \bar{q} \quad (\text{B.6})$$

Using the same nomenclature shown in Fig. A.4 of Appendix A, and carry out the discretization process:

$$\begin{aligned}
 & \frac{\frac{p}{\mu Z} \left[\frac{p}{\mu Z} |_{i+1/2,j} + \frac{p}{\mu Z} |_{i,j} \right]^{n+1}}{x_{i+1/2,j} - x_{i-1/2,j}} - \frac{\frac{p}{\mu Z} \left[\frac{p}{\mu Z} |_{i-1/2,j} + \frac{p}{\mu Z} |_{i,j} \right]^{n+1}}{x_{i,j} - x_{i-1,j}} \\
 & + \frac{\frac{p}{\mu Z} \left[\frac{p}{\mu Z} |_{i,j+1/2} + \frac{p}{\mu Z} |_{i,j} \right]^{n+1}}{y_{i,j+1/2} - y_{i,j-1/2}} - \frac{\frac{p}{\mu Z} \left[\frac{p}{\mu Z} |_{i,j-1/2} + \frac{p}{\mu Z} |_{i,j} \right]^{n+1}}{y_{i,j} - y_{i,j-1}} \\
 & = \frac{\Phi_{i,j}^{n+1} p_{i,j}^{n+1}}{Z_{i,j}^{n+1} \Delta t} - \frac{\Phi_{i,j}^n p_{i,j}^n}{Z_{i,j}^n \Delta t} + \frac{RT}{M} \frac{q}{q}
 \end{aligned} \tag{B.7}$$

Break up the transmissivity as shown in Section B.3, and collect terms:

$$\begin{aligned}
 & \frac{k_{i-1/2,j}^{n+1} \left[\frac{p}{\mu Z} |_{i-1,j} + \frac{p}{\mu Z} |_{i,j} \right]^{n+1}}{2 \left[x_{i,j} - x_{i-1,j} \right] \left[x_{i+1/2,j} - x_{i-1/2,j} \right]} p_{i-1,j}^{n+1} + \frac{k_{i,j+1/2}^{n+1} \left[\frac{p}{\mu Z} |_{i,j+1} + \frac{p}{\mu Z} |_{i,j} \right]^{n+1}}{2 \left[y_{i,j+1} - y_{i,j} \right] \left[y_{i,j+1/2} - y_{i,j-1/2} \right]} p_{i,j+1}^{n+1} \\
 & - \left[\frac{k_{i-1/2,j}^{n+1} \left[\frac{p}{\mu Z} |_{i-1,j} + \frac{p}{\mu Z} |_{i,j} \right]^{n+1}}{2(x_{i,j} - x_{i-1,j})(x_{i+1/2,j} - x_{i-1/2,j})} + \frac{k_{i+1/2,j}^{n+1} \left[\frac{p}{\mu Z} |_{i+1,j} + \frac{p}{\mu Z} |_{i,j} \right]^{n+1}}{2(x_{i+1,j} - x_{i,j})(x_{i+1/2,j} - x_{i-1/2,j})} \right. \\
 & + \frac{k_{i,j-1/2}^{n+1} \left[\frac{p}{\mu Z} |_{i,j-1} + \frac{p}{\mu Z} |_{i,j} \right]^{n+1}}{2(y_{i,j+1/2} - y_{i,j-1/2})(y_{i,j} - y_{i,j-1})} + \frac{k_{i,j+1/2}^{n+1} \left[\frac{p}{\mu Z} |_{i,j+1} + \frac{p}{\mu Z} |_{i,j} \right]^{n+1}}{2(y_{i,j+1} - y_{i,j})(y_{i,j+1/2} - y_{i,j-1/2})} \\
 & \left. + \frac{\Phi_{i,j}^{n+1}}{Z_{i,j}^{n+1} \Delta t} \right] p_{i,j}^{n+1} \\
 & + \frac{k_{i+1/2,j}^{n+1} \left[\frac{p}{\mu Z} |_{i+1,j} + \frac{p}{\mu Z} |_{i,j} \right]^{n+1}}{2(x_{i+1,j} - x_{i,j})(x_{i+1/2,j} - x_{i-1/2,j})} p_{i+1,j}^{n+1} + \frac{k_{i,j-1/2}^{n+1} \left[\frac{p}{\mu Z} |_{i,j} + \frac{p}{\mu Z} |_{i,j-1} \right]^{n+1}}{2(y_{i,j+1/2} - y_{i,j-1/2})(y_{i,j} - y_{i,j-1})} p_{i,j-1}^{n+1} \\
 & = - \frac{\Phi_{i,j}^n p_{i,j}^n}{Z_{i,j}^n \Delta t} + \frac{RT q_{ij}}{M(x_{i+1/2,j} - x_{i-1/2,j})(y_{i,j+1/2} - y_{i,j-1/2})h}
 \end{aligned} \tag{B.8}$$

Notice $\bar{q}_{ij} = \frac{q_{ij}}{\Delta x \Delta y h} = \frac{q_{ij}}{\Delta V}$

Apply the conversion factor associated with permeability and the appropriate units for each term:

Conversion factor associated with $k = 7.3243814 \times 10^{-5}$

$\Delta t = \text{sec}$	$p = \text{psia}$	$q = \text{lbm/sec}$
$\rho_{STC} = \text{lbm/ft}^3$	$\Delta x = \text{ft}$	$k = \text{Darcy}$
$\mu = \text{cp}$	$\Delta y = \text{ft}$	$M = (28.97)(\gamma_g)$
$B = \text{RB/STB}$	$h = \text{ft}$	$R = 10.73$

The final discretized equation is:

$$\begin{aligned}
 & \frac{k_{i,j-1/2}^{n+1} \left[\frac{p}{\mu Z} |_{i,j} + \frac{p}{\mu Z} |_{i,j-1} \right]^{n+1}}{\Delta y_{i,j} \Delta y_{i,j}^-} p_{i,j-1}^{n+1} + \frac{k_{i-1/2,j}^{n+1} \left[\frac{p}{\mu Z} |_{i-1,j} + \frac{p}{\mu Z} |_{i,j} \right]^{n+1}}{\Delta x_{i,j} \Delta x_{i,j}^-} p_{i-1,j}^{n+1} \\
 & - \left[\frac{k_{i-1/2,j}^{n+1} \left[\frac{p}{\mu Z} |_{i-1,j} + \frac{p}{\mu Z} |_{i,j} \right]^{n+1}}{\Delta x_{i,j} \Delta x_{i,j}^-} + \frac{k_{i+1/2,j}^{n+1} \left[\frac{p}{\mu Z} |_{i+1,j} + \frac{p}{\mu Z} |_{i,j} \right]^{n+1}}{\Delta x_{i,j} \Delta x_{i,j}^+} \right. \\
 & + \frac{k_{i,j-1/2}^{n+1} \left[\frac{p}{\mu Z} |_{i,j-1} + \frac{p}{\mu Z} |_{i,j} \right]^{n+1}}{\Delta y_{i,j} \Delta y_{i,j}^-} + \frac{k_{i,j+1/2}^{n+1} \left[\frac{p}{\mu Z} |_{i,j+1} + \frac{p}{\mu Z} |_{i,j} \right]^{n+1}}{\Delta y_{i,j} \Delta y_{i,j}^+} \\
 & \left. + \frac{\phi_{i,j}^{n+1}}{3.6621907 \times 10^{-5} Z_{i,j}^{n+1} \Delta t} \right] p_{i,j}^{n+1} \\
 & + \frac{k_{i+1/2,j}^{n+1} \left[\frac{p}{\mu Z} |_{i+1,j} + \frac{p}{\mu Z} |_{i,j} \right]^{n+1}}{\Delta x_{i,j} \Delta x_{i,j}^+} p_{i+1,j}^{n+1} + \frac{k_{i,j+1/2}^{n+1} \left[\frac{p}{\mu Z} |_{i,j+1} + \frac{p}{\mu Z} |_{i,j} \right]^{n+1}}{\Delta y_{i,j} \Delta y_{i,j}^+} p_{i,j+1}^{n+1} \\
 & = - \frac{\phi_{i,j}^n p_{i,j}^n}{3.6621907 \times 10^{-5} Z_{i,j}^n \Delta t} + \frac{10115.589 T q_{ij}}{(\gamma_g) h \Delta x_{i,j} \Delta y_{i,j}} \quad (B.9)
 \end{aligned}$$

The final simulation Eq. (B.9) is solved by the same method described in Appendix A.

B.5 USER INSTRUCTIONS AND INPUT FORMAT

The user instructions are similar to the ones mentioned in Appendix A.13 (page 55).

INPUT FORMAT FOR GAS SIMULATOR

- (1) No. of blocks in the x direction (always use 21 for this version)
IB (i)
- (2) No. of blocks in the y direction (always use 21 for this version)
JB (i)
- (3) Thickness of the reservoir (ft)
H (r)
- (4) Uniform block length indicator for the x direction (0 for yes, 1 for no)
IX (i)
- (5) Base length for blocks in the x direction (ft)
BX (r)
- (6) No. of blocks that have different length in the x direction
IDX (i)
- (7) I of the block , length of the block (ft)
NOX (i) BX1 (r)
IDX times
- (8) Uniform block length indicator for the y direction (0 for yes, 1 for no)
IY (i)
- (9) Base length for blocks in the y direction (ft)
BY (r)
- (10) No. of blocks that have different length in the y direction
IDY (i)
- (11) I of the block , Length of the block (ft)
NOY (i) BY1 (r)
IDY times
- (12) Uniform k_x indicator (0 for yes, 1 for no)
KXI (i)

omit
if
line (4)
is = 0

omit
if
line (8)
is = 0

(13) k_x base value (md)
BKX (r)

omit
 if
 line (12)
 is = 0

(14) $\frac{\text{No. of blocks that have different } k_x}{\text{NKX (i)}}$

(15) $\frac{\text{I of the block}}{\text{I (i)}} , \frac{\text{J of the block}}{\text{J (i)}} , \frac{k_x \text{ of the block (md)}}{\text{XK1 (r)}}$

NKX times

(16) Uniform k_y indicator (0 for yes, 1 for no)
KYI (i)

(17) k_y base value (md)
BKY (r)

omit
 if
 line (16)
 is = 0

(18) $\frac{\text{No. of blocks that have different } k_y}{\text{NKY (i)}}$

(19) $\frac{\text{I of the block}}{\text{I (i)}} , \frac{\text{J of the block}}{\text{J (i)}} , \frac{k_y \text{ of the block (md)}}{\text{YK1 (r)}}$

NKY times

(20) Uniform φ indicator (0 for yes, 1 for no)
IPHI (i)

(21) φ base value (fraction)
BPPII (r)

omit
 if
 line (20)
 is = 0

(22) $\frac{\text{No. of blocks that have different } \varphi}{\text{NPIII (i)}}$

(23) $\frac{\text{I No. of the block}}{\text{I (i)}} , \frac{\text{J No. of the block}}{\text{J (i)}} , \frac{\varphi \text{ of the block (fraction)}}{\text{PIII (r)}}$

NPIII times

(24) Uniform initial pressure indicator (0 for yes, 1 for no)

IPOI (i)

(25) Initial pressure base value (psia)

BPOI (r)

omit
if
line (24)
is = 0

(26) No. of blocks that have a different initial pressure

NPOI (i)

(27) I of the block , J of the block , Initial pressure (psia)

I (i)

J (i)

POI1 (r)

NPOI times

(28) S.G. of gas

SG (r)

(29) Reservoir temperature (° F)

TEMP (r)

(30) No. of PVT entries (maximum 50)

NPVT (i)

(31) P (psia) , μ (cp) , Z

PT (r)

VT (r)

ZT (r)

NPVT times

(32) Uniform time step indicator (0 for yes, 1 for no)

NTIME (i)

(33) Total No. of time step assigned (maximum 500 for this version)

NTOT (i)

omit
if
line (32)
is = 1

(34) Constant time step size (days)

TIME1 (r)

omit
if
line (32)
is = 0

(35) No. of groups of different time steps

NGT (i)

(36) Time step size(days) , Duration of this time step(no. of times)

TIME1 (r)

LAST (i)

(37) Standard pressure (psia)

PSTD (r)

(38) Standard temperature (°F)

TSTD (r)

(39) No. of blocks that have injection or production

NPOD (i)

omit
if
line (39)
is = 0

(40) I of the block , J of the block , Rate (SCF/D, - for inj., + for prod.)
I (i) J (i) Q1 (r)

NPOD times

(41) Maximum no. of iteration allowed

MAXIN (i)

(42) Maximum no. of time steps allowed to be executed

MAXEXE (i)

(43) Dummy (always input a 0)

ICHECK (i)

(44) Convergence criteria (psia)

CONVER (r)

(45) Force iteration indicator (0 for no, 1 for yes)

IFORCE (i)

omit
if
line (45)
is = 0

(46) No. of iteration forced to perform
NFORIT (i)

(47) No. of time steps to be printed (enter 0 if all is to be printed)

NPRINT (i)

omit
if
line (47)
is = 0

(48) Numbers of the time steps to be printed
NOPRT (i)

NPRINT times

(49) Omit pressure map indicator (0 for not omit, 1 for omit)

ISKIPP (i)

omit
if
line (40)
is = 0

(50) I of the block to be printed , J of the block to be printed
IBLPR (i) JBLPR (i)

(51) I of the block , J of the block (to be output to file PWOUT)
IBLPR2 (i) JBLPR2 (i)

APPENDIX C VALIDATION OF THE SIMULATOR FOR SLIGHTLY COMPRESSIBLE FLUIDS

It is mandatory to check the simulator with a test case for which analytical results are available in order to determine if the numerical model is functioning correctly. The case of a single well located in the center of a closed square reservoir was chosen. The analytical solution for this case is well known and can be found in the reference by Earlougher *et al.* (1968).

Figure C.1 shows the physical system to be simulated.

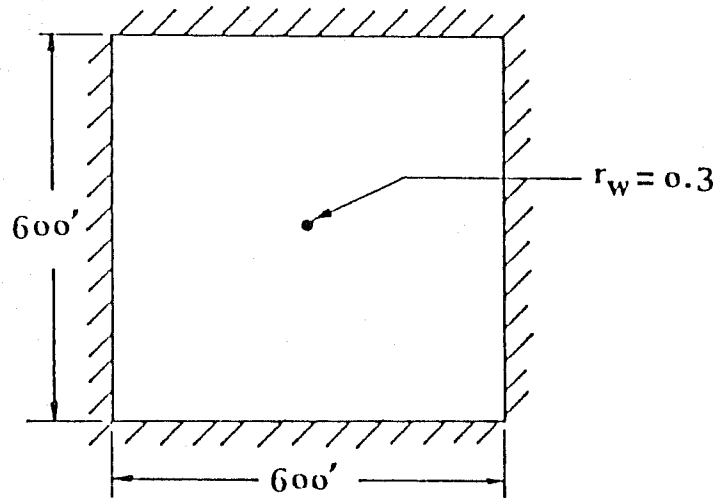


Fig. C.1 Well in the Center of a Closed Square Reservoir

Table C.1 shows the results of an analytical solution to this problem. Table C.1 is the dimensionless pressure solution for a closed outer boundary square reservoir with \sqrt{A}/r_w equal to 2000, and one well located in the center of the square. The quantity A is the area of the reservoir, and r_w is the wellbore radius. The dimensionless pressure p_D and the dimensionless time t_{DA} have the following definitions:

$$p_D = \frac{kh (p_i - p_{wf})}{141.2qB\mu} \quad (C.1)$$

$$t_{DA} = \frac{0.0002637kt}{\phi\mu c_r A} \quad (C.2)$$

where :

- k = permeability (md)
- h = formation thickness (ft)
- p_i = initial pressure (psi)
- p_{wf} = well pressure (psi)
- q = flow rate (STB/D)
- B = formation volume factor (RV/STV)
- μ = viscosity (cp)
- t = time (hrs)
- ϕ = porosity (fraction)
- c_t = total system compressibility (1/psi)

TABLE C.1

DIMENSIONLESS PRESSURE AT VARIOUS POINTS IN A CLOSED SQUARE WITH A WELL AT THE CENTER, NO WELLBORE STORAGE, NO SKIN, $\sqrt{A}/r_w = 2,000$.
 After Earlougher, Ramey, Miller, and Mueller. (1968)

r_{DA}	P_D							
	$r_D=0.000$ YD=0.000	$r_D=0.750$ YD=0.000	$r_D=0.250$ YD=0.250	$r_D=0.500$ YD=0.000	$r_D=0.100$ YD=0.750	$r_D=0.500$ YD=0.500	$r_D=0.750$ YD=0.000	$r_D=0.750$ YD=0.750
0.0010	4.5514	0.0021	0.0000	0.0000	0.0000	0.0000	0.0000	0.0000
0.0015	4.7543	0.0109	0.0004	0.0000	0.0000	0.0000	0.0000	0.0000
0.0020	4.8981	0.0261	0.0021	0.0000	0.0000	0.0000	0.0000	0.0000
0.0025	5.0097	0.0454	0.0054	0.0001	0.0000	0.0000	0.0000	0.0000
0.0030	5.1009	0.0673	0.0109	0.0004	0.0001	0.0000	0.0000	0.0000
0.0040	5.2447	0.1141	0.0241	0.0021	0.0007	0.0000	0.0000	0.0000
0.0050	5.3543	0.1607	0.0454	0.0054	0.0021	0.0001	0.0001	0.0000
0.0060	5.4474	0.2053	0.0673	0.0109	0.0047	0.0004	0.0007	0.0001
0.0070	5.5243	0.2473	0.0904	0.0174	0.0073	0.0011	0.0016	0.0003
0.0080	5.5913	0.2871	0.1141	0.0241	0.0109	0.0017	0.0024	0.0007
0.0090	5.6502	0.3243	0.1374	0.0309	0.0146	0.0024	0.0031	0.0011
0.0100	5.7029	0.3592	0.1607	0.0454	0.0183	0.0031	0.0038	0.0015
0.0110	5.7504	0.3923	0.1837	0.0604	0.0220	0.0038	0.0045	0.0019
0.0120	5.7929	0.4237	0.2053	0.0754	0.0257	0.0045	0.0052	0.0023
0.0130	5.8304	0.4537	0.2257	0.0904	0.0294	0.0052	0.0059	0.0027
0.0140	5.8629	0.4823	0.2443	0.1049	0.0331	0.0059	0.0066	0.0031
0.0150	5.8904	0.5097	0.2613	0.1189	0.0368	0.0066	0.0073	0.0035
0.0160	5.9139	0.5359	0.2767	0.1324	0.0405	0.0073	0.0080	0.0039
0.0170	5.9334	0.5611	0.2907	0.1454	0.0442	0.0080	0.0087	0.0043
0.0180	5.9499	0.5853	0.3037	0.1579	0.0479	0.0087	0.0094	0.0047
0.0190	5.9634	0.6087	0.3157	0.1700	0.0516	0.0094	0.0101	0.0051
0.0200	5.9739	0.6313	0.3267	0.1817	0.0553	0.0101	0.0108	0.0055
0.0210	5.9814	0.6531	0.3367	0.1930	0.0590	0.0108	0.0115	0.0059
0.0220	5.9869	0.6741	0.3457	0.2039	0.0627	0.0115	0.0122	0.0063
0.0230	5.9904	0.6943	0.3537	0.2144	0.0664	0.0122	0.0129	0.0067
0.0240	5.9929	0.7137	0.3607	0.2245	0.0701	0.0129	0.0136	0.0071
0.0250	5.9944	0.7323	0.3667	0.2343	0.0738	0.0136	0.0143	0.0075
0.0260	5.9949	0.7501	0.3717	0.2437	0.0775	0.0143	0.0150	0.0079
0.0270	5.9944	0.7671	0.3767	0.2527	0.0812	0.0150	0.0157	0.0083
0.0280	5.9929	0.7833	0.3813	0.2613	0.0849	0.0157	0.0164	0.0087
0.0290	5.9904	0.7987	0.3857	0.2694	0.0886	0.0164	0.0171	0.0091
0.0300	5.9869	0.8133	0.3897	0.2771	0.0923	0.0171	0.0178	0.0095
0.0310	5.9824	0.8271	0.3937	0.2843	0.0960	0.0178	0.0185	0.0099
0.0320	5.9769	0.8401	0.3977	0.2910	0.0997	0.0185	0.0192	0.0103
0.0330	5.9704	0.8523	0.4017	0.2971	0.1034	0.0192	0.0199	0.0107
0.0340	5.9629	0.8637	0.4057	0.3027	0.1071	0.0199	0.0206	0.0111
0.0350	5.9544	0.8743	0.4097	0.3077	0.1108	0.0206	0.0213	0.0115
0.0360	5.9449	0.8841	0.4137	0.3123	0.1145	0.0213	0.0220	0.0119
0.0370	5.9344	0.8931	0.4177	0.3163	0.1182	0.0220	0.0227	0.0123
0.0380	5.9229	0.9013	0.4217	0.3200	0.1219	0.0227	0.0234	0.0127
0.0390	5.9104	0.9087	0.4257	0.3233	0.1256	0.0234	0.0241	0.0131
0.0400	5.8969	0.9153	0.4297	0.3263	0.1293	0.0241	0.0248	0.0135
0.0410	5.8824	0.9211	0.4337	0.3290	0.1330	0.0248	0.0255	0.0139
0.0420	5.8669	0.9261	0.4377	0.3313	0.1367	0.0255	0.0262	0.0143
0.0430	5.8504	0.9303	0.4417	0.3333	0.1404	0.0262	0.0269	0.0147
0.0440	5.8329	0.9337	0.4457	0.3350	0.1441	0.0269	0.0276	0.0151
0.0450	5.8144	0.9363	0.4497	0.3363	0.1478	0.0276	0.0283	0.0155
0.0460	5.7949	0.9381	0.4537	0.3373	0.1515	0.0283	0.0290	0.0159
0.0470	5.7744	0.9391	0.4577	0.3380	0.1552	0.0290	0.0297	0.0163
0.0480	5.7529	0.9393	0.4617	0.3383	0.1589	0.0297	0.0304	0.0167
0.0490	5.7304	0.9387	0.4657	0.3383	0.1626	0.0304	0.0311	0.0171
0.0500	5.7069	0.9373	0.4697	0.3377	0.1663	0.0311	0.0318	0.0175
0.0510	5.6824	0.9351	0.4737	0.3367	0.1700	0.0318	0.0325	0.0179
0.0520	5.6569	0.9321	0.4777	0.3353	0.1737	0.0325	0.0332	0.0183
0.0530	5.6304	0.9283	0.4817	0.3333	0.1774	0.0332	0.0339	0.0187
0.0540	5.6029	0.9237	0.4857	0.3307	0.1811	0.0339	0.0346	0.0191
0.0550	5.5744	0.9183	0.4897	0.3277	0.1848	0.0346	0.0353	0.0195
0.0560	5.5449	0.9121	0.4937	0.3243	0.1885	0.0353	0.0360	0.0199
0.0570	5.5144	0.9051	0.4977	0.3200	0.1922	0.0360	0.0367	0.0203
0.0580	5.4829	0.8973	0.5017	0.3153	0.1959	0.0367	0.0374	0.0207
0.0590	5.4504	0.8887	0.5057	0.3100	0.2000	0.0374	0.0381	0.0211
0.0600	5.4169	0.8793	0.5097	0.3043	0.2041	0.0381	0.0388	0.0215
0.0610	5.3824	0.8691	0.5137	0.2980	0.2082	0.0388	0.0395	0.0219
0.0620	5.3469	0.8581	0.5177	0.2913	0.2123	0.0395	0.0402	0.0223
0.0630	5.3104	0.8463	0.5217	0.2843	0.2164	0.0402	0.0409	0.0227
0.0640	5.2729	0.8337	0.5257	0.2770	0.2205	0.0409	0.0416	0.0231
0.0650	5.2344	0.8203	0.5297	0.2694	0.2246	0.0416	0.0423	0.0235
0.0660	5.1949	0.8061	0.5337	0.2613	0.2287	0.0423	0.0430	0.0239
0.0670	5.1544	0.7911	0.5377	0.2527	0.2328	0.0430	0.0437	0.0243
0.0680	5.1129	0.7753	0.5417	0.2437	0.2369	0.0437	0.0444	0.0247
0.0690	5.0704	0.7587	0.5457	0.2343	0.2410	0.0444	0.0451	0.0251
0.0700	5.0269	0.7413	0.5497	0.2243	0.2451	0.0451	0.0458	0.0255
0.0710	4.9824	0.7231	0.5537	0.2137	0.2492	0.0458	0.0465	0.0259
0.0720	4.9369	0.7041	0.5577	0.2027	0.2533	0.0465	0.0472	0.0263
0.0730	4.8904	0.6843	0.5617	0.1910	0.2574	0.0472	0.0479	0.0267
0.0740	4.8429	0.6637	0.5657	0.1787	0.2615	0.0479	0.0486	0.0271
0.0750	4.7944	0.6423	0.5697	0.1657	0.2656	0.0486	0.0493	0.0275
0.0760	4.7449	0.6201	0.5737	0.1520	0.2697	0.0493	0.0500	0.0279
0.0770	4.6944	0.5971	0.5777	0.1377	0.2738	0.0500	0.0507	0.0283
0.0780	4.6429	0.5733	0.5817	0.1227	0.2779	0.0507	0.0514	0.0287
0.0790	4.5904	0.5487	0.5857	0.1070	0.2820	0.0514	0.0521	0.0291
0.0800	4.5369	0.5233	0.5897	0.0907	0.2861	0.0521	0.0528	0.0295
0.0810	4.4824	0.4971	0.5937	0.0737	0.2902	0.0528	0.0535	0.0299
0.0820	4.4269	0.4701	0.5977	0.0560	0.2943	0.0535	0.0542	0.0303
0.0830	4.3704	0.4423	0.6017	0.0377	0.2984	0.0542	0.0549	0.0307
0.0840	4.3129	0.4137	0.6057	0.0187	0.3025	0.0549	0.0556	0.0311
0.0850	4.2544	0.3843	0.6097	0.0	0.3066	0.0556	0.0563	0.0315
0.0860	4.1949	0.3541	0.6137	0.0	0.3107	0.0563	0.0570	0.0319
0.0870	4.1344	0.3231	0.6177	0.0	0.3148	0.0570	0.0577	0.0323
0.0880	4.0729	0.2913	0.6217	0.0	0.3189	0.0577	0.0584	0.0327
0.0890	4.0104	0.2587	0.6257	0.0	0.3230	0.0584	0.0591	0.0331
0.0900	3.9469	0.2253	0.6297	0.0	0.3271	0.0591	0.0598	0.0335
0.0910	3.8824	0.1911	0.6337	0.0	0.3312	0.0598	0.0605	0.0339
0.0920	3.8169	0.1561	0.6377	0.0	0.3353	0.0605	0.0612	0.0343
0.0930	3.7504	0.1203	0.6417	0.0	0.3394	0.0612	0.0619	0.0347
0.0940	3.6829	0.0837	0.6457	0.0	0.3435	0.0619	0.0626	0.0351
0.0950	3.6144	0.0463	0.6497	0.0	0.3476	0.0626	0.0633	0.0355
0.0960	3.5449	0.0081	0.6537	0.0	0.3517	0.0633	0.0640	0.0359
0.0970	3.4744	0.0	0.6577	0.0	0.3558	0.0640	0.0647	0.0363
0.0980	3.4029	0.0	0.6617	0.0	0.3599	0.0647	0.0654	0.0367
0.0990	3.3304	0.0	0.6657	0.0	0.3640	0.0654	0.0661	0.0371
0.1000	3.2569	0.0	0.6697	0.0	0.3681	0.0661	0.0668	0.0375
0.1010	3.1824	0.0	0.6737	0.0	0.3722	0.0668	0.0675	0.0379
0.1020	3.1069	0.0	0.6777	0.0	0.3763	0.0675	0.0682	0.0383
0.1030	3.0304	0.0	0.6817	0.0	0.3804	0.0682	0.0689	0.0387
0.1040	2.9529	0.0	0.6857	0.0	0.3845	0.0689	0.0696	0.0391
0.1050	2.8744	0.0	0.6897	0.0	0.3886	0.0696	0.0703	0.0395
0.1060	2.7949	0.0	0.6937	0.0	0.3927	0.0703	0.0710	0.0399
0.1070	2.7144	0.0	0.6977	0.0	0.3968	0.0710	0.0717	0.0403
0.1080	2.6329	0.0	0.7017	0.0	0.4009	0.0717	0.0724	0.0407
0.1090	2.5504	0.0	0.7057	0.0	0.4050	0.0724	0.0731	0.0411
0.1100	2.4669	0.0	0.7097	0.0	0.4091	0.0731	0.0738	0.0415
0.1110	2.3824	0.0	0.7137	0.0	0.4132	0.0738	0.0745	0.0419

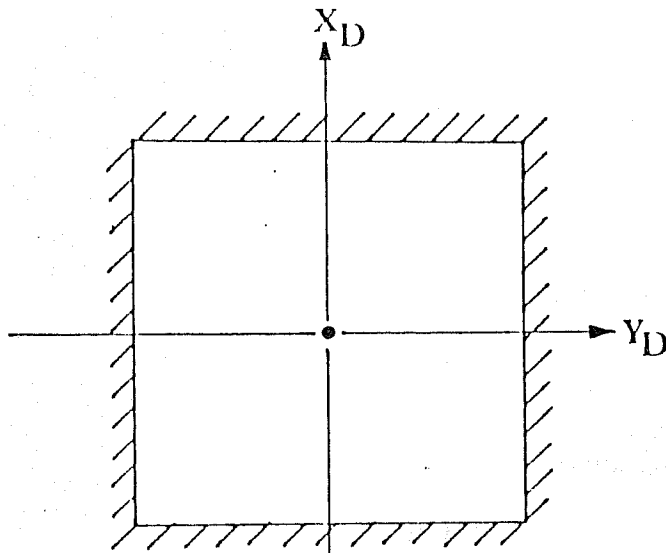


Fig. C.2 Physical Dimensions of Well in the Center of a Closed Square Reservoir

TABLE C.2 FLUID DATA

ρ_{STD}	= 62.4 lbm/ft ³
B_{STD}	= 1 RB/STB
c_t	= 3.0×10^{-6} 1/psi
h	= 100 ft
ϕ	= 0.2
k	= 25 md
p_i	= 1000 psia
$T_{reservoir}$	= 150°F

Two sets of grid dimensions were used to test the validity of the well-block pressure interpretation method described in section A.11 of Appendix A. Both runs utilized a grid of 21×21 blocks. The first run was a full-scale simulation with the well block dimension chosen so that $0.2\Delta X = r_w$. The second run simulated one quarter of the reservoir with the flow rate reduced to one quarter of the first run. The well-block dimension of the second run was calculated with Eq. (A.34) as described in Appendix A.

Figure C.3 presents the results from the first run, and Fig. C.4 presents the results from the second run. They agree favorably with the analytical solution. The results agree favorably with a maximum difference of less than 0.25% between the two runs. The quarter-reservoir run gave a closer answer to the analytical solution than the full-reservoir run. This is expected since the second run has a higher resolution in grid spacing than the first. Both sets of results indicate that the simulator functioned correctly.

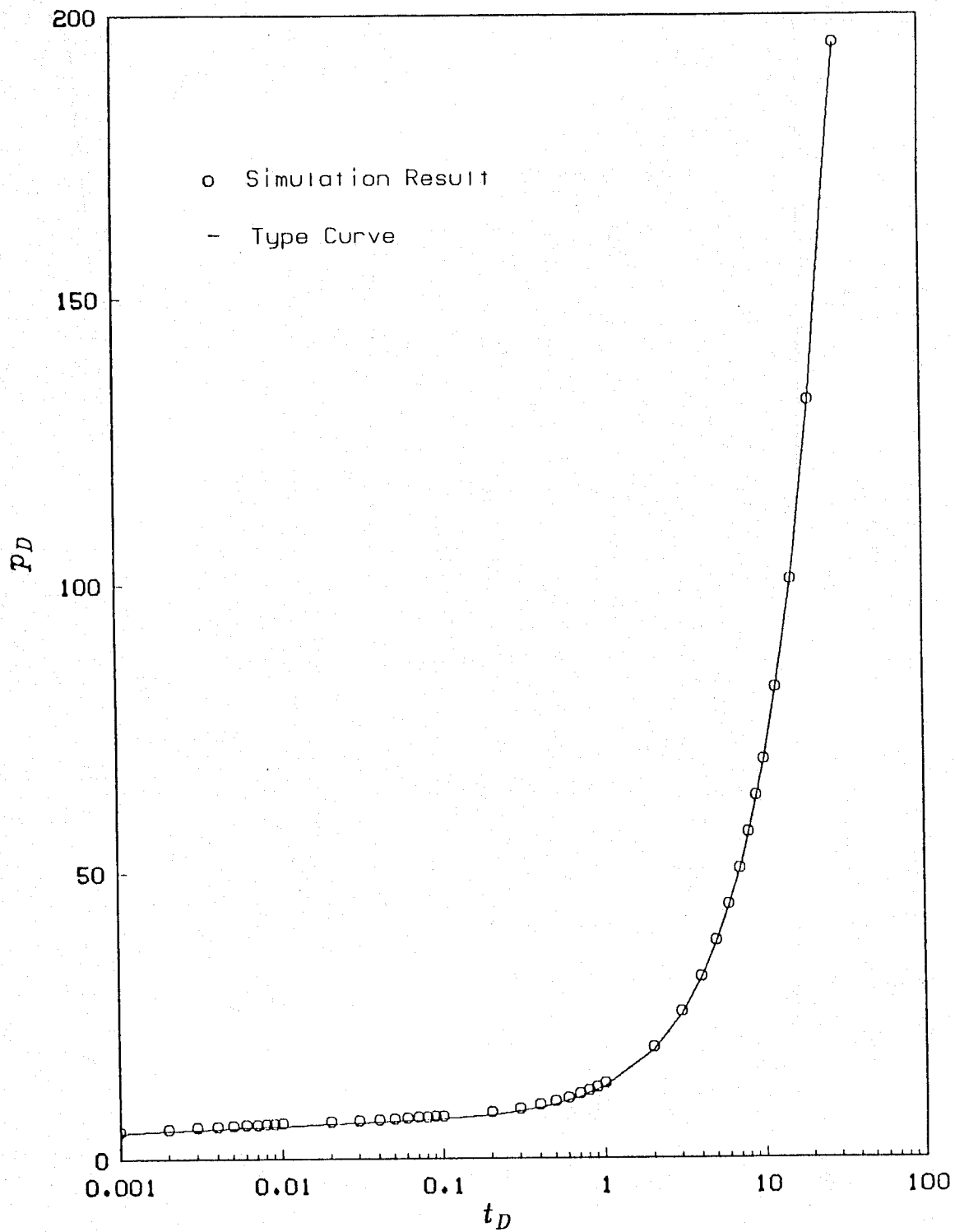


Fig. C.3 Dimensionless Pressure Solution for a Well in a Closed, Square Reservoir (Full-Scale Reservoir Simulation)

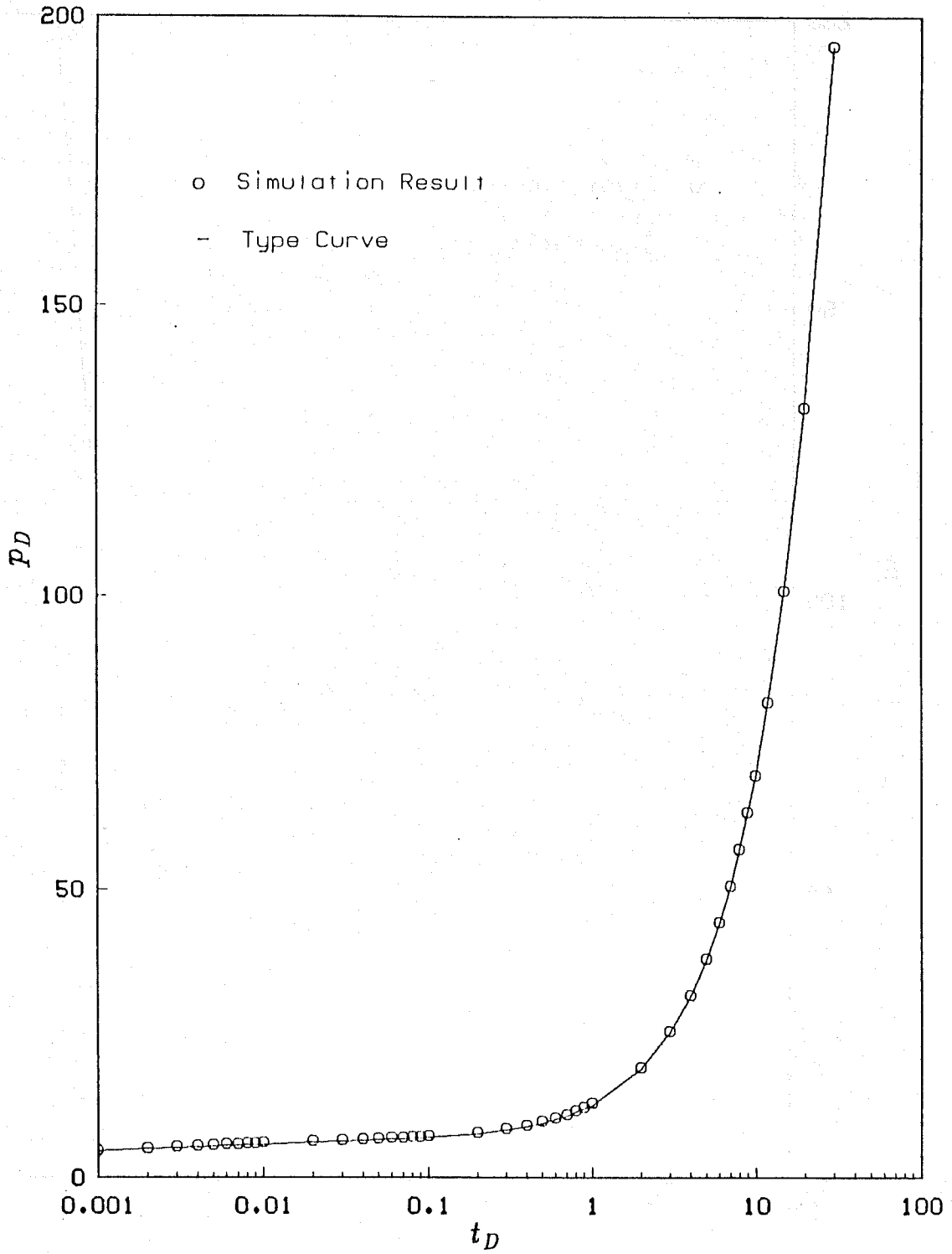


Fig. C.4 Dimensionless Pressure Solution for a Well in a Closed, Square Reservoir (One-Quarter Reservoir Simulation)

APPENDIX D

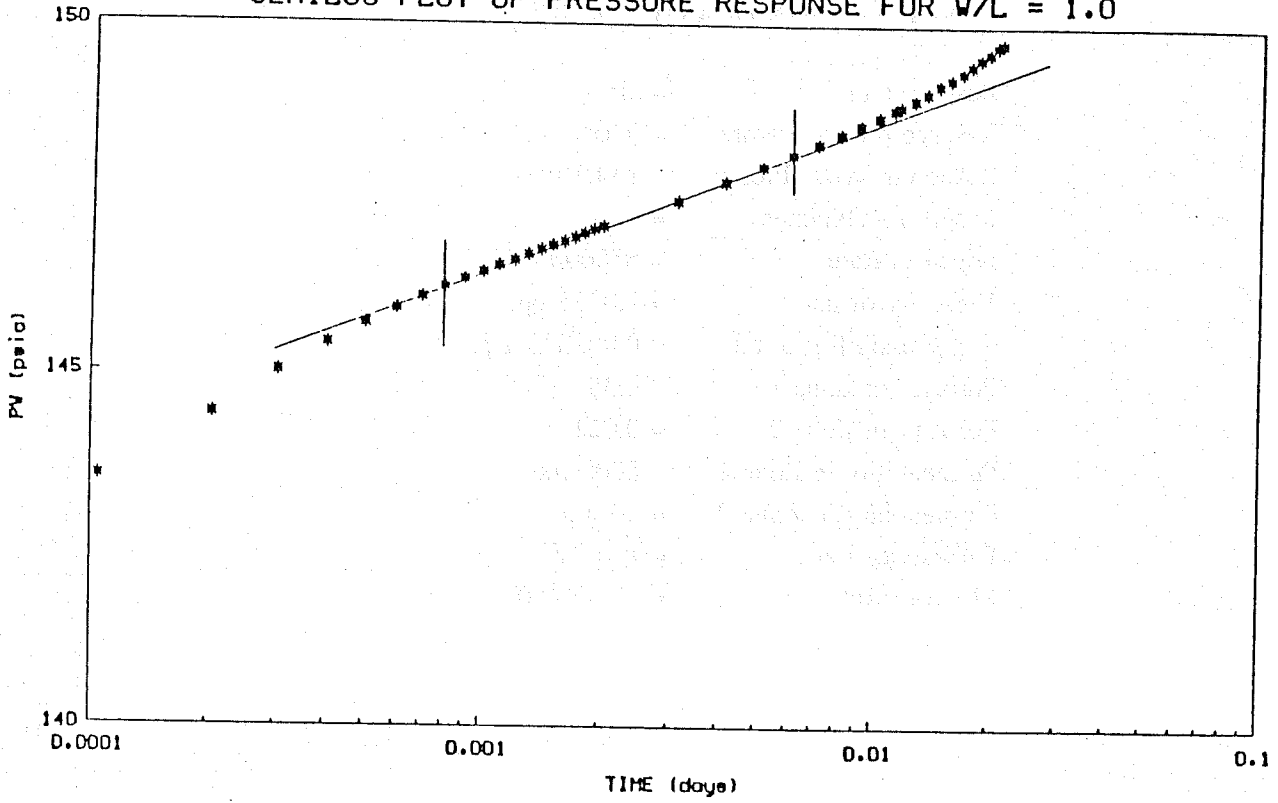
FLUID AND ROCK PROPERTIES USED FOR SIMULATION RUNS

Reservoir Fluid	= air
Reservoir Temperature	= 500°F
Reservoir Initial Pressure	= 134.5 psia
Reservoir Thickness	= 30 ft
Injection Rate	= 650000 STB/D
Viscosity of air	= 0.0275 cp
Compressibility of air	= 0.003333 1/psi
Porosity in Zone 1	= 0.35
Porosity in Zone 2	= 0.021
Permeability in Zone 1	= 8000 md
Permeability in Zone 2	= 40 md
Diffusivity Ratio	= $\eta = 12.0$
Mobility Ratio	= $\lambda = 200.0$

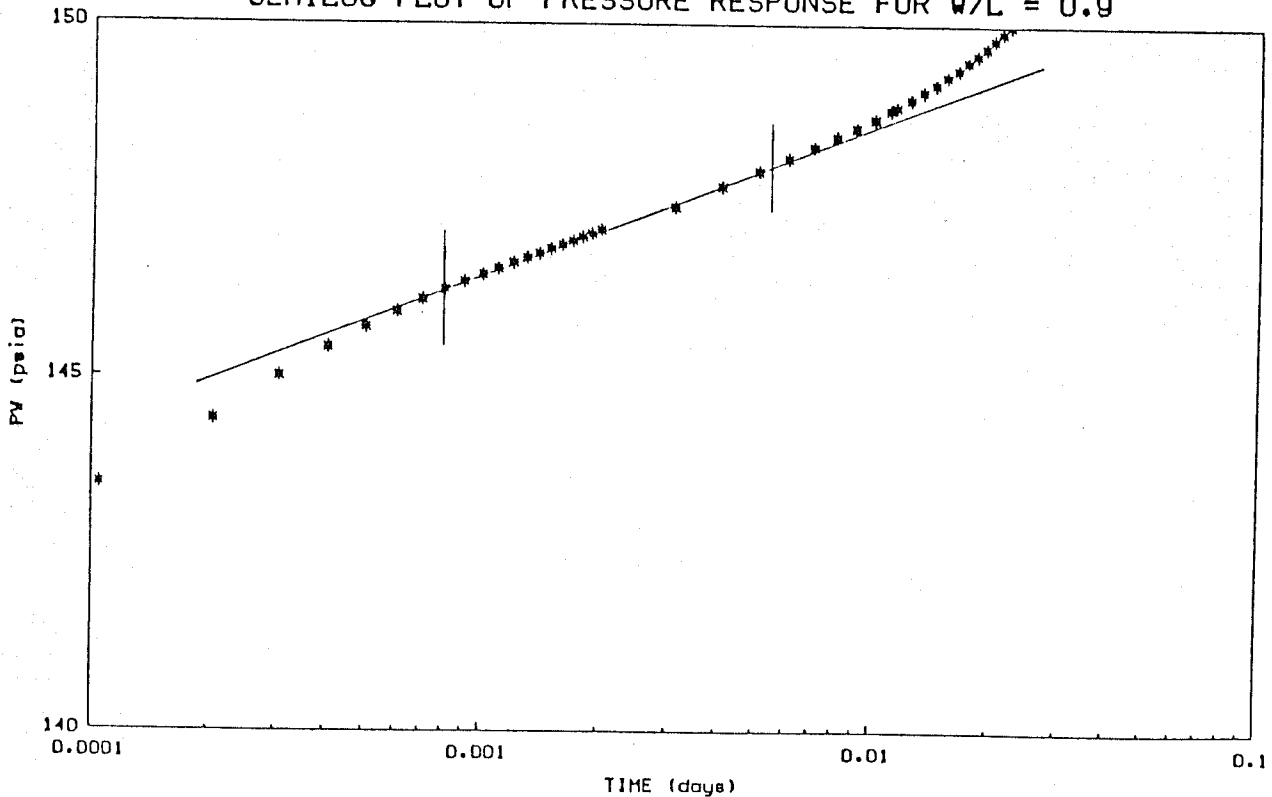
APPENDIX E

SEMILOG AND CARTESIAN PLOTS OF PRESSURE RESPONSES

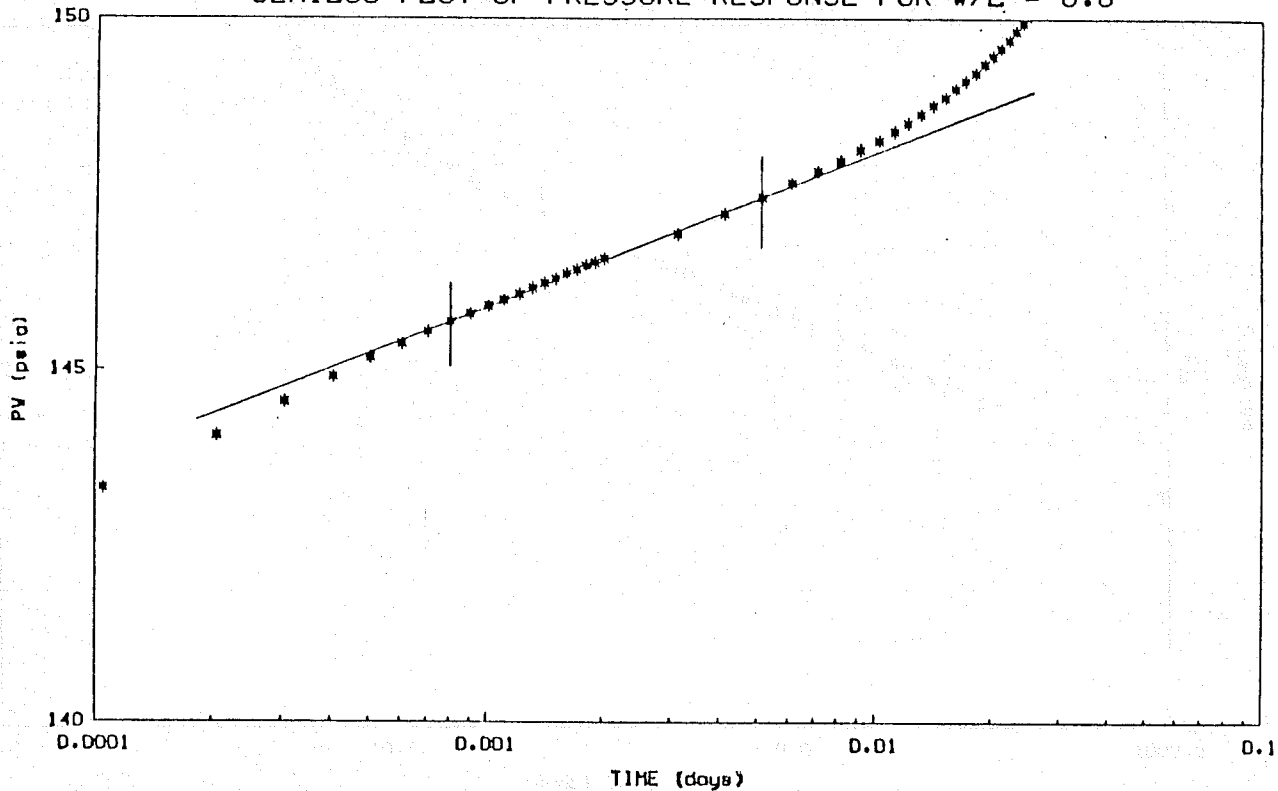
SEMILOG PLOT OF PRESSURE RESPONSE FOR W/L = 1.0



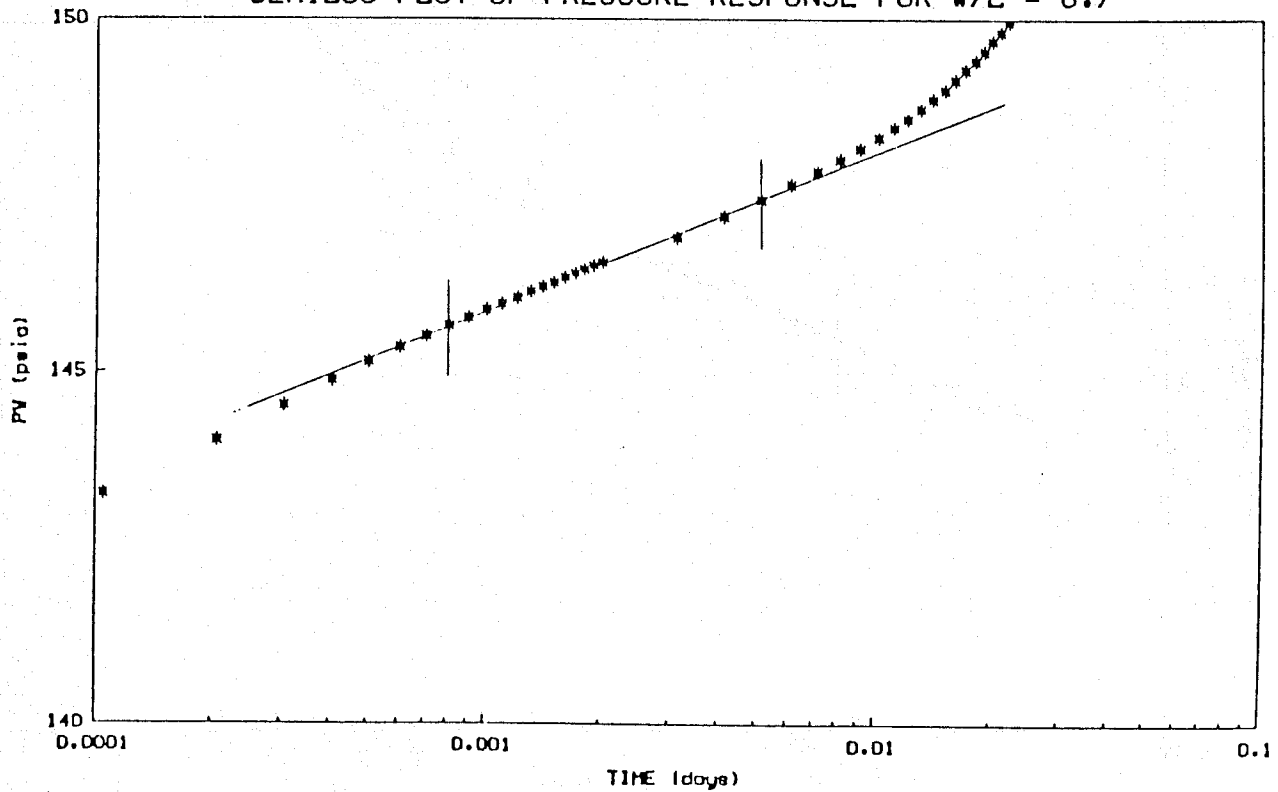
SEMILOG PLOT OF PRESSURE RESPONSE FOR W/L = 0.9



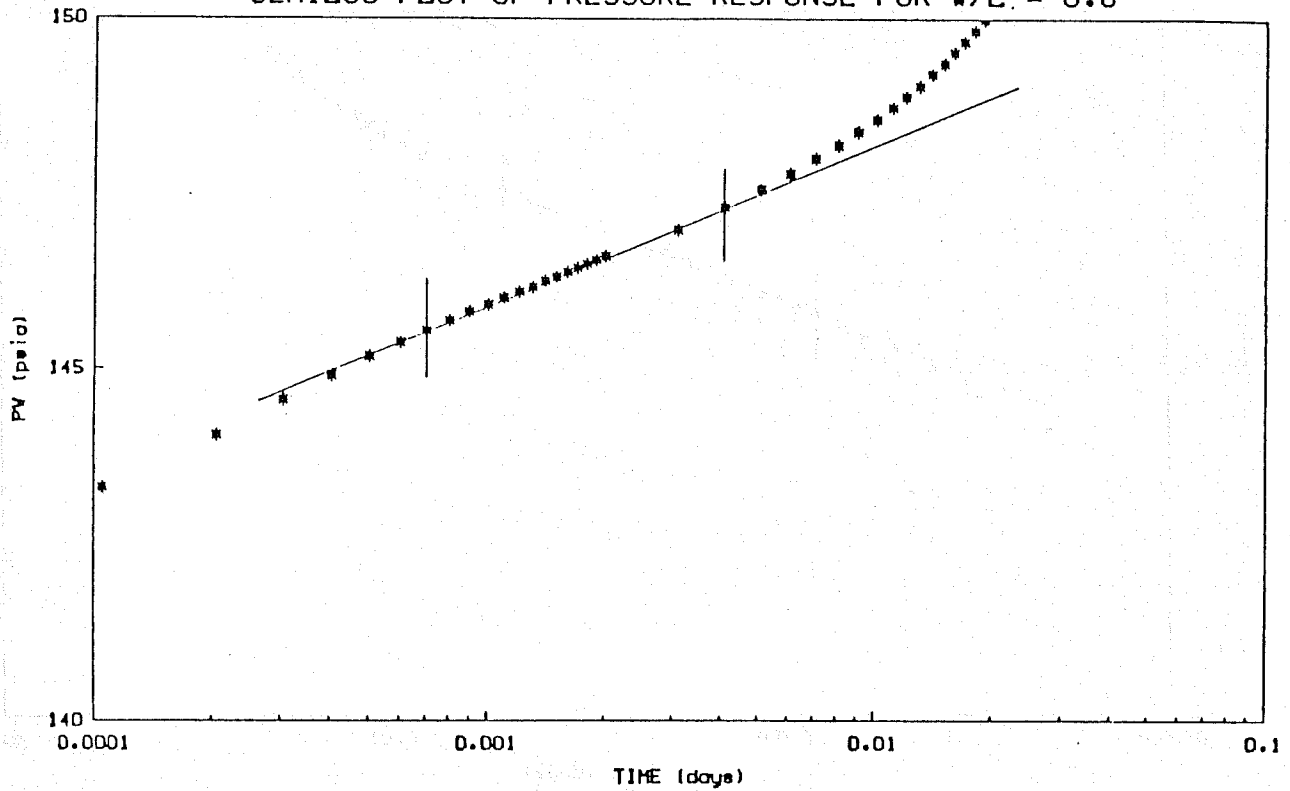
SEMILOG PLOT OF PRESSURE RESPONSE FOR W/L = 0.8



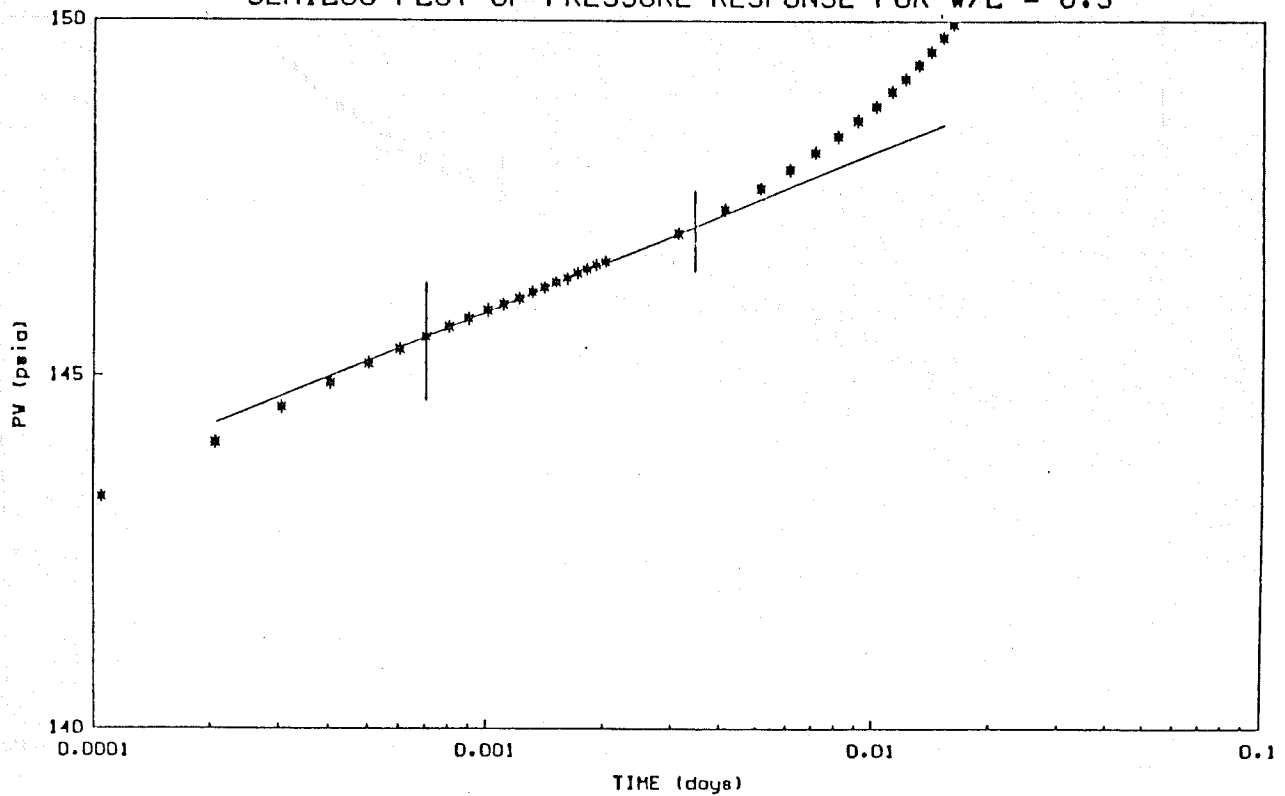
SEMILOG PLOT OF PRESSURE RESPONSE FOR W/L = 0.7



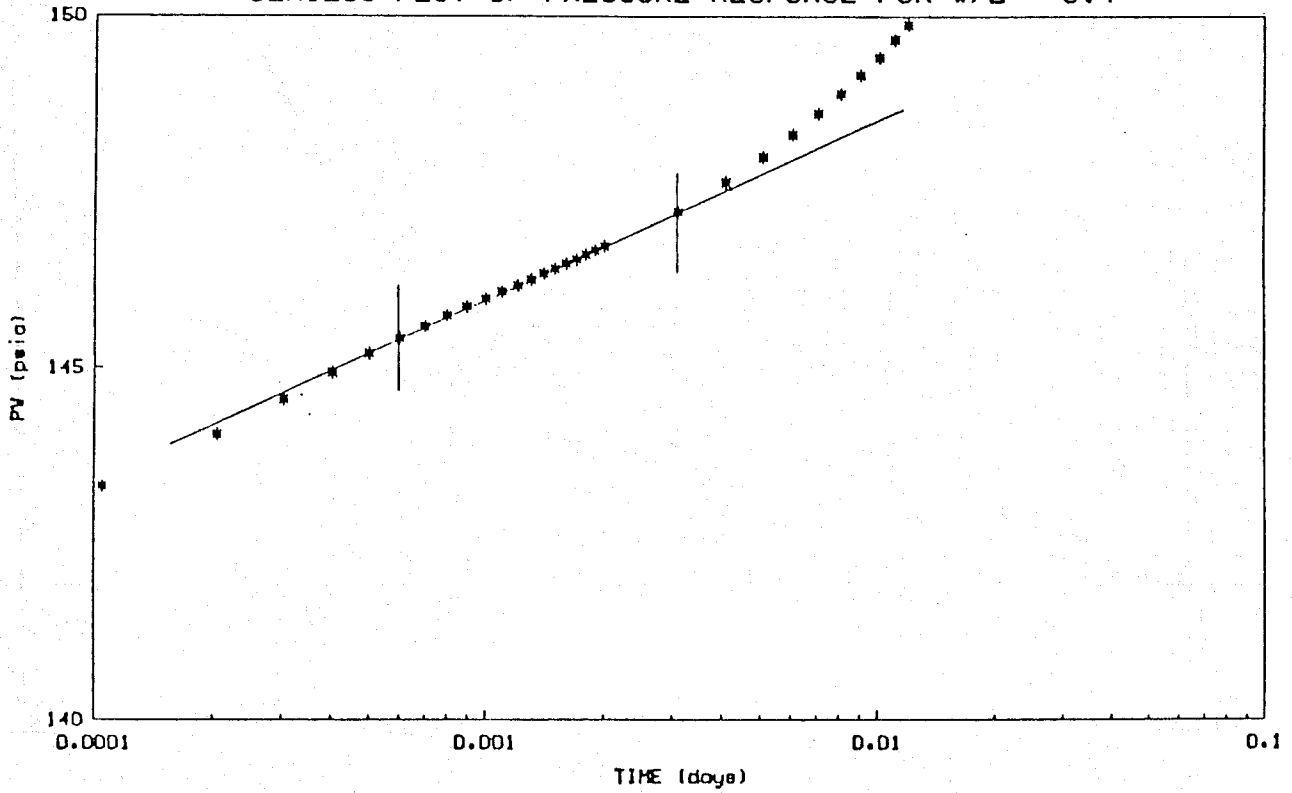
SEMILOG PLOT OF PRESSURE RESPONSE FOR W/L = 0.6



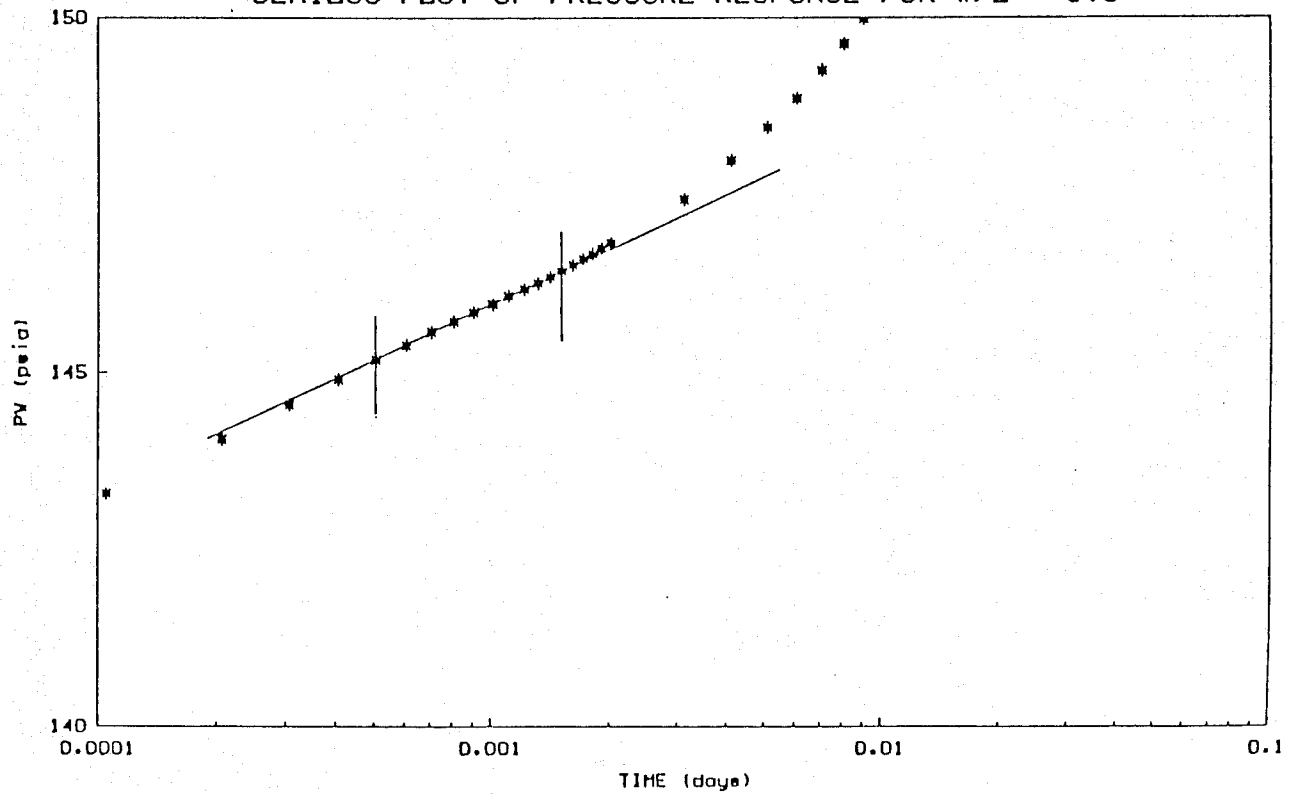
SEMILOG PLOT OF PRESSURE RESPONSE FOR W/L = 0.5



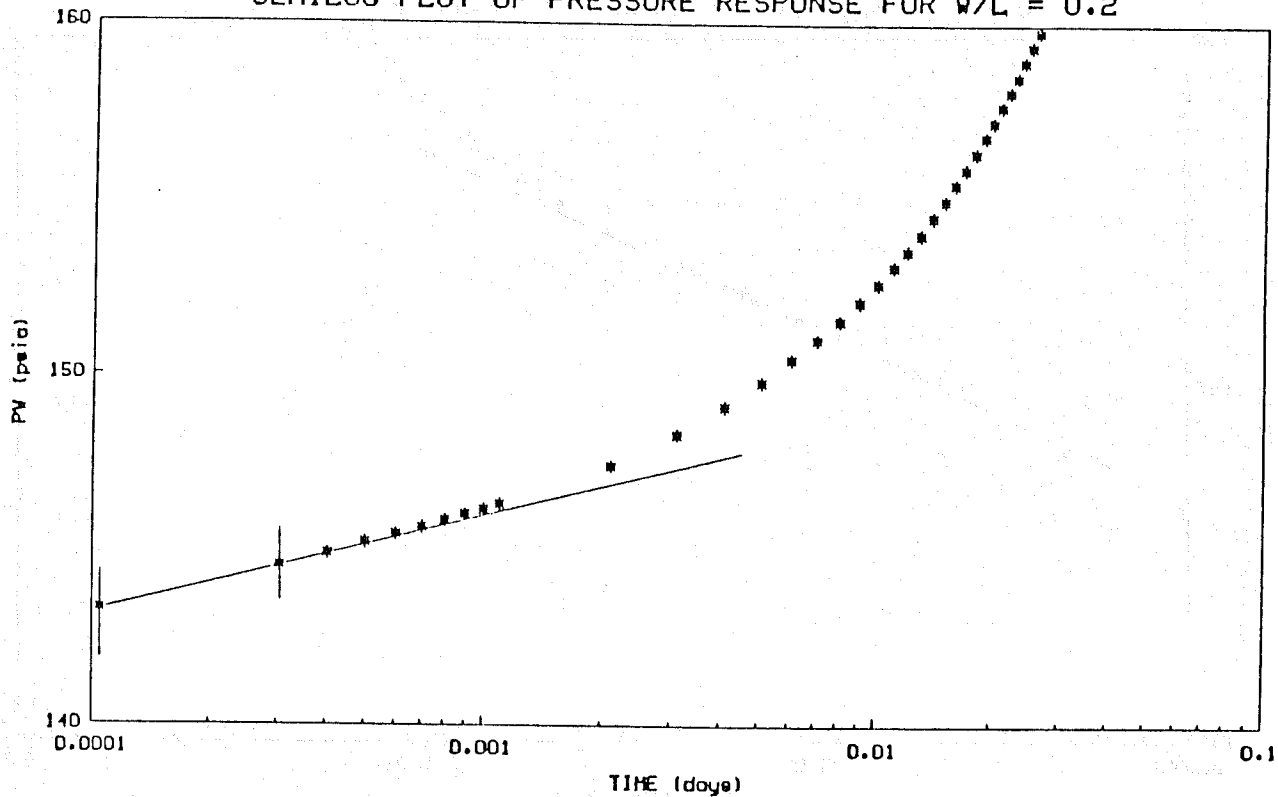
SEMILOG PLOT OF PRESSURE RESPONSE FOR W/L = 0.4



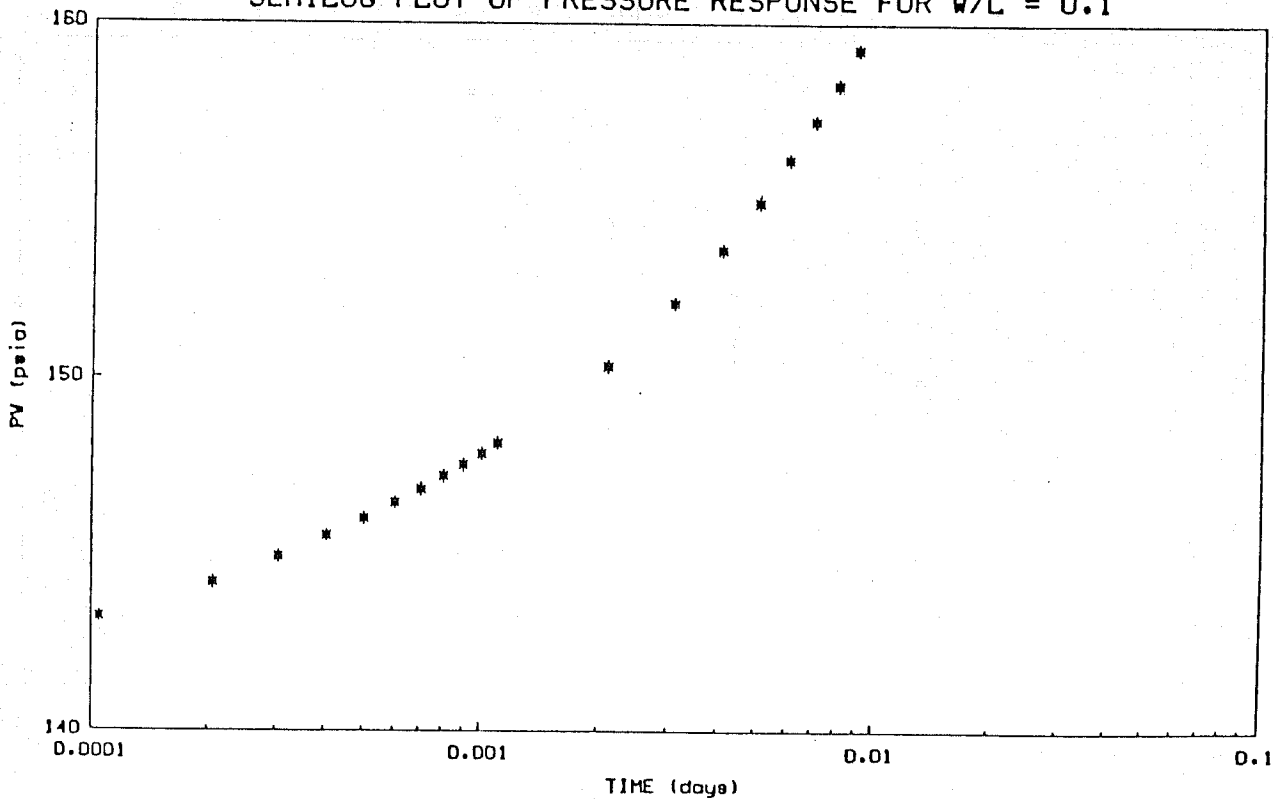
SEMILOG PLOT OF PRESSURE RESPONSE FOR W/L = 0.3



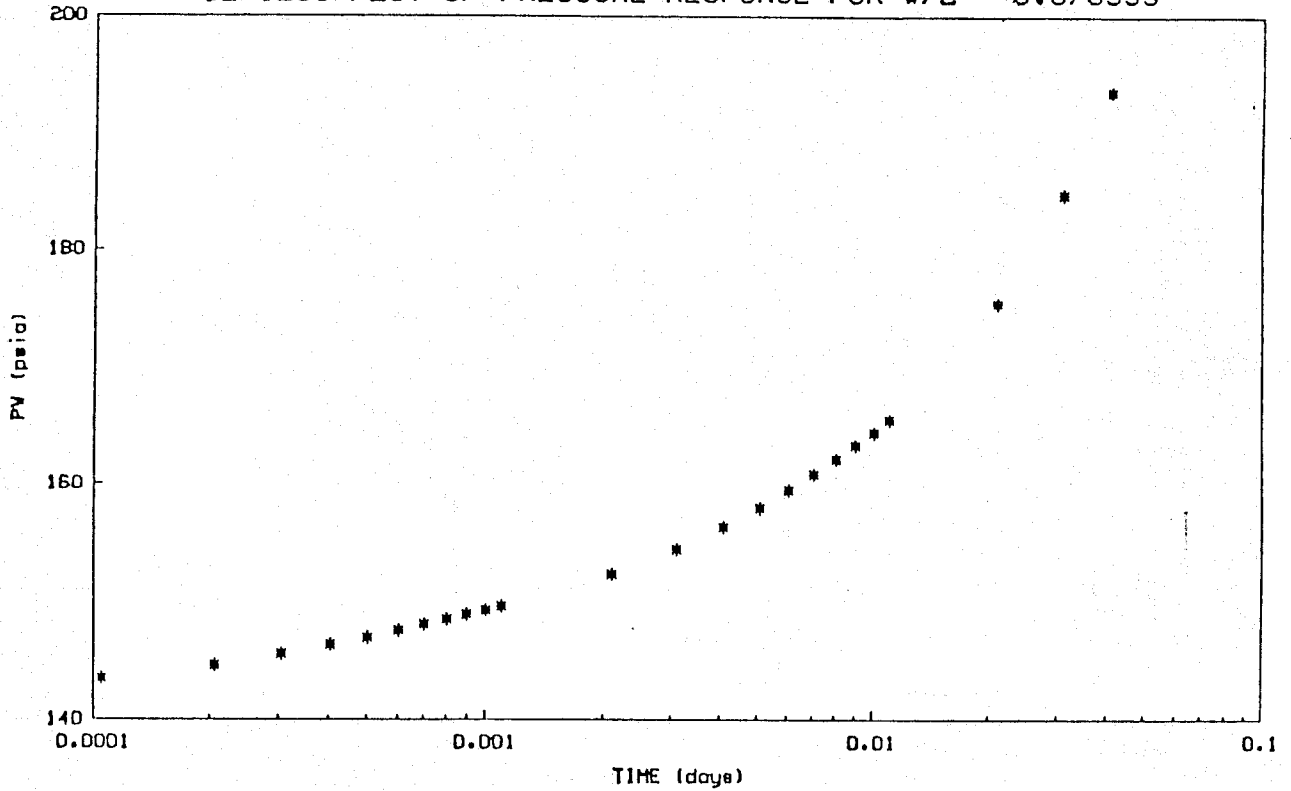
SEMILOG PLOT OF PRESSURE RESPONSE FOR W/L = 0.2



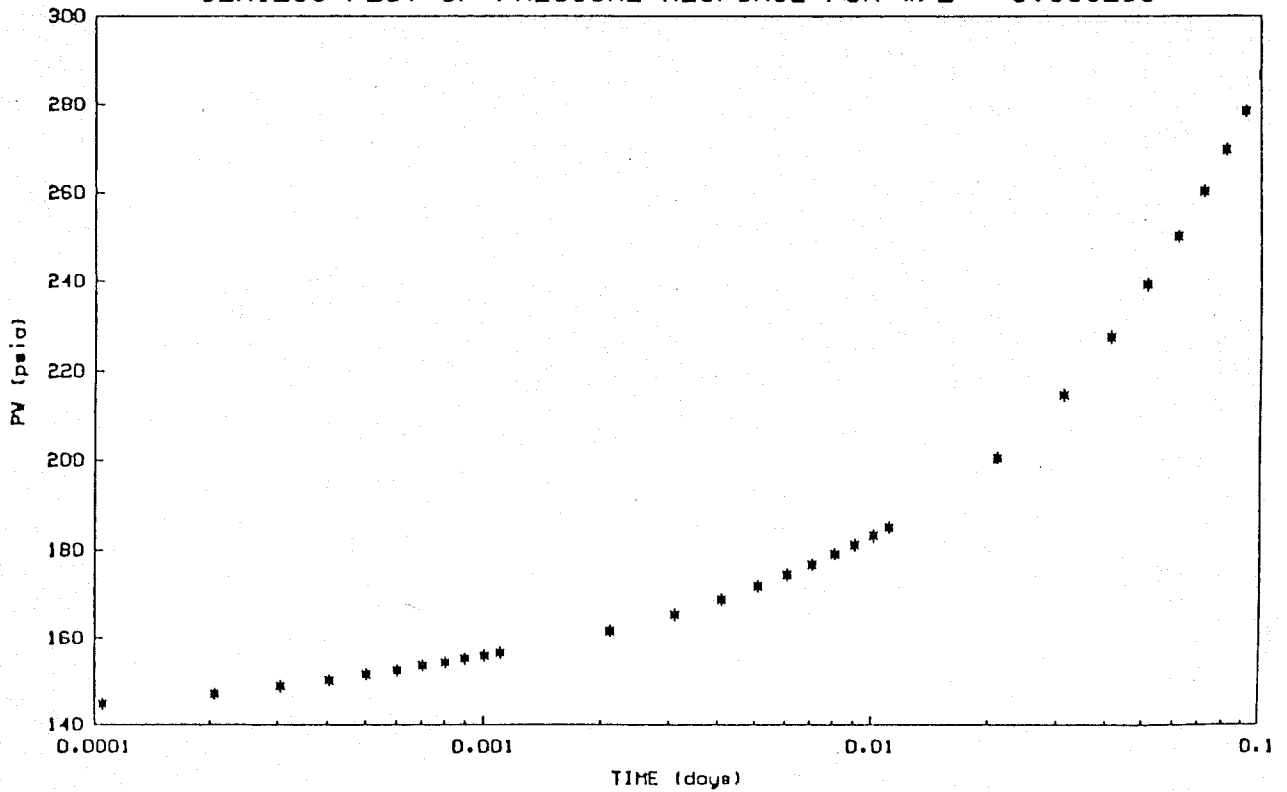
SEMILOG PLOT OF PRESSURE RESPONSE FOR W/L = 0.1



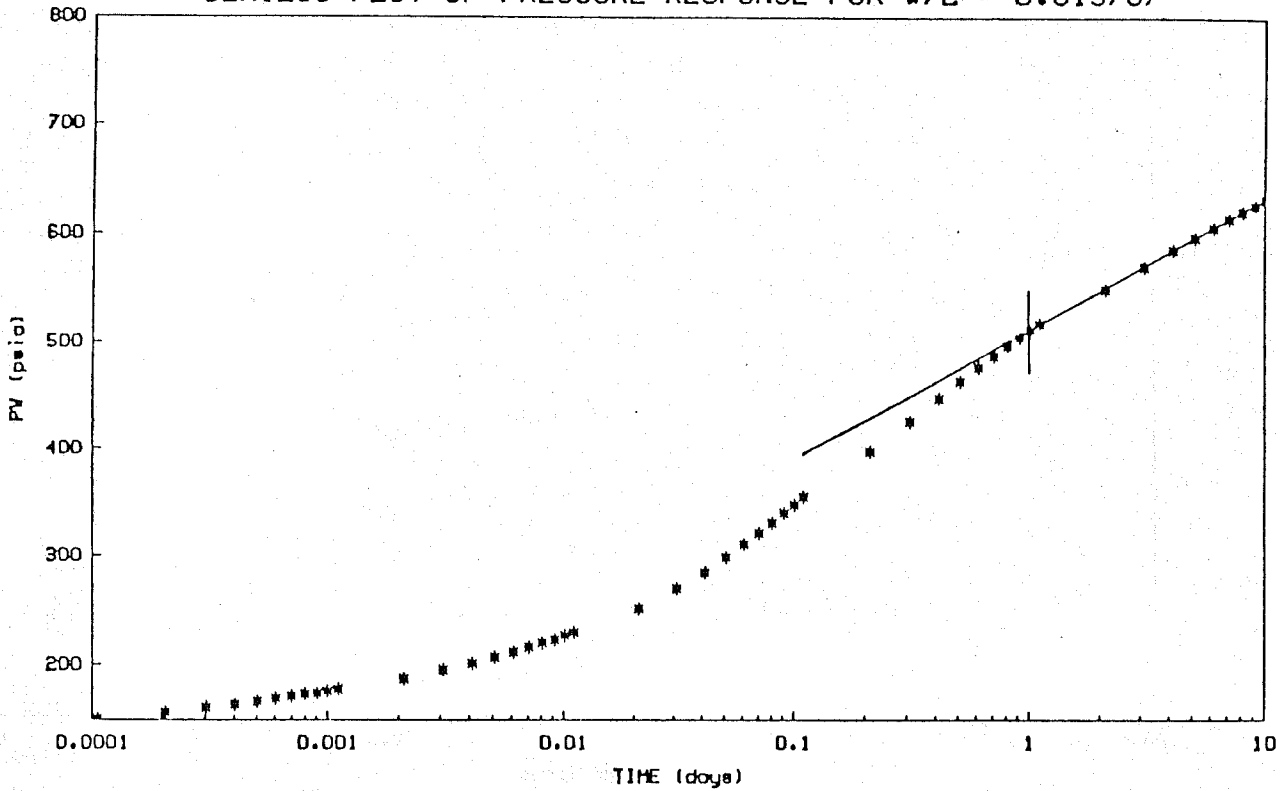
SEMILOG PLOT OF PRESSURE RESPONSE FOR W/L = 0.078539



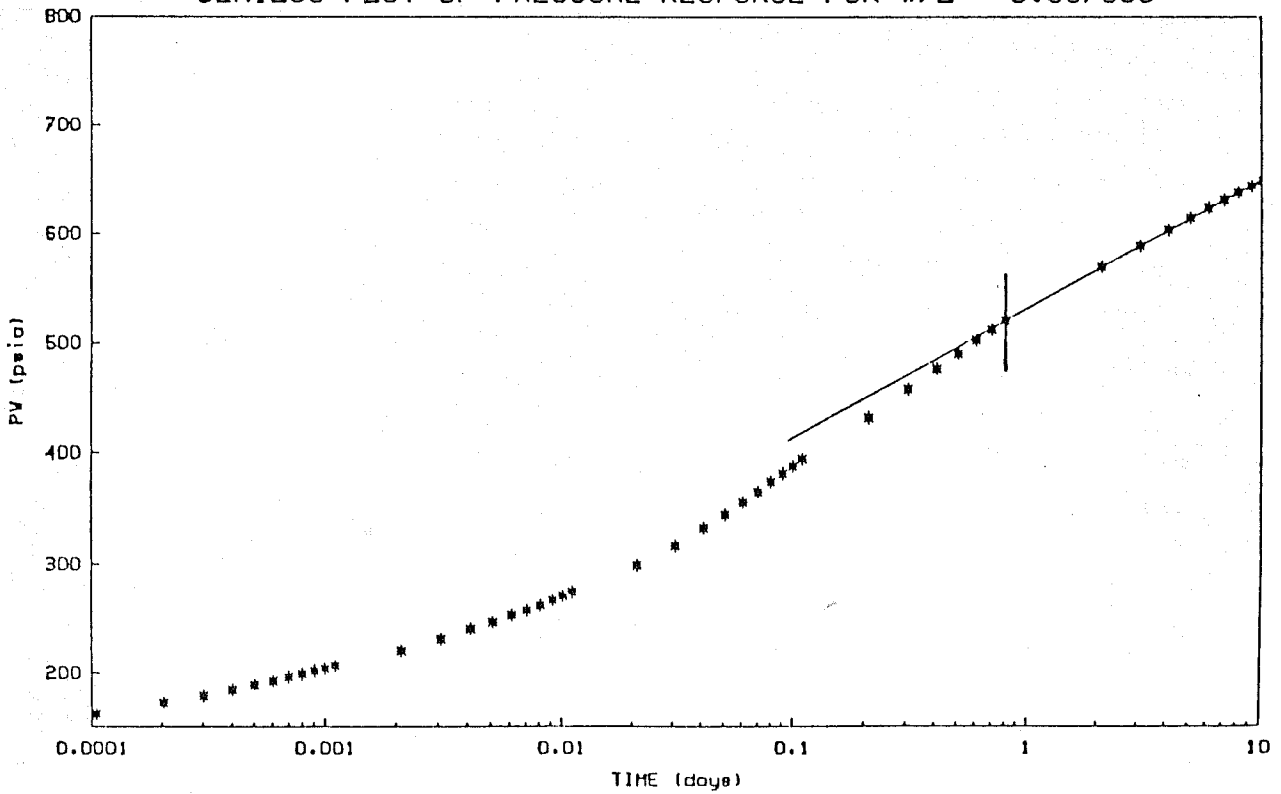
SEMILOG PLOT OF PRESSURE RESPONSE FOR W/L = 0.039269



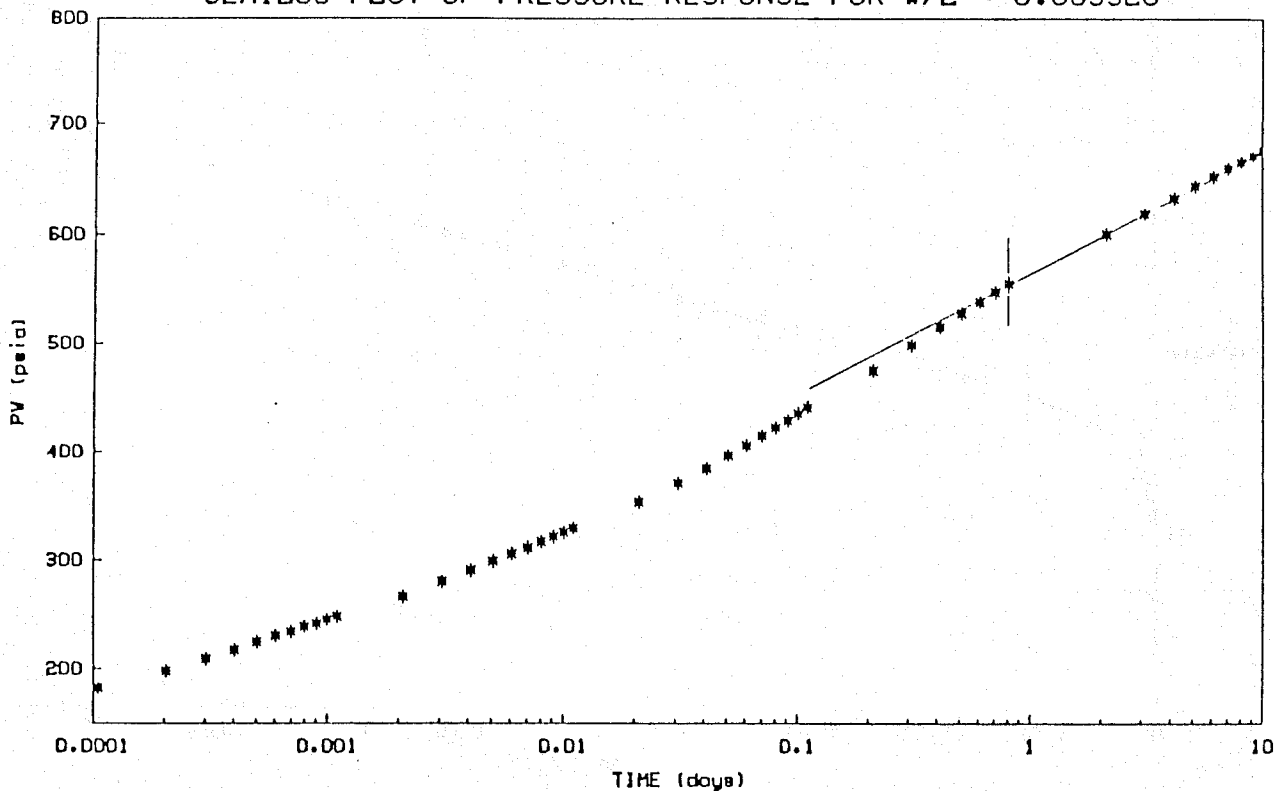
SEMILOG PLOT OF PRESSURE RESPONSE FOR W/L = 0.015707



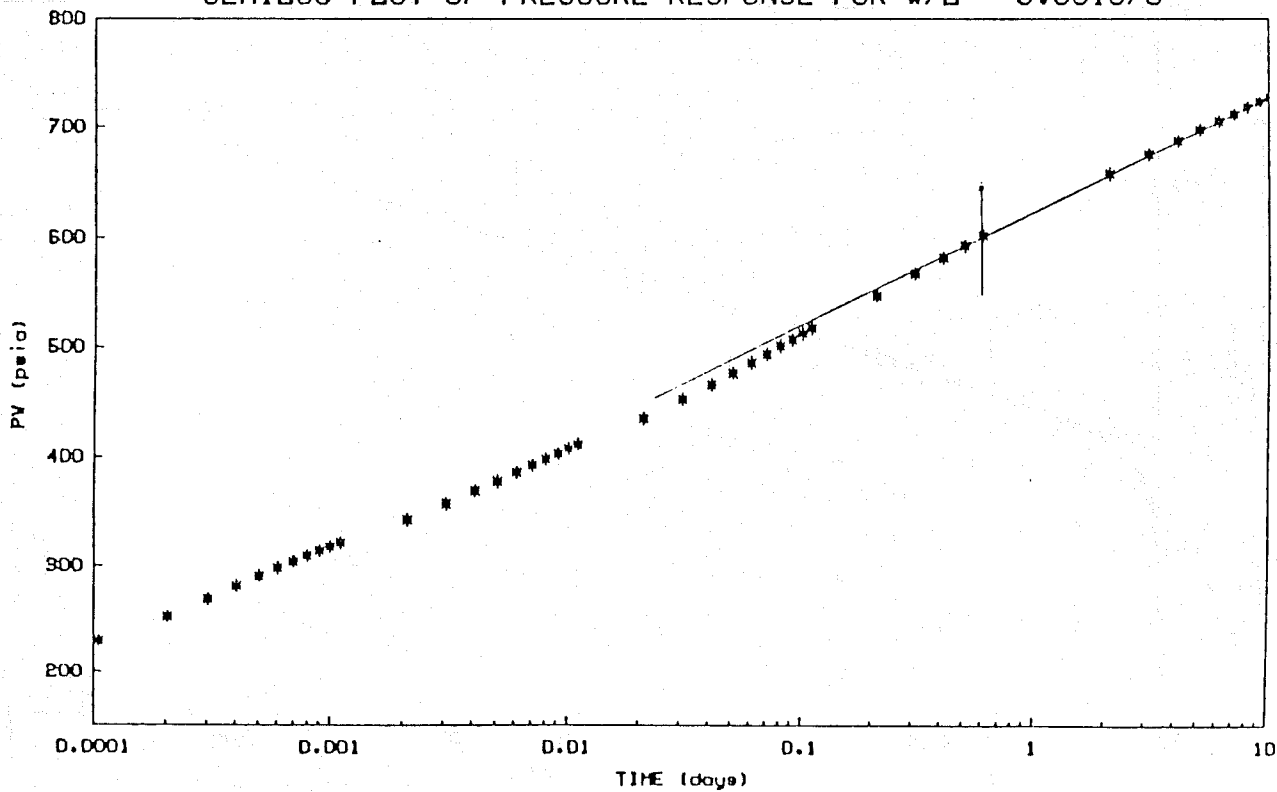
SEMILOG PLOT OF PRESSURE RESPONSE FOR W/L = 0.007853



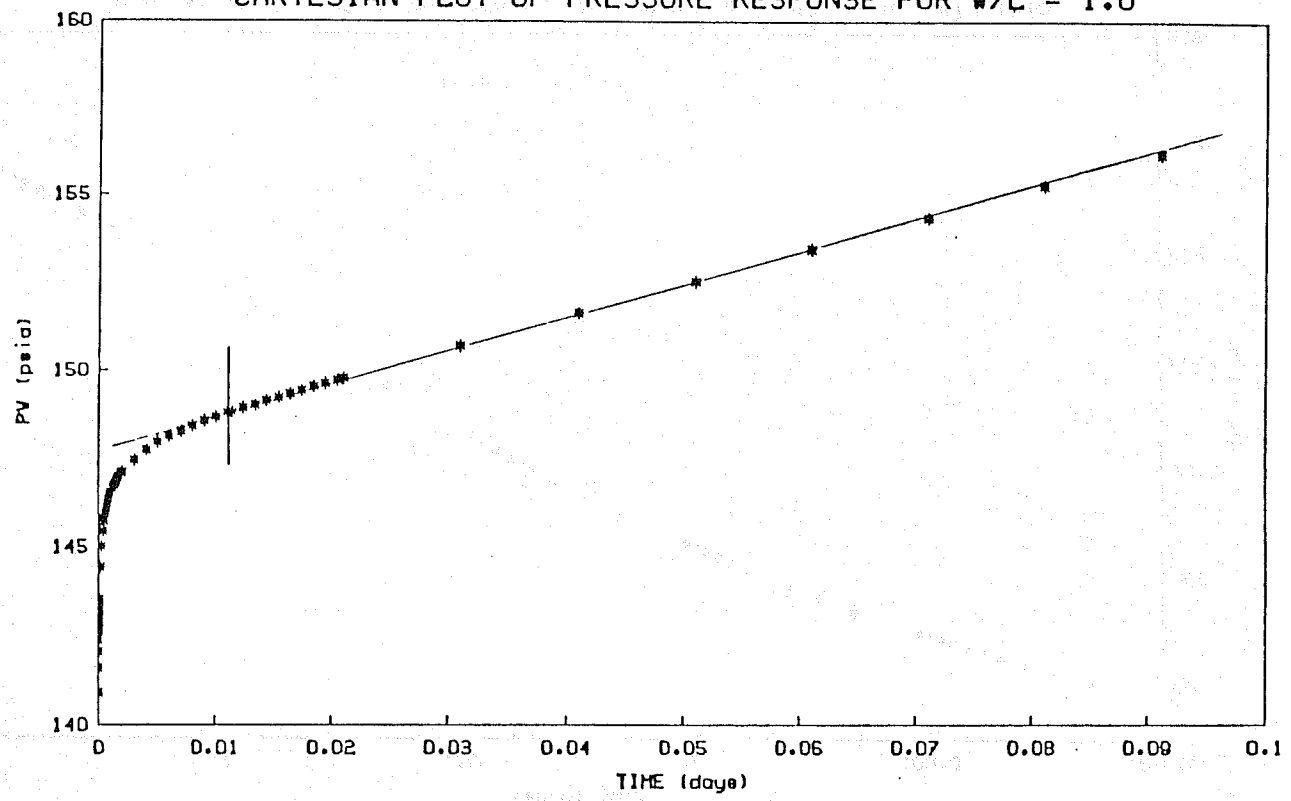
SEMILOG PLOT OF PRESSURE RESPONSE FOR W/L = 0.003926



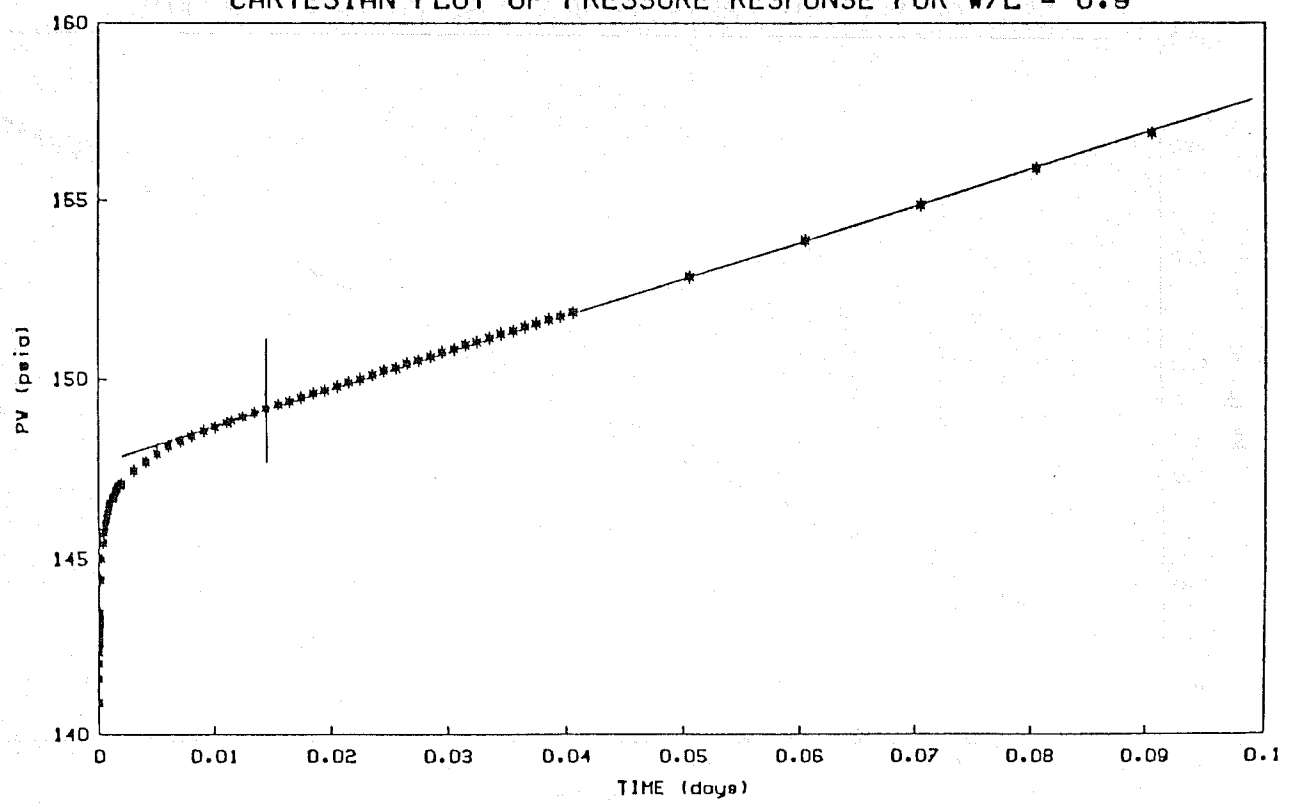
SEMILOG PLOT OF PRESSURE RESPONSE FOR W/L = 0.001570



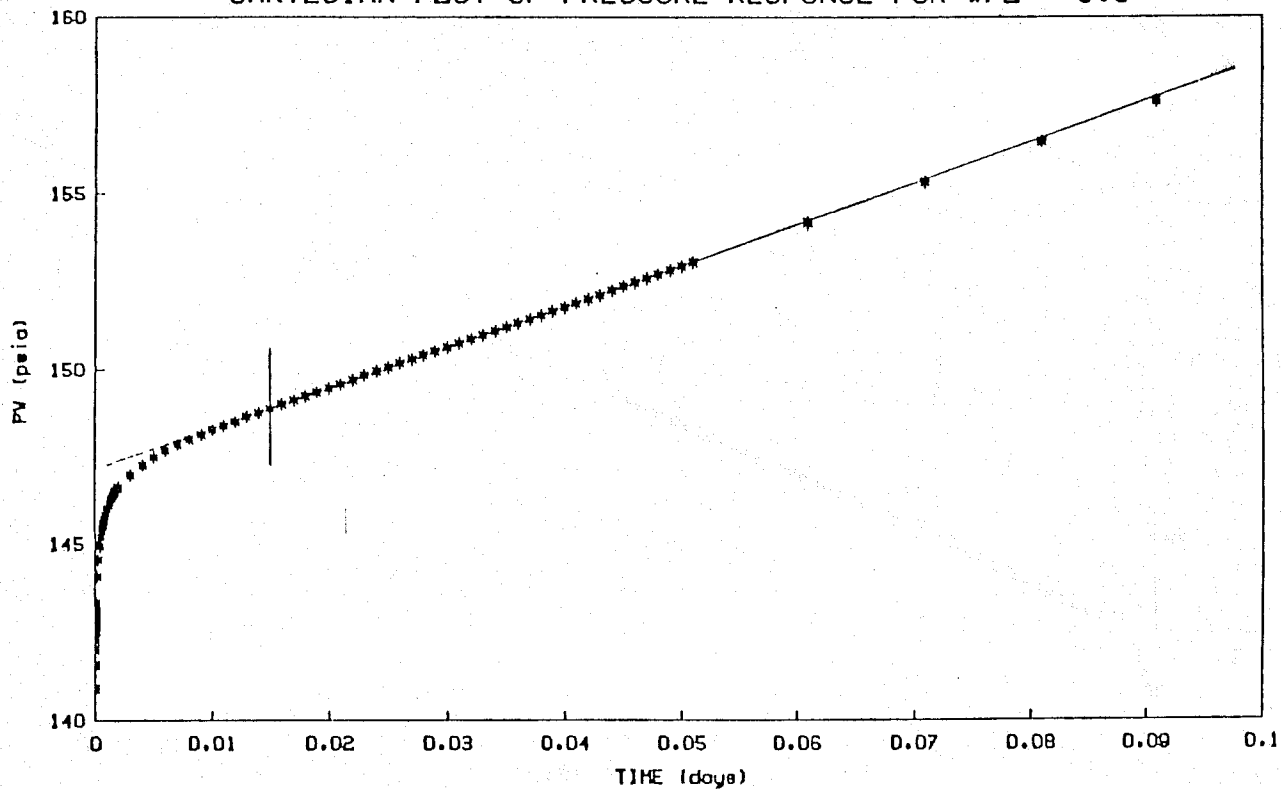
CARTESIAN PLOT OF PRESSURE RESPONSE FOR W/L = 1.0



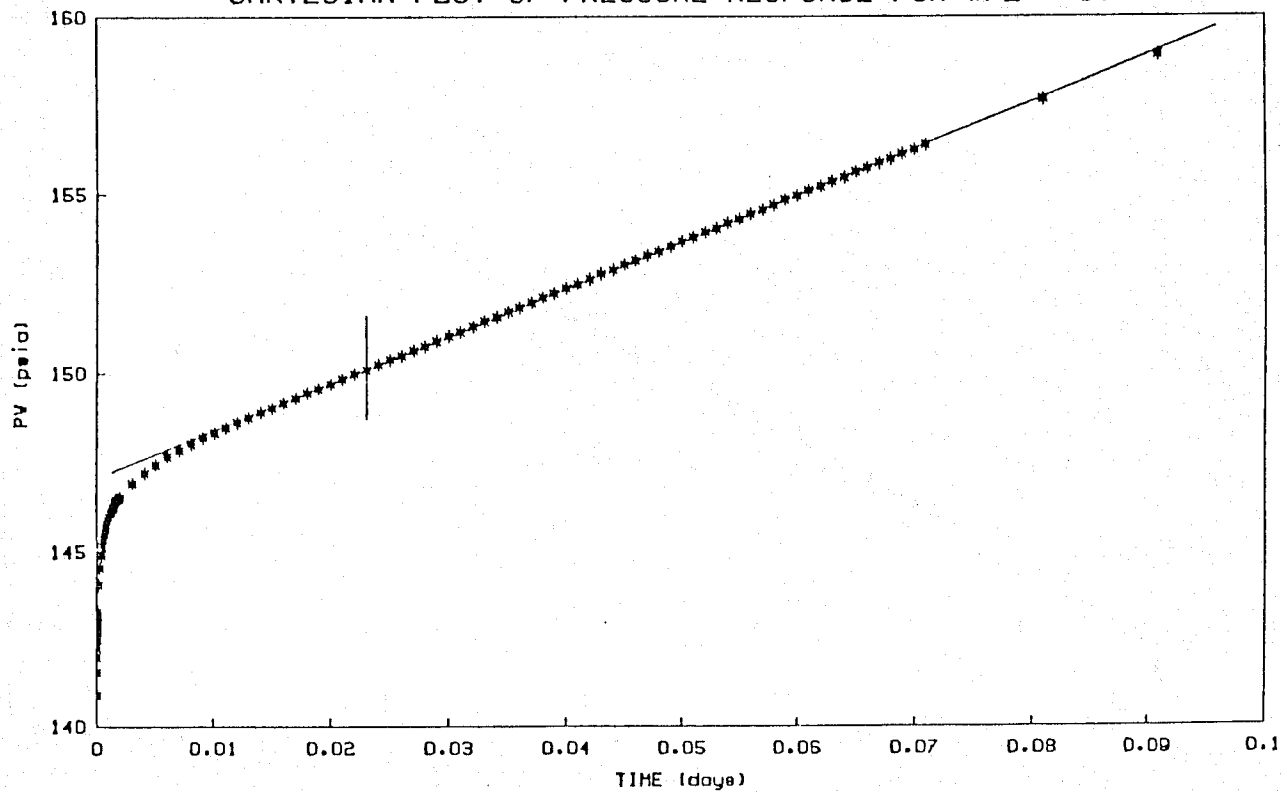
CARTESIAN PLOT OF PRESSURE RESPONSE FOR W/L = 0.9



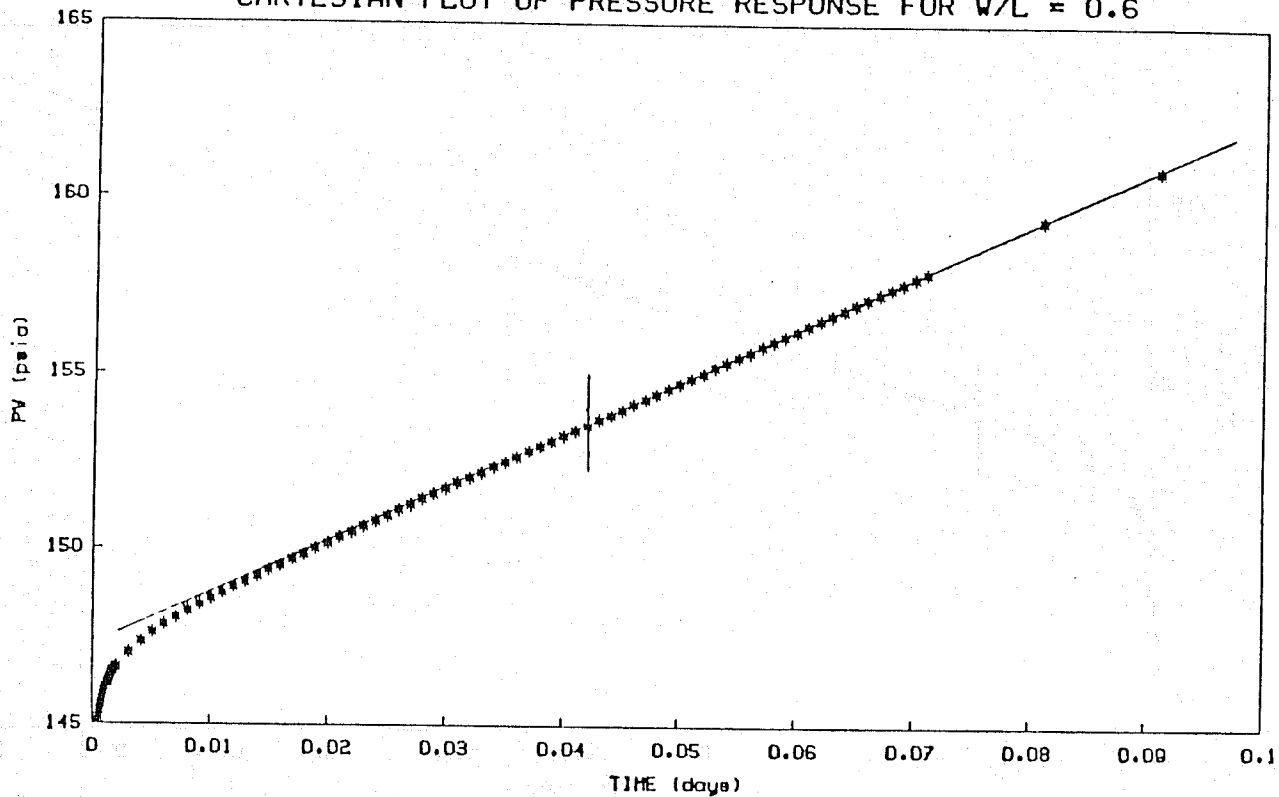
CARTESIAN PLOT OF PRESSURE RESPONSE FOR W/L = 0.8



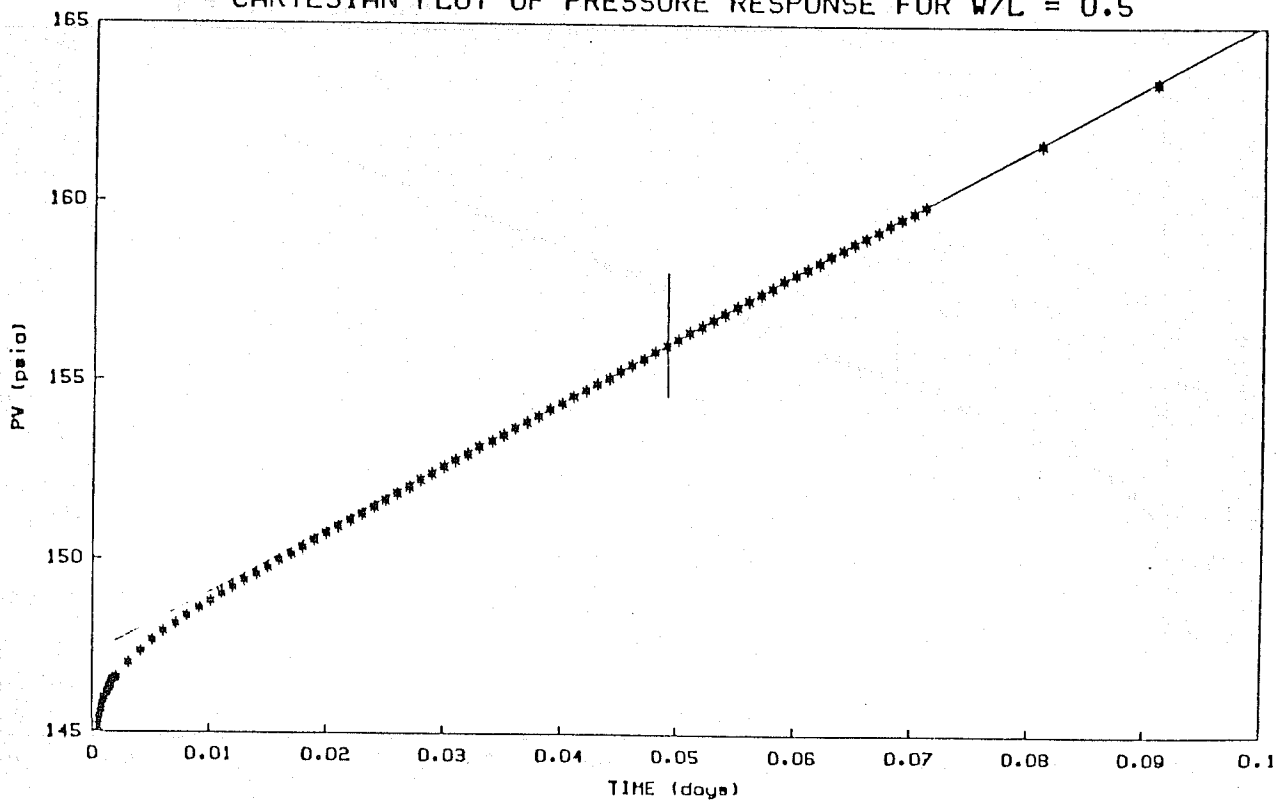
CARTESIAN PLOT OF PRESSURE RESPONSE FOR W/L = 0.7



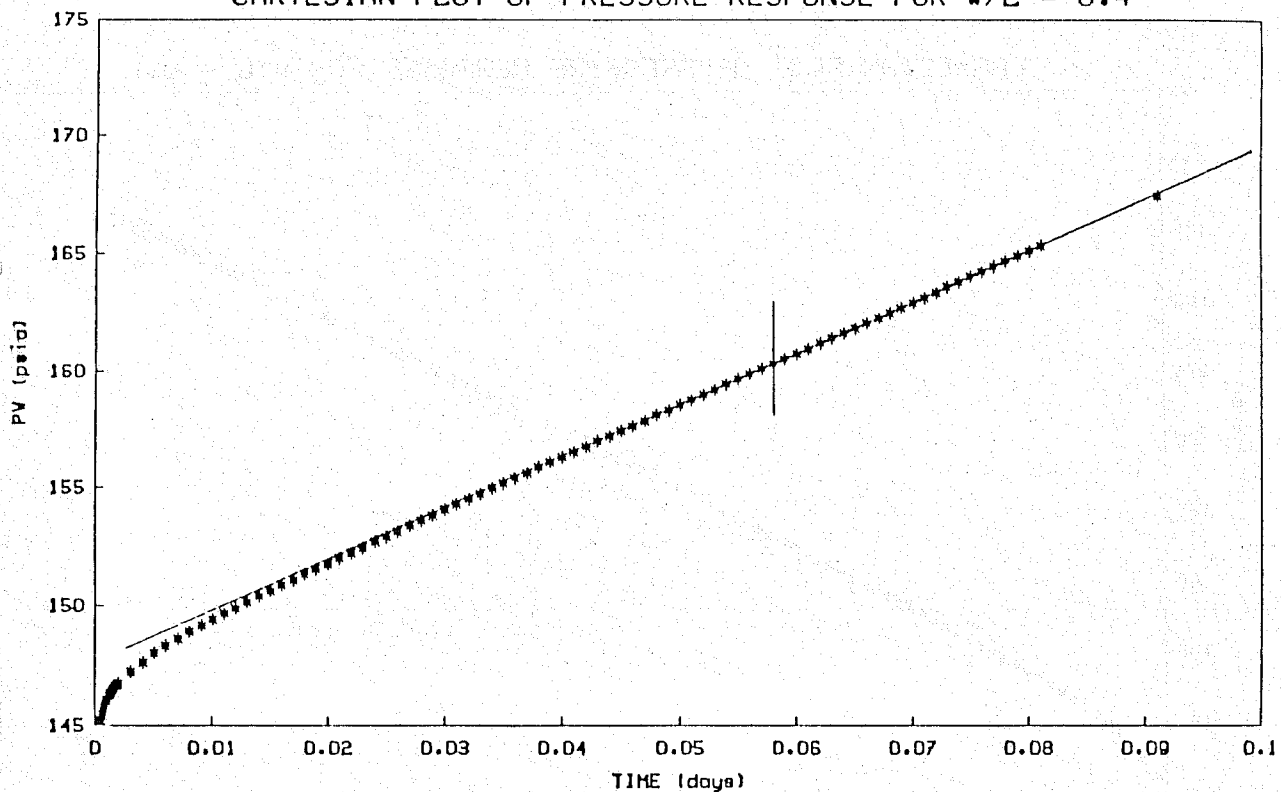
CARTESIAN PLOT OF PRESSURE RESPONSE FOR W/L = 0.6



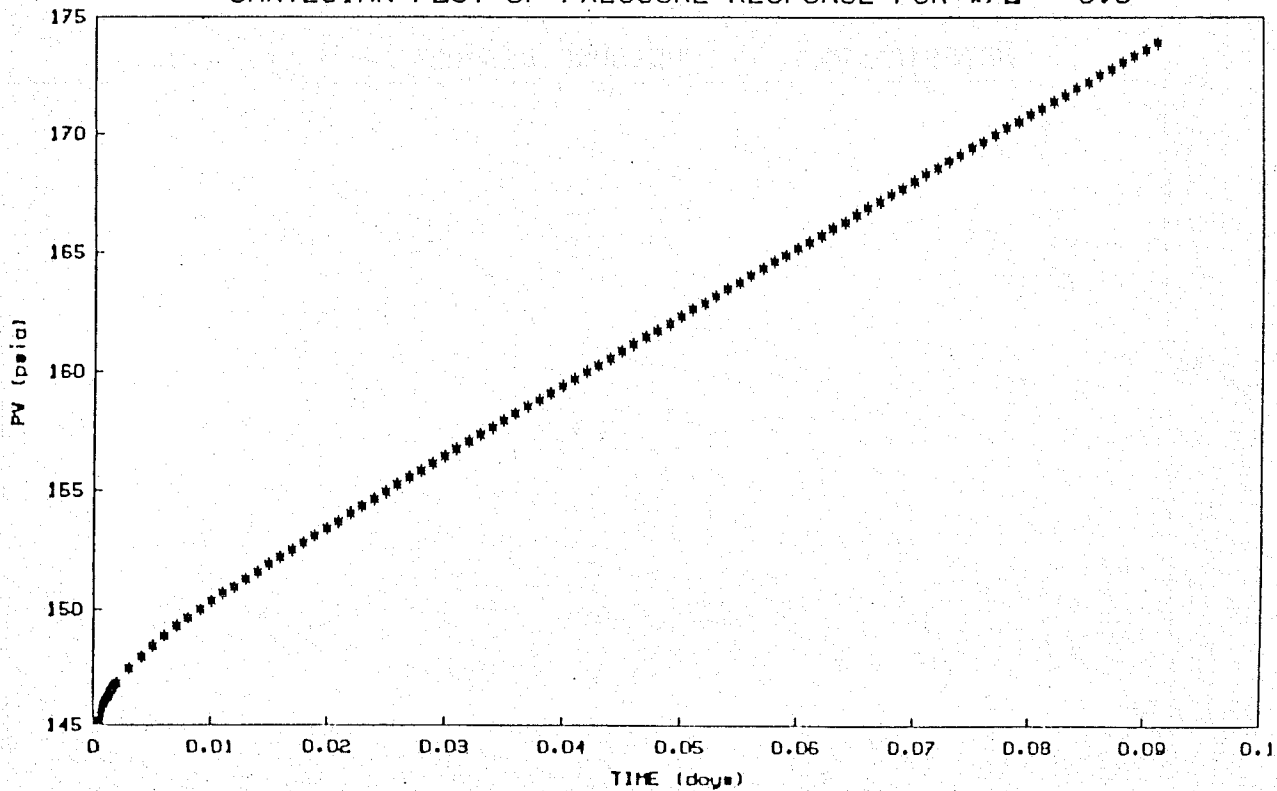
CARTESIAN PLOT OF PRESSURE RESPONSE FOR W/L = 0.5



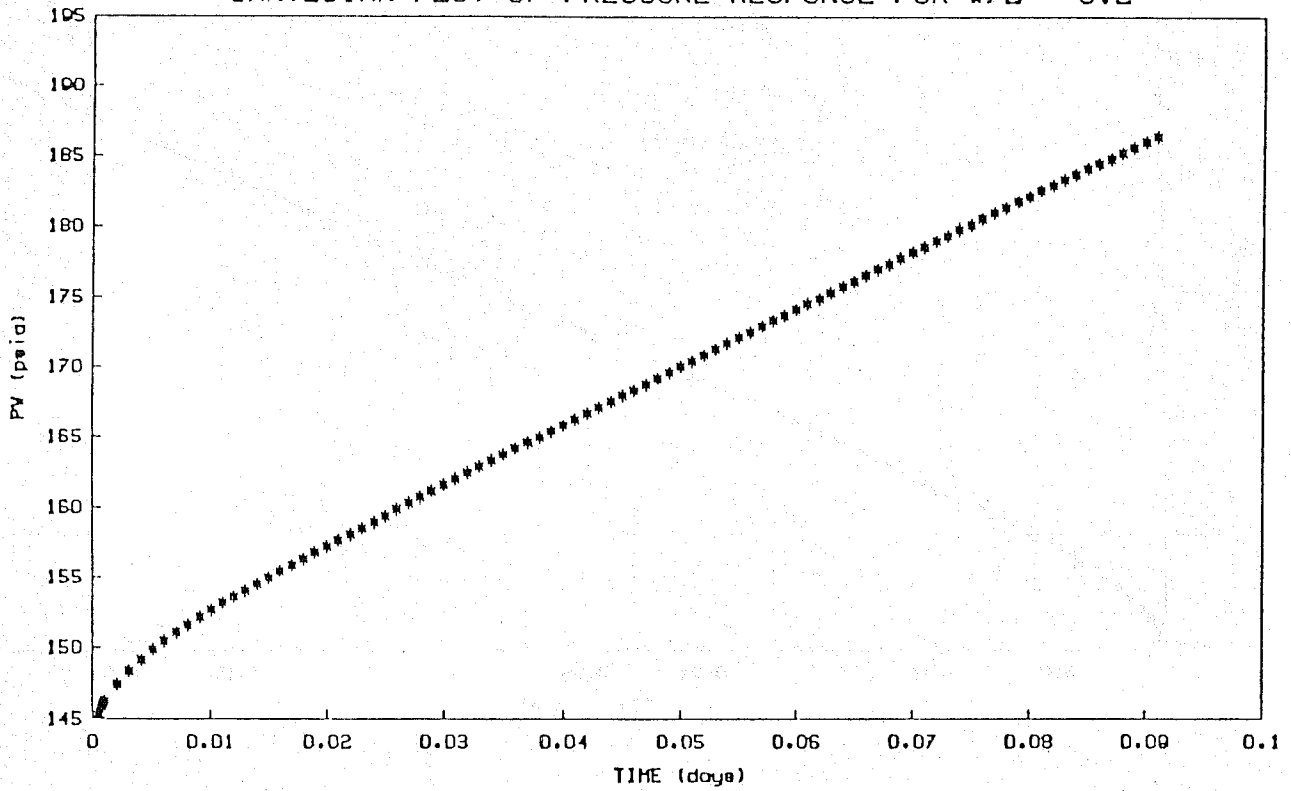
CARTESIAN PLOT OF PRESSURE RESPONSE FOR W/L = 0.4



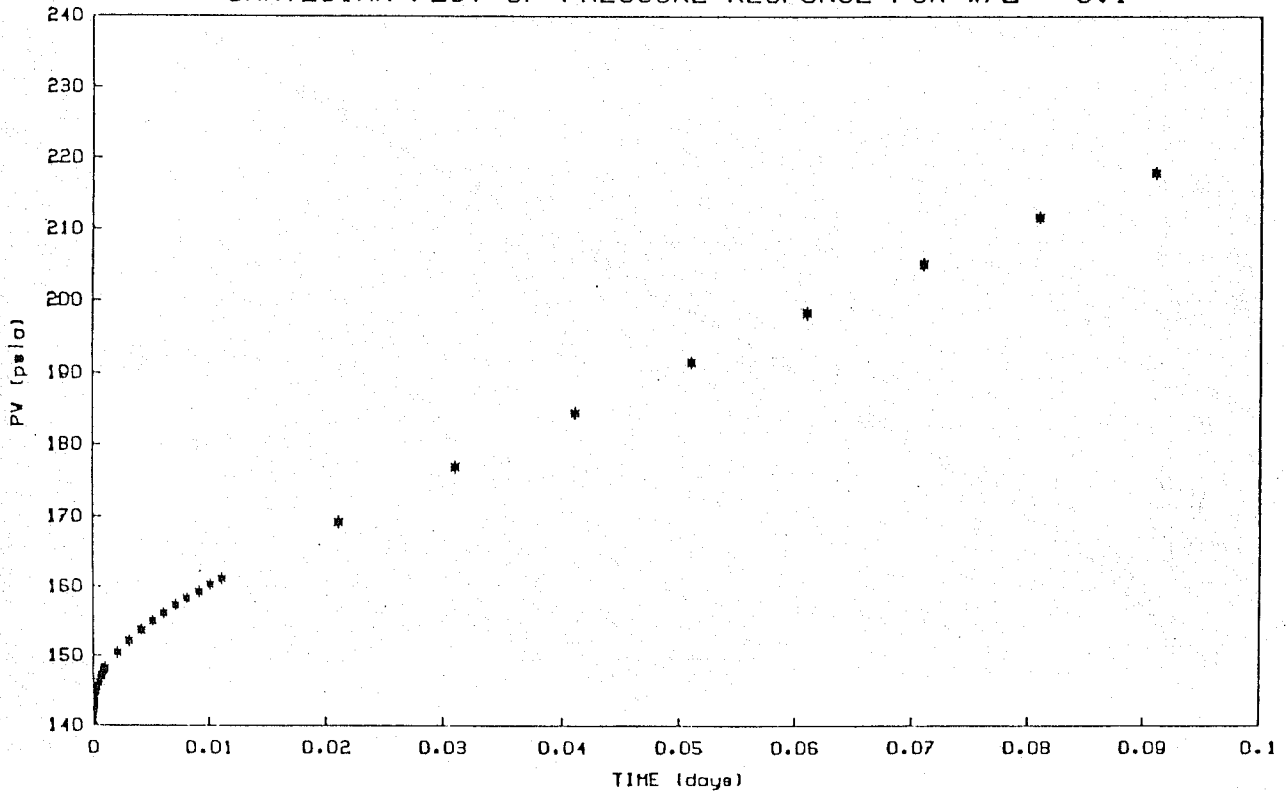
CARTESIAN PLOT OF PRESSURE RESPONSE FOR W/L = 0.3



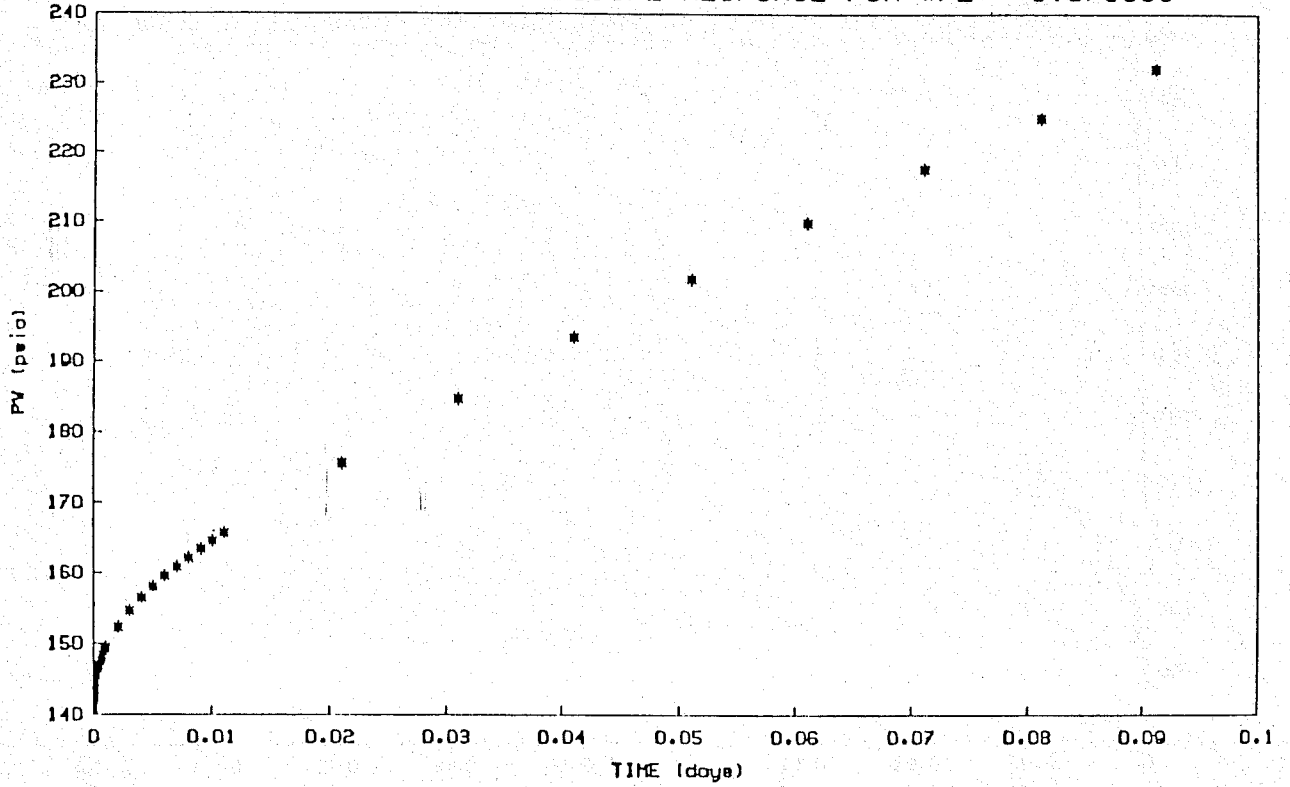
CARTESIAN PLOT OF PRESSURE RESPONSE FOR W/L = 0.2



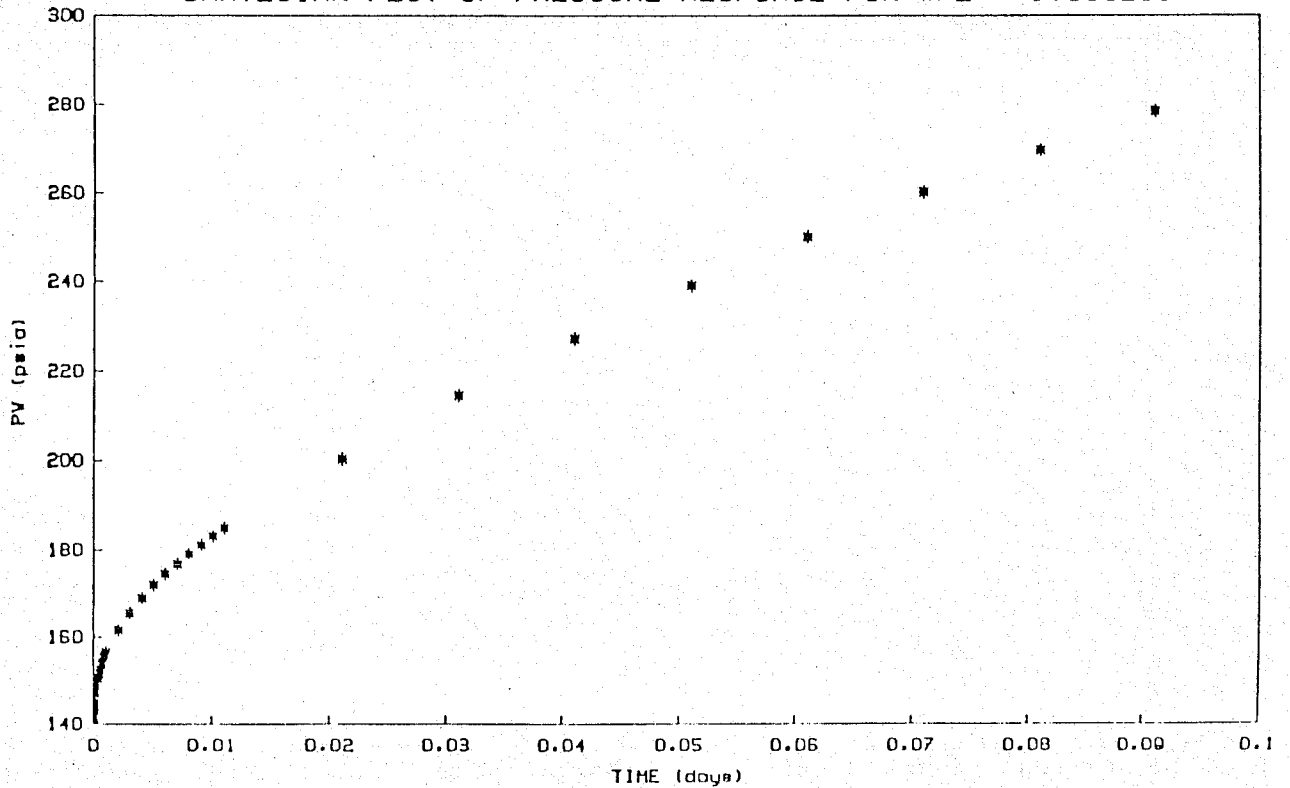
CARTESIAN PLOT OF PRESSURE RESPONSE FOR W/L = 0.1



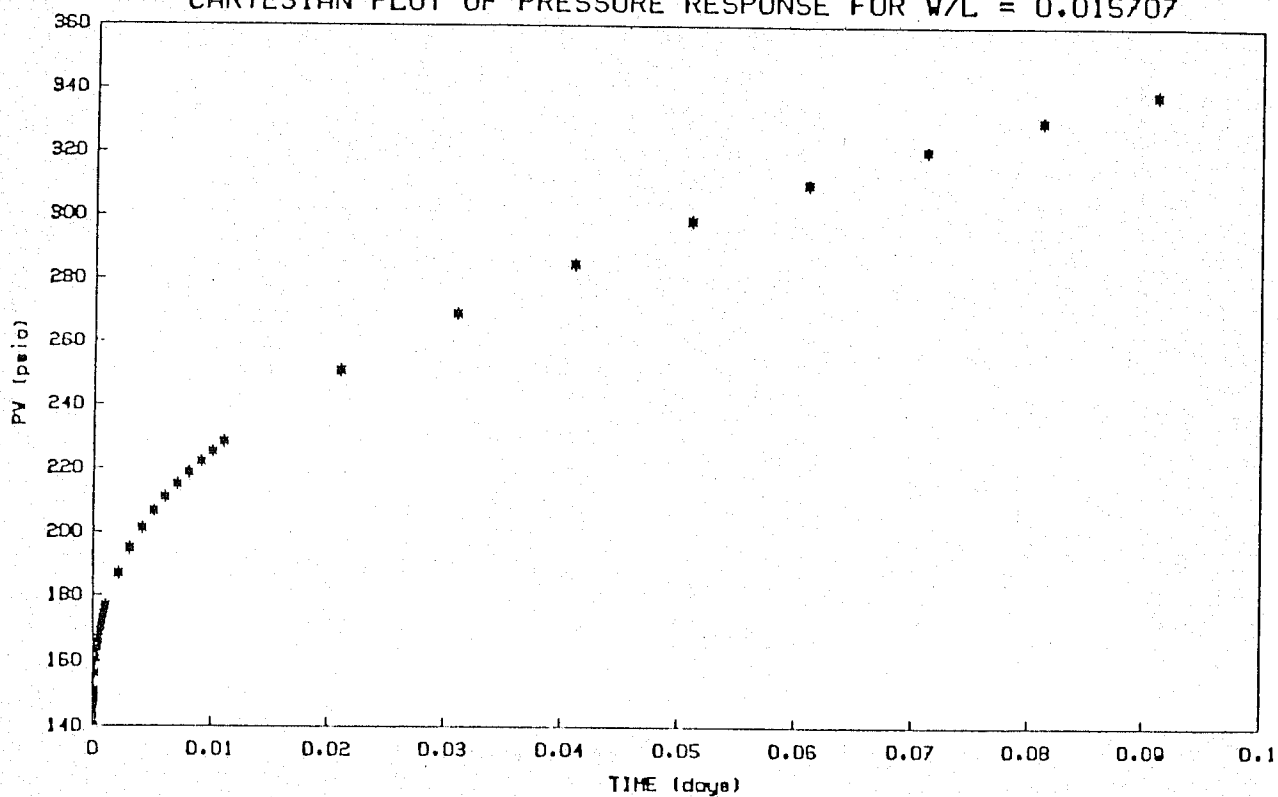
CARTESIAN PLOT OF PRESSURE RESPONSE FOR W/L = 0.078539



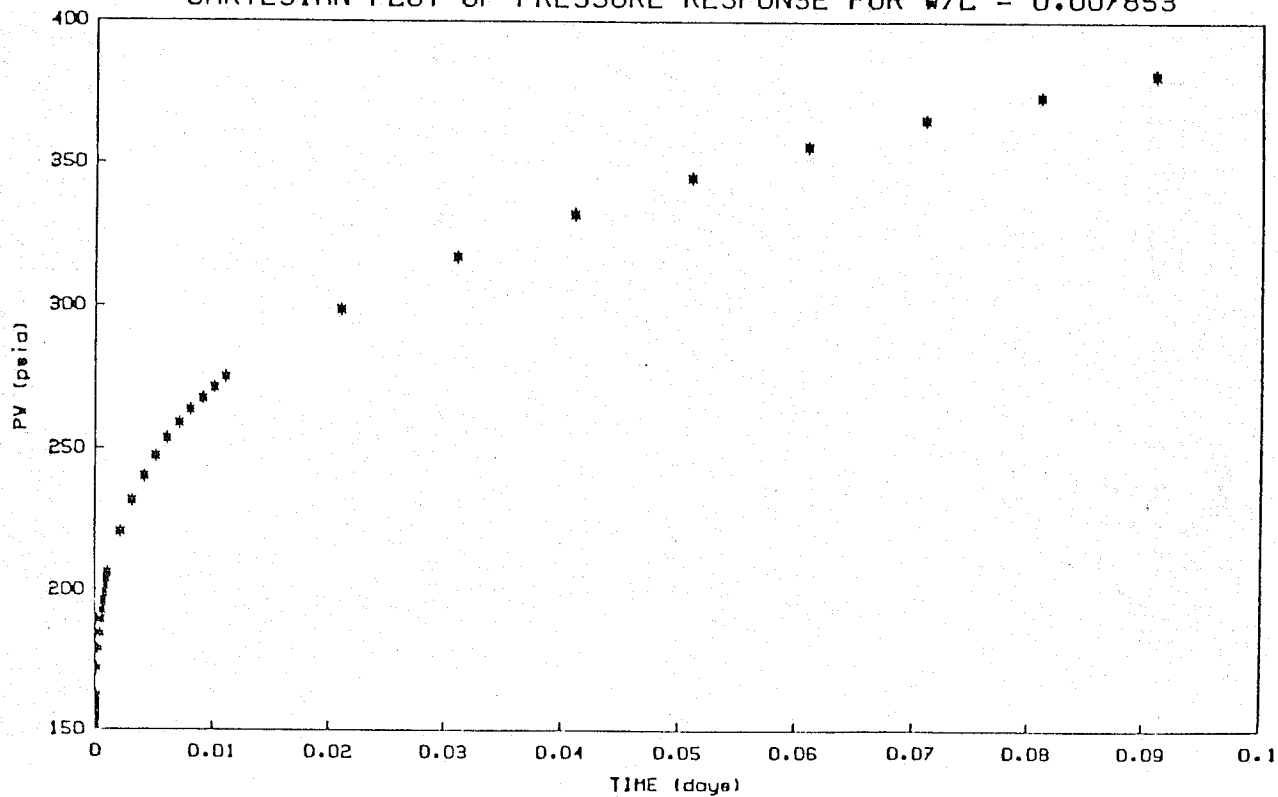
CARTESIAN PLOT OF PRESSURE RESPONSE FOR W/L = 0.039269

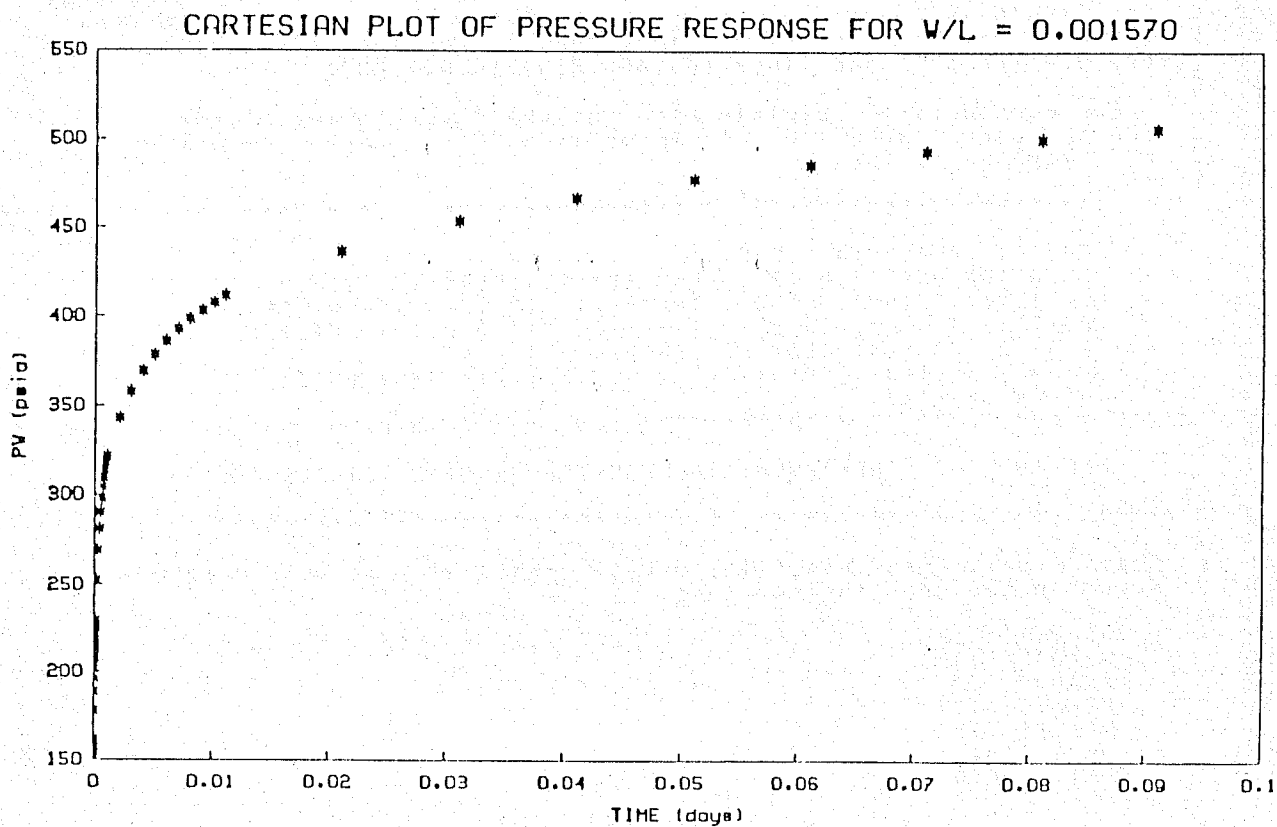
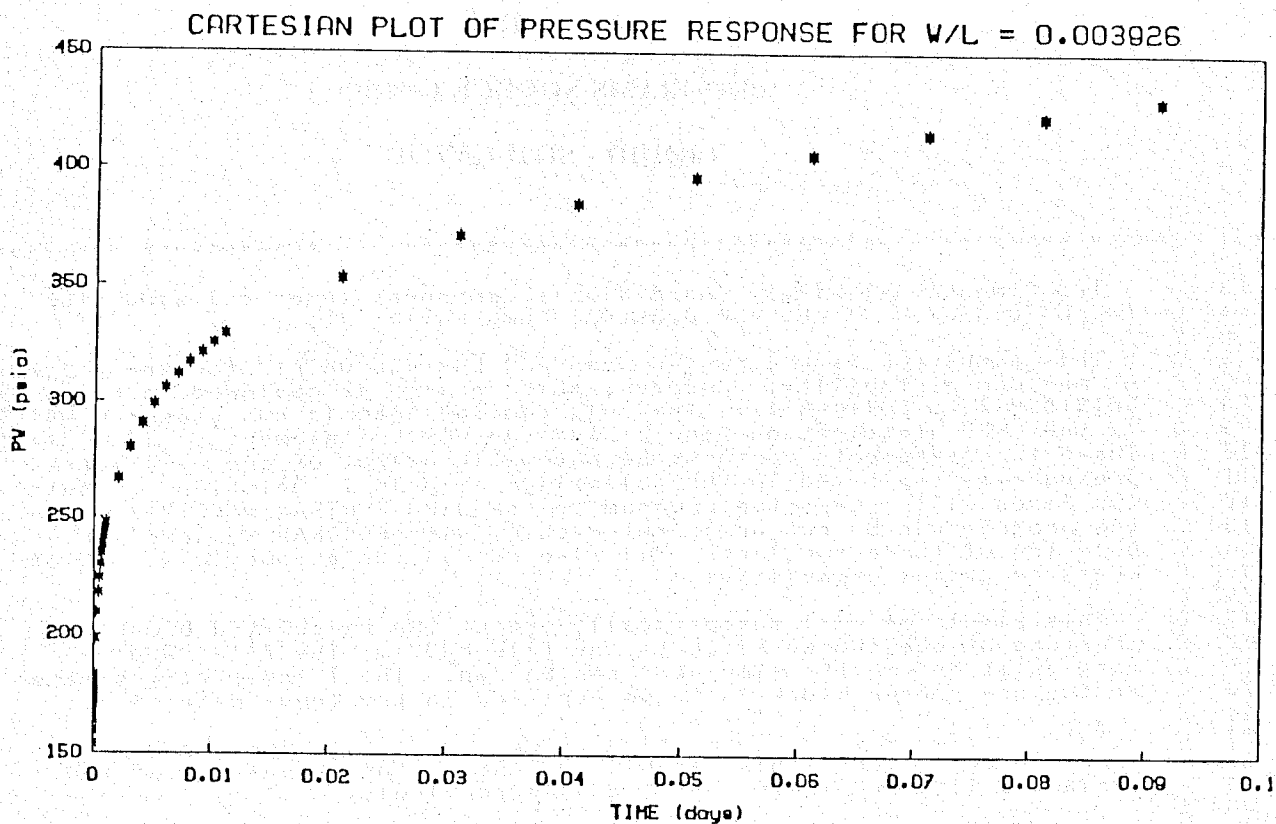


CARTESIAN PLOT OF PRESSURE RESPONSE FOR W/L = 0.015707



CARTESIAN PLOT OF PRESSURE RESPONSE FOR W/L = 0.007853





APPENDIX F
PROGRAMS SOURCE CODES
LIQUID - SIMULATOR

```
1 C*****
2 C
3 C Two Dimensional Single Phase Single Component Numerical Simulator
4 C for Liquid with Slight and Constant Compressibility
5 C
6 C This simulator is written in standard Fortran WATFIV for the purpose
7 C of maximum portability. However, this version is designed to run under
8 C UNIX(BSD 4.2)-FORTRAN 77. The only command that is non standard WATFIV
9 C is the OPEN statement on line 51 and the WRITE statement on line 914 & 915.
10 C These two statements perform the automatic output of one well-block
11 C pressure as explained in the following paragraph. Deletion of these
12 C two lines will return the program to standard FORTRAN WATFIV and
13 C the program can be run under any machine with FORTRAN 66 compiler.
14 C Deletion of these two lines will also remove the automatic well-block
15 C pressure output capability.
16 C
17 C This simulator will automatically output the calculated block
18 C pressure of one chosen block to the file PWOUT. The file PWOUT
19 C must exist before the simulator can be run. The I and J co-ordinate
20 C of the one chosen block is to be supplied in the input data file.
21 C
22 C This version will perform calculations up to 500 time steps. To
23 C increase or decrease this capability, change the dimensions of the
24 C variables TIME and IPRINT on line 44 accordingly.
25 C
26 C This version has a material balance calculation scheme that is
27 C designed for liquid with slight and constant compressibility. If
28 C gas is to be the flowing fluid and the gas is to be simulated as
29 C a fluid with constant compressibility. The material balance scheme
30 C must be changed accordingly. Included in this version is the modified
31 C material balance calculation for gas. However, the material balance
32 C for liquid is currently active in this version. To switch to the
33 C gas material balance calculation, deactivate lines 468,469,812,813
34 C 829,835 and activate lines 465,466,815,816,831,837.
35 C
36 C For more detailed explanation and the input format please
37 C see the user instructions in Appendix A in the master report by
38 C E.Y. Teng(Sept. 1984).
39 C
40 C*****
41 C
42 C IMPLICIT REAL*8(A-H,O-Z)
43 C DIMENSION DX(21),DY(21),PERMX(21,21),PERMY(21,21),PHI(21,21),
44 C +PO(21,21),PT(500),VT(500),TIME(500),Q(21,21),IPRINT(500)
45 C +,PG(21,21),A(21,21),B(21,21),C(21,21),D(21,21),E(21,21)
46 C +,F(21,21),AA(441),BB(441),PGO(21,21)
47 C +,XX(441),CC(441),DD(441),EE(441),FF(441),AAA(18501)
48 C INTEGER KDR(441)
49 C***** open the file PWOUT to accept P Input
50 C
51 C OPEN(UNIT=2,FILE='PWOUT',ACCESS='SEQUENTIAL',STATUS='OLD')
52 C
53 C*****
54 C
55 C Read in data from data file, detail explanation of each term can be
56 C found in the user instructions
57 C
58 C READ(5,*)IB
59 C READ(5,*)JB
60 C READ(5,*)H
61 C READ(5,*)IX
62 C READ(5,*)BX
63 C DO 1 I1=1,21
64 C DX(I1)=0.0
```

```
65      1 CONTINUE
66      DO 2 I2=1,1B
67      DX(I2)=BX
68      2 CONTINUE
69      IF(IX.EQ.0)GO TO 5
70      READ(5,*)IDX
71      DO 3 I3=1,IDX
72      READ(5,*)NOX,BX1
73      DX(NOX)=BX1
74      3 CONTINUE
75      5 CONTINUE
76      DO 6 I6=1,21
77      DY(I6)=0.0
78      6 CONTINUE
79      READ(5,*)IY
80      READ(5,*)BY
81      DO 7 I7=1,JB
82      DY(I7)=BY
83      7 CONTINUE
84      IF(IY.EQ.0)GO TO 10
85      READ(5,*)IDY
86      DO 8 I8=1,IDY
87      READ(5,*)NOY,BY1
88      DY(NOY)=BY1
89      8 CONTINUE
90      10 CONTINUE
91      DO 11 I11=1,21
92      DO 12 I12=1,21
93      PERMX(I11,I12)=0.0
94      PERMY(I11,I12)=0.0
95      12 CONTINUE
96      11 CONTINUE
97      READ(5,*)KXI
98      READ(5,*)BKX
99      BKX=BKX/1000.0
100     DO 13 I13=1,1B
101     DO 14 I14=1,JB
102     PERMX(I13,I14)=BKX
103     14 CONTINUE
104     13 CONTINUE
105     IF(KXI.EQ.0)GO TO 17
106     READ(5,*)NKX
107     DO 15 I15=1,NKX
108     READ(5,*)I,J,XK1
109     XK1=XK1/1000.0
110     PERMX(I,J)=XK1
111     15 CONTINUE
112     17 CONTINUE
113     READ(5,*)KYI
114     READ(5,*)BKY
115     BKY=BKY/1000.0
116     DO 18 I18=1,1B
117     DO 19 I19=1,JB
118     PERMY(I18,I19)=BKY
119     19 CONTINUE
120     18 CONTINUE
121     IF(KYI.EQ.0)GO TO 22
122     READ(5,*)NKY
123     DO 20 I20=1,NKY
124     READ(5,*)I,J,YK1
125     YK1=YK1/1000.0
126     PERMY(I,J)=YK1
127     20 CONTINUE
128     22 CONTINUE
```

```
129      READ(5,*)IPHI
130      READ(5,*)BPHI
131      DO 24 I24=1,21
132      DO 25 I25=1,21
133      PHI(I24,I25)=0.0
134      25 CONTINUE
135      24 CONTINUE
136      DO 26 I26=1,IB
137      DO 27 I27=1,JB
138      PHI(I26,I27)=BPHI
139      27 CONTINUE
140      26 CONTINUE
141      IF(IPHI.EQ.0)GO TO 30
142      READ(5,*)NPHI
143      DO 28 I28=1,NPHI
144      READ(5,*)I,J,PHI1
145      PHI(I,J)=PHI1
146      28 CONTINUE
147      30 CONTINUE
148      READ(5,*)IPOI
149      READ(5,*)BPOI
150      DO 31 I31=1,21
151      DO 32 I32=1,21
152      PO(I31,I32)=0.0
153      32 CONTINUE
154      31 CONTINUE
155      DO 33 I33=1,IB
156      DO 34 I34=1,JB
157      PO(I33,I34)=BPOI
158      34 CONTINUE
159      33 CONTINUE
160      IF(IPOI.EQ.0)GO TO 38
161      READ(5,*)NPOI
162      DO 35 I35=1,NPOI
163      READ(5,*)I,J,POI1
164      PO(I,J)=POI1
165      35 CONTINUE
166      38 CONTINUE
167      READ(5,*)ROOW
168      READ(5,*)CFL
169      READ(5,*)BSTD
170      READ(5,*)TEMP
171      TEMP=TEMP+463.0
172      READ(5,*)NPVT
173      DO 41 I41=1,NPVT
174      READ(5,*)PT(I41),VT(I41)
175      41 CONTINUE
176      READ(5,*)NTIME
177      READ(5,*)NTOT
178      DO 42 I42=1,NTOT
179      TIME(I42)=0.0
180      42 CONTINUE
181      IF(NTIME.EQ.1)GO TO 50
182      READ(5,*)TIME1
183      TIME1=TIME1*86400.0
184      DO 43 I43=1,NTOT
185      TIME(I43)=TIME1
186      43 CONTINUE
187      50 CONTINUE
188      IF(NTIME.EQ.0)GO TO 60
189      READ(5,*)NGT
190      IC=1
191      DO 51 I51=1,NGT
192      READ(5,*)TIME1,LAST
```

```

193     TIME1=TIME1*86400.0
194     DO 52 I52=1, LAST
195     TIME(IC)=TIME1
196     IC=IC+1
197     52 CONTINUE
198     51 CONTINUE
199     60 CONTINUE
200     READ(5,*)PSTD
201     READ(5,*)TSTD
202     TSTD=TSTD+460.0
203     READ(5,*)NPOD
204     DO 53 I53=1,21
205     DO 54 I54=1,21
206     Q(I53,I54)=0.0
207     54 CONTINUE
208     53 CONTINUE
209     IF(NPOD.EQ.0)GO TO 61
210     DEN=ROOW
211     DO 55 I55=1,NPOD
212     READ(5,*)I,J,Q1
213     Q1=(Q1/86400.0)*DEN*5.615
214     Q(I,J)=Q1
215     55 CONTINUE
216     61 CONTINUE
217     READ(5,*)MAXIN
218     READ(5,*)MAXEXE
219     READ(5,*)ICHECK
220     READ(5,*)CONVER
221     READ(5,*)IFORCE
222     IF(IFORCE.EQ.0)GO TO 500
223     READ(5,*)NFORIT
224     500 CONTINUE
225     DO 62 I62=1,NTOT
226     IPRINT(I62)=0
227     62 CONTINUE
228     READ(5,*)NPRINT
229     IF(NPRINT.EQ.0)GO TO 70
230     DO 63 I63=1,NPRINT
231     READ(5,*)NOPRT
232     IPRINT(NOPRT)=1
233     63 CONTINUE
234     GO TO 75
235     70 CONTINUE
236     DO 71 I71=1,MAXEXE
237     IPRINT(I71)=1
238     71 CONTINUE
239     75 CONTINUE
240     READ(5,*)ISKIPP
241     IF(ISKIPP.EQ.0)GO TO 510
242     READ(5,*)IBLPR,JBLPR
243     510 CONTINUE
244     READ(5,*)IBLPR2,JBLPR2
245     C
246     C*****
247     C
248     C   The following part of the program perform the echo check of all
249     C   read in data by writing them to the standard output
250     C
251     C*****
252     C
253     WRITE(6,99)
254     99 FORMAT(1X,' ')
255     WRITE(6,100)
256     100 FORMAT(/,1X,'*****',

```

```
257 + '*****',
258 + '*****')
259 WRITE(6,101)
260 101 FORMAT(1X,'*',118X,'*')
261 WRITE(6,102)
262 102 FORMAT(1X,'*',3X,'TWO DIMENSIONAL SINGLE PHASE AREAL',1X,
263 +'HORIZONTAL LIQUID SIMULATOR (CONSTANT & SLIGHT CF)',5X,
264 +'E.T.',6X,'MAY 84',8X,'*')
265 WRITE(6,103)
266 103 FORMAT(1X,'*',118X,'*')
267 WRITE(6,104)
268 104 FORMAT(1X,'*****',
269 + '*****',
270 + '*****')
271 WRITE(6,105)
272 105 FORMAT(//,50X,'-----')
273 WRITE(6,106)
274 106 FORMAT(53X,'INPUT DATA')
275 WRITE(6,107)
276 107 FORMAT(50X,'-----')
277 IJB=IB*JB
278 WRITE(6,109)IJB
279 109 FORMAT(///,10X,'TOTAL NO. OF BLOCKS ASSIGNED = ',I3)
280 WRITE(6,110)IB
281 110 FORMAT(10X,'NO. OF BLOCKS IN X DIRECTION = ',I3)
282 WRITE(6,111)JB
283 111 FORMAT(10X,'NO. OF BLOCKS IN Y DIRECTION = ',I3)
284 WRITE(6,112)H
285 112 FORMAT(//,10X,'RESERVOIR THICKNESS = ',F9.4,1X,'(FT)')
286 WRITE(6,113)TEMP
287 113 FORMAT(10X,'RESERVOIR TEMPERATURE = ',F9.4,1X,'(R)')
288 WRITE(6,114)ROOW
289 114 FORMAT(//,10X,'FLUID DENSITY (LBS/FT**3) = ',F7.4)
290 WRITE(6,501)CFL
291 501 FORMAT(10X,'FLUID COMPRESSIBILITY = ',E15.8,1X,'(1/psfa)')
292 WRITE(6,115)PSTD
293 115 FORMAT(10X,'STANDARD PRESSURE = ',F9.4,1X,'(PSIA)')
294 WRITE(6,116)TSTD
295 116 FORMAT(10X,'STANDARD TEMPERATURE = ',F9.4,1X,'(R)')
296 WRITE(6,117)
297 117 FORMAT(//,10X,'BLOCK ORDERING CONVENTION : ')
298 WRITE(6,118)
299 118 FORMAT(/,35X,'Y')
300 WRITE(6,119)
301 119 FORMAT(/,20X,'(1,1) (1,2) (1,3) . . . .')
302 WRITE(6,120)
303 120 FORMAT(15X,'X (2,1) (2,2) (2,3) . . . .')
304 WRITE(6,121)
305 121 FORMAT(20X,'(3,1) (3,2) (3,3) . . . .')
306 WRITE(6,122)
307 122 FORMAT(//,10X,'BLOCK LENGTH : ')
308 WRITE(6,123)
309 123 FORMAT(/,20X,'BLOCK NO.',16X,'DX(FT)',25X,'DY(FT)')
310 WRITE(6,124)
311 124 FORMAT(20X,'-----',16X,'-----',25X,'-----')
312 DO 125 I125=1,21
313 WRITE(6,126)I125,DX(I125),DY(I125)
314 126 FORMAT(/,23X,I2,10X,F20.13,10X,F20.13)
315 125 CONTINUE
316 WRITE(6,127)
317 127 FORMAT(//,10X,'POROSITY MAP (FRACTION) :')
318 DO 128 L1=1,21
319 WRITE(6,129)PHI(L1,1),PHI(L1,2),PHI(L1,3),PHI(L1,4),PHI(L1,5),
320 +PHI(L1,6),PHI(L1,7),PHI(L1,8),PHI(L1,9),PHI(L1,10),PHI(L1,11),
```

```
321      +PHI(L1,12),PHI(L1,13),PHI(L1,14),PHI(L1,15),PHI(L1,16),
322      +PHI(L1,17),PHI(L1,18),PHI(L1,19),PHI(L1,20),PHI(L1,21)
323 129 FORMAT(/,2X,21F6.3)
324 128 CONTINUE
325      WRITE(6,130)
326 130 FORMAT(/,10X,'X DIR. PERMEABILITY MAP (DARCY) :')
327      DO 131 L2=1,21
328          WRITE(6,132)PERMX(L2,1),PERMX(L2,2),PERMX(L2,3),PERMX(L2,4),
329          +PERMX(L2,5),PERMX(L2,6),PERMX(L2,7),PERMX(L2,8),PERMX(L2,9),
330          +PERMX(L2,10),PERMX(L2,11),PERMX(L2,12),PERMX(L2,13),
331          +PERMX(L2,14),PERMX(L2,15),PERMX(L2,16),PERMX(L2,17),
332          +PERMX(L2,18),PERMX(L2,19),PERMX(L2,20),PERMX(L2,21)
333 132 FORMAT(/,2X,21F6.3)
334 131 CONTINUE
335      WRITE(6,133)
336 133 FORMAT(/,10X,'Y DIR. PERMEABILITY MAP (DARCY) :')
337      DO 134 L3=1,21
338          WRITE(6,132)PERMY(L3,1),PERMY(L3,2),PERMY(L3,3),PERMY(L3,4),
339          +PERMY(L3,5),PERMY(L3,6),PERMY(L3,7),PERMY(L3,8),PERMY(L3,9),
340          +PERMY(L3,10),PERMY(L3,11),PERMY(L3,12),PERMY(L3,13),
341          +PERMY(L3,14),PERMY(L3,15),PERMY(L3,16),PERMY(L3,17),
342          +PERMY(L3,18),PERMY(L3,19),PERMY(L3,20),PERMY(L3,21)
343 134 CONTINUE
344      WRITE(6,135)
345 135 FORMAT(/,10X,'ORIGINAL PRESSURE MAP (PSIA) :')
346      DO 136 L4=1,21
347          WRITE(6,137)PO(L4,1),PO(L4,2),PO(L4,3),PO(L4,4),PO(L4,5),PO(L4
348          +,6),PO(L4,7),PO(L4,8),PO(L4,9),PO(L4,10),PO(L4,11),PO(L4,12),
349          +PO(L4,13),PO(L4,14),PO(L4,15),PO(L4,16),PO(L4,17),
350          +PO(L4,18),PO(L4,19),PO(L4,20),PO(L4,21)
351 137 FORMAT(/,2X,21F6.0)
352 136 CONTINUE
353      WRITE(6,138)
354 138 FORMAT(/,10X,'FLOW RATE MAP (LBM/SEC)',1X,
355      + '(- FOR INJ. & + FOR PROD.) :')
356      DO 139 L5=1,21
357          WRITE(6,140)Q(L5,1),Q(L5,2),Q(L5,3),Q(L5,4),Q(L5,5),Q(L5,6),
358          +Q(L5,7),Q(L5,8),Q(L5,9),Q(L5,10),Q(L5,11),Q(L5,12),Q(L5,13),
359          +Q(L5,14),Q(L5,15),Q(L5,16),Q(L5,17),Q(L5,18),Q(L5,19),
360          +Q(L5,20),Q(L5,21)
361 140 FORMAT(/,2X,21F6.2)
362 139 CONTINUE
363      WRITE(6,141)
364 141 FORMAT(/,50X,'-----')
365      WRITE(6,142)
366 142 FORMAT(51X,'FLUID P.V.T. DATA')
367      WRITE(6,143)
368 143 FORMAT(50X,'-----')
369      WRITE(6,144)
370 144 FORMAT(/,3X,'PRESSURE',27X,'
371      + '
372          ,25X,'VISCOSITY',28X,
373          + '
374          WRITE(6,145)
375 145 FORMAT(3X,'(PSIA)',64X,'(CP)')
376      WRITE(6,146)
377 146 FORMAT(1X,'-----')
378      + '-----'
379      + '-----'
380      DO 147 I147=1,NPVT
381          WRITE(6,148)PT(I147),VT(I147)
382 148 FORMAT(/,1X,F10.4,59X,F10.7)
383 147 CONTINUE
384      WRITE(6,146)
385      WRITE(6,150)
386 150 FORMAT(/,50X,'-----')
```

```
385      WRITE(6,151)
386 151  FORMAT(50X,'TIME STEP CONTROL')
387      WRITE(6,152)
388 152  FORMAT(50X,'-----')
389      WRITE(6,153)NTOT
390 153  FORMAT(//,1X,'TOTAL NO. OF TIME STEP ASSIGNED = ',I4)
391      WRITE(6,154)
392 154  FORMAT(//,20X,'TIME STEP NO.',20X,'TIME STEP SIZE (DAYS)')
393      WRITE(6,155)
394 155  FORMAT(20X,'-----',20X,'-----')
395      DO 156 I156=1,NTOT
396      TIMTEP=TIME(I156)/86400.0
397      WRITE(6,157)I156,TIMTEP
398 157  FORMAT(/,24X,14,23X,F17.11)
399 156  CONTINUE
400      WRITE(6,158)
401 158  FORMAT(/,20X,'-----',
402      +,'-----')
403      WRITE(6,159)
404 159  FORMAT(//,50X,'-----')
405      WRITE(6,160)
406 160  FORMAT(51X,'EXECUTION CONTROL')
407      WRITE(6,161)
408 161  FORMAT(50X,'-----')
409      WRITE(6,162)MAXEXE
410 162  FORMAT(//,1X,'NO. OF TIME STEP ALLOWED TO BE EXECUTED = ',I4)
411      WRITE(6,163)MAXIN
412 163  FORMAT(1X,'MAX. NO. OF ITERATION ALLOWED = ',I4)
413      IF(IFORCE.EQ.0)WRITE(6,502)
414 502  FORMAT(1X,'FORCE ITERATION = NOT ENGAGED')
415      IF(IFORCE.EQ.1)WRITE(6,503)
416 503  FORMAT(1X,'FORCE ITERATION = ENGAGED')
417      IF(IFORCE.EQ.1)WRITE(6,504)NFORIT
418 504  FORMAT(1X,'NUMBER OF ITERATION FORCED TO PERFORM = ',1X,I4)
419      WRITE(6,164)CONVER
420 164  FORMAT(1X,'CONVERGENCE CRITERIA = ',F8.5,1X,'(PSIA)')
421      WRITE(6,165)
422 165  FORMAT(//,50X,'-----')
423      WRITE(6,166)
424 166  FORMAT(51X,'OUTPUT CONTROL')
425      WRITE(6,167)
426 167  FORMAT(50X,'-----')
427      IF(ISKIPP.EQ.0)WRITE(6,511)
428 511  FORMAT(//,1X,'PRESSURE MAP OMIT = NOT ENGAGED')
429      IF(ISKIPP.EQ.1)WRITE(6,512)
430 512  FORMAT(//,1X,'PRESSURE MAP OMIT = ENGAGED')
431      IF(ISKIPP.EQ.1)WRITE(6,513)IBLPR,JBLPR
432 513  FORMAT(1X,'THE ONE BLOCK THAT HAS PRESSURE PRINTED = BLOCK('
433      +,I2,',',I2,')')
434      WRITE(6,168)
435 168  FORMAT(//,25X,'TIME STEP NO. PRINTED',25X,'TOTAL TIME ELASPED')
436      WRITE(6,169)
437 169  FORMAT(65X,'FROM START OF SIMULATION (DAYS)')
438      WRITE(6,170)
439 170  FORMAT(25X,'-----',18X,'-----',
440      +,'-----')
441      WRITE(6,171)
442 171  FORMAT(/,1X,' ')
443      ADDTM=0.0
444      DO 180 I180=1,MAXEXE
445      ADDTM=ADDTM+TIME(I180)
446      ADDTM1=ADDTM/86400.0
447      IF(IPRINT(I180).EQ.1)WRITE(6,190)I180,ADDTM1
448 190  FORMAT(/,30X,14,33X,F17.11)
```

```

449 100 CONTINUE
450 WRITE(6,181)
451 181 FORMAT(/,25X,'-----',
452 + '-----')
453 WRITE(6,182)
454 182 FORMAT(//,1X,'*****',
455 + '*****',
456 + '*****')
457 C
458 C##### START OF PROGRAM #####
459 C
460 C##### Calculate initial mass in place
461 TMASS=0.0
462 DO 200 I200=1,IB
463 DO 201 I201=1,JB
464 C deactivated gas m.b. calculation
465 C TMASS=TMASS+(DX(I200)*DY(I201)*PHI(I200,I201)*H)*
466 C +((28.97*PO(I200,I201))/(1.0*10.72*960.0))
467 C
468 TMASS=TMASS+(DX(I200)*DY(I201)*PHI(I200,I201)*H)*
469 C +((1.0+CFL*(PO(I200,I201)-PSTD))*ROOW)
470 201 CONTINUE
471 200 CONTINUE
472 C#####
473 C set all block pressure to initial pressure
474 DO 205 I205=1,21
475 DO 206 I206=1,21
476 PG(I205,I206)=PO(I205,I206)
477 206 CONTINUE
478 205 CONTINUE
479 C start time step
480 DO 900 I900=1,MAXEXE
481 C set all block p to p of last time step
482 DO 300 I300=1,21
483 DO 301 I301=1,21
484 PO(I300,I301)=PG(I300,I301)
485 301 CONTINUE
486 300 CONTINUE
487 INNUB=0
488 801 CONTINUE
489 INNUB=INNUB+1
490 C set all pgo of current iteration to current p, pgo is the p of last
491 C iteration
492 DO 207 I207=1,21
493 DO 208 I208=1,21
494 PGO(I207,I208)=PG(I207,I208)
495 208 CONTINUE
496 207 CONTINUE
497 C initial the 5-diagonal matrix to 0
498 DO 203 I203=1,441
499 AA(I203)=0.0
500 BB(I203)=0.0
501 CC(I203)=0.0
502 DD(I203)=0.0
503 EE(I203)=0.0
504 FF(I203)=0.0
505 203 CONTINUE
506 DO 211 I211=1,21
507 DO 210 I210=1,21
508 A(I211,I210)=0.0
509 B(I211,I210)=0.0
510 C(I211,I210)=0.0
511 D(I211,I210)=0.0
512 E(I211,I210)=0.0

```

```

513     F(I211,I210)=0.0
514     210 CONTINUE
515     211 CONTINUE
516 C calculate transmissibilities for all blocks
517     DO 800 J=1,21
518     DO 850 I=1,21
519     IF(I.EQ.1)PERMXM=0.0
520     IF(I.NE.1)PERMXM=(DX(I)+DX(I-1))/((DX(I-1)/PERMX(I-1,J))+
521     +(DX(I)/PERMX(I,J)))
522     IF(I.EQ.21)PERMXP=0.0
523     IF(I.NE.21)PERMXP=(DX(I)+DX(I+1))/((DX(I+1)/PERMX(I+1,J))
524     ++(DX(I)/PERMX(I,J)))
525     IF(J.EQ.1)PERMYM=0.0
526     IF(J.NE.1)PERMYM=(DY(J)+DY(J-1))/((DY(J-1)/PERMY(I,J-1))+
527     +(DY(J)/PERMY(I,J)))
528     IF(J.EQ.21)PERMYP=0.0
529     IF(J.NE.21)PERMYP=(DY(J)+DY(J+1))/((DY(J+1)/PERMY(I,J+1))+
530     +(DY(J)/PERMY(I,J)))
531     IF(I.EQ.1)DELXM=DX(I)
532     IF(I.NE.1)DELXM=(DX(I)+DX(I-1))*0.5
533     IF(I.EQ.21)DELXP=DX(I)
534     IF(I.NE.21)DELXP=(DX(I)+DX(I+1))*0.5
535     IF(J.EQ.1)DELYM=DY(J)
536     IF(J.NE.1)DELYM=(DY(J)+DY(J-1))*0.5
537     IF(J.EQ.21)DELYP=DY(J)
538     IF(J.NE.21)DELYP=(DY(J)+DY(J+1))*0.5
539     CALL SSCH(NPVT,PT,VT,PG(I,J),VCOIJ,NCODE,6)
540     PVB=1.0/(VCOIJ*(BSTD/(1.0+CFL*(PG(I,J)-PSTD))))
541     IF(I.NE.1)CALL SSCH(NPVT,PT,VT,PG(I-1,J),VCOIM1,NCODE,6)
542     IF(I.NE.1)PVBIM1=1.0/(VCOIM1*(BSTD/(1.0+CFL*(PG(I-1,J)-PSTD))))
543     IF(I.NE.21)CALL SSCH(NPVT,PT,VT,PG(I+1,J),VCOIP1,NCODE,6)
544     IF(I.NE.21)PVBIP1=1.0/(VCOIP1*(BSTD/(1.0+CFL*(PG(I+1,J)-PSTD))))
545     IF(J.NE.1)CALL SSCH(NPVT,PT,VT,PG(I,J-1),VCOJM1,NCODE,6)
546     IF(J.NE.1)PVBJM1=1.0/(VCOJM1*(BSTD/(1.0+CFL*(PG(I,J-1)-PSTD))))
547     IF(J.NE.21)CALL SSCH(NPVT,PT,VT,PG(I,J+1),VCOJPI,NCODE,6)
548     IF(J.NE.21)PVBJP1=1.0/(VCOJPI*(BSTD/(1.0+CFL*(PG(I,J+1)-PSTD))))
549 C set matrix element to the calculated values
550     A(I,J)=(PERMYM*(PVB+PVBJM1))/(DY(J)*DELYM)
551     B(I,J)=(PERMXM*(PVBIM1+PVB))/(DX(I)*DELXM)
552     D(I,J)=(PERMXP*(PVBIP1+PVB))/(DX(I)*DELXP)
553     E(I,J)=(PERMYP*(PVBJP1+PVB))/(DY(J)*DELYP)
554     C(I,J)=(B(I,J)+D(I,J)+A(I,J)+E(I,J)+
555     +((27306.06*PHI(I,J)*CFL)/(BSTD*TIME(1900))))*(-1.0)
556     F(I,J)=(((27306.06)*PHI(I,J)*CFL*PO(I,J))/(BSTD*TIME(1900)))+
557     +((27306.06*Q(I,J))/(ROOW*H*DX(I)*DY(J)))
558     850 CONTINUE
559     800 CONTINUE
560 C routine used to check matrix, it will print all elements out
561     IF(ICHECK.EQ.0)GO TO 1240
562     DO 1234 I1234=1,21
563     DO 1235 I1235=1,21
564     WRITE(6,1236)A(I1235,I1234),B(I1235,I1234),C(I1235,I1234)
565     +,D(I1235,I1234),E(I1235,I1234),F(I1235,I1234)
566     1236 FORMAT(6(2x,F15.8))
567     1235 CONTINUE
568     1234 CONTINUE
569     1240 CONTINUE
570 C align matrix element to go into GBAND matrix solver
571     DO 600 I600=1,21
572     AA(I600)=A(I600,1)
573     BB(I600)=B(I600,1)
574     CC(I600)=C(I600,1)
575     DD(I600)=D(I600,1)
576     EE(I600)=E(I600,1)

```

577 FF(1600)=F(1600,1)
578 600 CONTINUE
579 DO 601 I601=22,42
580 AA(1601)=A(1601-21,2)
581 BB(1601)=B(1601-21,2)
582 CC(1601)=C(1601-21,2)
583 DD(1601)=D(1601-21,2)
584 EE(1601)=E(1601-21,2)
585 FF(1601)=F(1601-21,2)
586 601 CONTINUE
587 DO 602 I602=43,63
588 AA(1602)=A(1602-42,3)
589 BB(1602)=B(1602-42,3)
590 CC(1602)=C(1602-42,3)
591 DD(1602)=D(1602-42,3)
592 EE(1602)=E(1602-42,3)
593 FF(1602)=F(1602-42,3)
594 602 CONTINUE
595 DO 603 I603=64,84
596 AA(1603)=A(1603-63,4)
597 BB(1603)=B(1603-63,4)
598 CC(1603)=C(1603-63,4)
599 DD(1603)=D(1603-63,4)
600 EE(1603)=E(1603-63,4)
601 FF(1603)=F(1603-63,4)
602 603 CONTINUE
603 DO 604 I604=85,105
604 AA(1604)=A(1604-84,5)
605 BB(1604)=B(1604-84,5)
606 CC(1604)=C(1604-84,5)
607 DD(1604)=D(1604-84,5)
608 EE(1604)=E(1604-84,5)
609 FF(1604)=F(1604-84,5)
610 604 CONTINUE
611 DO 605 I605=106,126
612 AA(1605)=A(1605-105,6)
613 BB(1605)=B(1605-105,6)
614 CC(1605)=C(1605-105,6)
615 DD(1605)=D(1605-105,6)
616 EE(1605)=E(1605-105,6)
617 FF(1605)=F(1605-105,6)
618 605 CONTINUE
619 DO 606 I606=127,147
620 AA(1606)=A(1606-126,7)
621 BB(1606)=B(1606-126,7)
622 CC(1606)=C(1606-126,7)
623 DD(1606)=D(1606-126,7)
624 EE(1606)=E(1606-126,7)
625 FF(1606)=F(1606-126,7)
626 606 CONTINUE
627 DO 607 I607=148,168
628 AA(1607)=A(1607-147,8)
629 BB(1607)=B(1607-147,8)
630 CC(1607)=C(1607-147,8)
631 DD(1607)=D(1607-147,8)
632 EE(1607)=E(1607-147,8)
633 FF(1607)=F(1607-147,8)
634 607 CONTINUE
635 DO 608 I608=169,189
636 AA(1608)=A(1608-168,9)
637 BB(1608)=B(1608-168,9)
638 CC(1608)=C(1608-168,9)
639 DD(1608)=D(1608-168,9)
640 EE(1608)=E(1608-168,9)

641 FF(1608)=F(1608-168,9)
642 608 CONTINUE
643 DO 609 I609=190,210
644 AA(1609)=A(1609-189,10)
645 BB(1609)=B(1609-189,10)
646 CC(1609)=C(1609-189,10)
647 DD(1609)=D(1609-189,10)
648 EE(1609)=E(1609-189,10)
649 FF(1609)=F(1609-189,10)
650 609 CONTINUE
651 DO 610 I610=211,231
652 AA(1610)=A(1610-210,11)
653 BB(1610)=B(1610-210,11)
654 CC(1610)=C(1610-210,11)
655 DD(1610)=D(1610-210,11)
656 EE(1610)=E(1610-210,11)
657 FF(1610)=F(1610-210,11)
658 610 CONTINUE
659 DO 611 I611=232,252
660 AA(1611)=A(1611-231,12)
661 BB(1611)=B(1611-231,12)
662 CC(1611)=C(1611-231,12)
663 DD(1611)=D(1611-231,12)
664 EE(1611)=E(1611-231,12)
665 FF(1611)=F(1611-231,12)
666 611 CONTINUE
667 DO 612 I612=253,273
668 AA(1612)=A(1612-252,13)
669 BB(1612)=B(1612-252,13)
670 CC(1612)=C(1612-252,13)
671 DD(1612)=D(1612-252,13)
672 EE(1612)=E(1612-252,13)
673 FF(1612)=F(1612-252,13)
674 612 CONTINUE
675 DO 613 I613=274,294
676 AA(1613)=A(1613-273,14)
677 BB(1613)=B(1613-273,14)
678 CC(1613)=C(1613-273,14)
679 DD(1613)=D(1613-273,14)
680 EE(1613)=E(1613-273,14)
681 FF(1613)=F(1613-273,14)
682 613 CONTINUE
683 DO 614 I614=295,315
684 AA(1614)=A(1614-294,15)
685 BB(1614)=B(1614-294,15)
686 CC(1614)=C(1614-294,15)
687 DD(1614)=D(1614-294,15)
688 EE(1614)=E(1614-294,15)
689 FF(1614)=F(1614-294,15)
690 614 CONTINUE
691 DO 615 I615=316,336
692 AA(1615)=A(1615-315,16)
693 BB(1615)=B(1615-315,16)
694 CC(1615)=C(1615-315,16)
695 DD(1615)=D(1615-315,16)
696 EE(1615)=E(1615-315,16)
697 FF(1615)=F(1615-315,16)
698 615 CONTINUE
699 DO 616 I616=337,357
700 AA(1616)=A(1616-336,17)
701 BB(1616)=B(1616-336,17)
702 CC(1616)=C(1616-336,17)
703 DD(1616)=D(1616-336,17)
704 EE(1616)=E(1616-336,17)

```

705      FF(1616)=F(1616-336,17)
706 616 CONTINUE
707      DO 617 I617=358,378
708      AA(1617)=A(1617-357,18)
709      BB(1617)=B(1617-357,18)
710      CC(1617)=C(1617-357,18)
711      DD(1617)=D(1617-357,18)
712      EE(1617)=E(1617-357,18)
713      FF(1617)=F(1617-357,18)
714 617 CONTINUE
715      DO 618 I618=379,399
716      AA(1618)=A(1618-378,19)
717      BB(1618)=B(1618-378,19)
718      CC(1618)=C(1618-378,19)
719      DD(1618)=D(1618-378,19)
720      EE(1618)=E(1618-378,19)
721      FF(1618)=F(1618-378,19)
722 618 CONTINUE
723      DO 619 I619=400,420
724      AA(1619)=A(1619-399,20)
725      BB(1619)=B(1619-399,20)
726      CC(1619)=C(1619-399,20)
727      DD(1619)=D(1619-399,20)
728      EE(1619)=E(1619-399,20)
729      FF(1619)=F(1619-399,20)
730 619 CONTINUE
731      DO 2000 I2000=421,441
732      AA(I2000)=A(I2000-420,21)
733      BB(I2000)=B(I2000-420,21)
734      CC(I2000)=C(I2000-420,21)
735      DD(I2000)=D(I2000-420,21)
736      EE(I2000)=E(I2000-420,21)
737      FF(I2000)=F(I2000-420,21)
738 2000 CONTINUE
739 C routine used for debugging, will print matrix out
740      IF(ICHECK.EQ.0)GO TO 1241
741      DO 770 I770=1,441
742      WRITE(6,771)AA(I770),BB(I770),CC(I770),DD(I770),EE(I770)
743      +,FF(I770)
744      771 FORMAT(6(2X,F15.8))
745      770 CONTINUE
746 1241 CONTINUE
747      DO 544 I544=1,18501
748      AAA(I544)=0.0
749      544 CONTINUE
750      DO 540 I540=1,441
751      KDR(I540)=0
752      540 CONTINUE
753      KDR(1)=1
754      DO 541 L541=2,441
755      IF(L541.GT.21)GO TO 542
756      KDR(L541)=KDR(L541-1)+21+L541
757      GO TO 541
758      542 IF(L541.GT.420)GO TO 543
759      KDR(L541)=KDR(L541-1)+43
760      GO TO 541
761      543 KDR(L541)=KDR(L541-1)+441-L541+23
762      541 CONTINUE
763      DO 545 I545=1,441
764      AAA(KDR(I545))=CC(I545)
765      545 CONTINUE
766      AAA(2)=DD(1)
767      AAA(22)=EE(1)
768      DO 546 I546=2,21

```

```
769      AAA(KDR(I546)-1)=BB(I546)
770      AAA(KDR(I546)+1)=DD(I546)
771      AAA(KDR(I546)+21)=EE(I546)
772  546 CONTINUE
773      DO 547 I547=22,420
774      AAA(KDR(I547)-1)=BB(I547)
775      AAA(KDR(I547)-21)=AA(I547)
776      AAA(KDR(I547)+1)=DD(I547)
777      AAA(KDR(I547)+21)=EE(I547)
778  547 CONTINUE
779      DO 548 I548=421,440
780      AAA(KDR(I548)-21)=AA(I548)
781      AAA(KDR(I548)-1)=BB(I548)
782      AAA(KDR(I548)+1)=DD(I548)
783  548 CONTINUE
784      AAA(18500)=BB(441)
785      AAA(18480)=AA(441)
786      CALL GBAND(AAA,FF,XX,441,21,1.0,IERR,0)
787  C set pg to the calculated pressures
788      LLL=0
789      DO 752 J752=1,21
790      DO 753 I753=1,21
791      LLL=LLL+1
792      PG(I753,J752)=XX(LLL)
793  753 CONTINUE
794  752 CONTINUE
795  C calculate the difference, if converged, go to print out subroutine
796      DO 702 I702=1,21
797      DO 703 I703=1,21
798      DIFF=PG(I702,I703)-PGO(I702,I703)
799      DIFFA=DABS(DIFF)
800      IF(DIFFA.GT.CONVER.AND.INNUB.LT.MAXIN.AND.IFORCE.EQ.0)GO TO 801
801  703 CONTINUE
802  702 CONTINUE
803  C check if the force iteration option is engaged
804      IF(IFORCE.EQ.1.AND.INNUB.LT.NFORIT)GO TO 801
805      IF(1900.NE.1)CMASOLD=CURMAS
806      QTO=0.0
807      CURMAS=0.0
808  C calculate current mass in place
809      DO 710 I710=1,21
810      DO 711 I711=1,21
811
812      CURMAS=CURMAS+(DX(I710)*DY(I711)*PHI(I710,I711)*H)*
813      +((1.0+CFL*(PG(I710,I711)-PSTD))*ROOW)
814  C deactivate m.b. calculations for gas
815      CURMAS=CURMAS+(DX(I710)*DY(I711)*PHI(I710,I711)*H)*
816      C +((28.97*PG(I710,I711))/(1.0*10.72*960.0))
817  C
818      QTO=QTO+Q(I710,I711)
819  711 CONTINUE
820  710 CONTINUE
821      PROMAS=TMASS-CURMAS
822      IF(1900.EQ.1)CMASP=TMASS-CURMAS
823      IF(1900.NE.1)CMASP=CMASOLD-CURMAS
824      TIMETO=0.0
825      DO 715 I715=1,1900
826      TIMETO=TIMETO+TIME(I715)
827  715 CONTINUE
828  C*****
829      PROD=TIMETO*QTO
830  C deactivated m.b. calculation for gas
831  C      PROD=TIMETO*(QTO/ROOW)*0.076135636
832  C*****
```



```
897 20 FORMAT(//,2X,'PRESSURE MAP (RIGHT HALF) :')
898 DO 21 I21=1,21
899 WRITE(6,2001)PG(I21,11),PG(I21,12),PG(I21,13),PG(I21,14),
900 +PG(I21,15),PG(I21,16),PG(I21,17),PG(I21,18),PG(I21,19),
901 +PG(I21,20),PG(I21,21)
902 2001 FORMAT(/,1X,11F11.5)
903 21 CONTINUE
904 520 CONTINUE
905 IF (ISKIPP.EQ.1)WRITE(6,521)IBLPR,JBLPR,PG( IBLPR,JBLPR)
906 521 FORMAT(//,1X,'P(',I2,',',I2,') = ',F15.8,1X,'PSIA')
907 WRITE(6,14)INNUB
908 14 FORMAT(//,2X,'NO. OF ITERATION PERFORMED',1X,
909 + 'FOR THIS TIME STEP = ',I4)
910 WRITE(6,1)
911 WRITE(6,15)
912 15 FORMAT(1X,' ')
913 C*****
914 WRITE(2,3000)WTM2,PG( IBLPR2,JBLPR2)
915 3000 FORMAT(2X,F20.11,5X,F20.11)
916 C*****
917 RETURN
918 END
919 SUBROUTINE SSCH(N,X,Y,XIN,YOUT,NCODE,IW)
920 IMPLICIT REAL*8(A-H,O-Z)
921 DIMENSION X(N),Y(N)
922 IF(XIN.LT.X(1))NCODE=88
923 IF(XIN.LT.X(1))YOUT=0.0
924 IF(XIN.LT.X(1))WRITE(6,10)
925 10 FORMAT(//,'INPUT DATA EXCEED LOWER LIMIT')
926 IF(XIN.GT.X(N))NCODE=99
927 IF(XIN.GT.X(N))YOUT=0.0
928 IF(XIN.GT.X(N))WRITE(6,11)
929 11 FORMAT(//,'INPUT DATA EXCEED UPPER LIMIT')
930 IF(XIN.LT.X(1).OR.XIN.GT.X(N))GO TO 9999
931 K=1
932 GO TO 1
933 2 K=K+1
934 1 CONTINUE
935 IF(XIN.EQ.X(K))YOUT=Y(K)
936 IF(XIN.EQ.X(K))GO TO 999
937 IF(XIN.GT.X(K))GO TO 2
938 YOUT=Y(K-1)+(Y(K)-Y(K-1))*(XIN-X(K-1))/(X(K)-X(K-1))
939 999 CONTINUE
940 NCODE=1
941 9999 CONTINUE
942 RETURN
943 END
944 SUBROUTINE GBAND(A,D,X,N,M,EPS,IERR,IFRST)
945 IMPLICIT REAL*8(A-H,O-Z)
946 DIMENSION A(18501),D(441),X(441)
947 IERR=0
948 J=1
949 DO 10 I=1,N
950 IE=M
951 IF(I+M-N)21,21,22
952 22 IE=N-I
953 21 IEAUX=M
954 IF(I-M)23,23,24
955 23 IEAUX=I
956 24 IE1=IE+IEAUX
957 MBIG=IE
958 J1=J+IE1
959 J2=J1
960 IF(IFRST.GT.0)GO TO 27
```

```
961      IF(DABS(A(J))-EPS)25,25,27
962 25 IERR=IERR+1
963 27 IF(MBIG)10,10,26
964 26 DO 20 J0=1,MBIG
965     S=A(J1)/A(J)
966     IF(IFRST.GT.0)GO TO 35
967     DO 30 K=1,MBIG
968     J1K=J1+K
969     JK=J+K
970 30 A(J1K)=A(J1K) -A(JK)*S
971 35 CONTINUE
972     IAUX=J0+1
973     D(IAUX)=D(IAUX)-D(I)*S
974     IE=M
975     IF(IAUX+M-N)31,31,32
976 32 IE=N-IAUX
977 31 IEAUX=M
978     IF(IAUX-M)33,33,34
979 33 IEAUX=IAUX
980 34 IE1=IE+IEAUX
981 20 J1=J1+IE1
982 10 J=J2+1
983     J=J-M-1
984     NP1=N+1
985     DO 40 IINV=1,N
986     I=NP1-IINV
987     IE=M
988     IF(I+M-N)41,41,42
989 42 IE=N-I
990 41 MBIG=IE
991     X(I)=D(I)
992     IF(MBIG)44,44,43
993 43 DO 50 K=1,MBIG
994     IK=I+K
995     JK=J+K
996 50 X(I)=X(I)-X(IK)*A(JK)
997 44 X(I)=X(I)/A(J)
998     IE=M
999     IF(I+M-NP1)51,51,52
1000 52 IE=NP1-I
1001 51 IEAUX=M
1002     IF(I-1-M)53,53,54
1003 53 IEAUX=I-1
1004 54 IE1=IE+IEAUX
1005     J=J-IE1-1
1006 40 CONTINUE
1007     RETURN
1008     END
```

GAS - SIMULATOR

```

1 C*****
2 C
3 C   Two Dimensional Single Phase Single Component Numerical Simulator
4 C   for Fully Compressible Gas
5 C
6 C   This simulator is written in standard Fortran WATFIV for the purpose
7 C   of maximum portability. However, this version is designed to run under
8 C   Unix(BSD 4.2)-FORTRAN 77. The only command that is non standard WATFIV
9 C   is the OPEN statement on line 39 and the WRITE statement on line 879 & 880.
10 C   These two statements perform the automatic output of the well-block
11 C   pressure as explained in the following paragraph. Deletion of these
12 C   two lines will return the program to standard FORTRAN WATFIV and
13 C   the program can be run under any machine with FORTRAN 66 compiler.
14 C   Deletion of these two lines will also remove the automatic well-block
15 C   pressure output capability.
16 C
17 C   This simulator will automatically output the calculated block
18 C   pressure of one chosen block to the file GPWOUT. The file GPWOUT
19 C   must exist before the simulator can be run. The I and J co-ordinate
20 C   of the one chosen block is to be supplied in the input data file.
21 C
22 C   This version will perform calculations up to 100 time steps. To
23 C   increase or decrease this capability, change the dimensions of the
24 C   variables TIME and IPRINT on line 33 accordingly.
25 C
26 C   For more detailed explanation and the input format please
27 C   see the user instructions in Appendix A in the master report by
28 C   E.Y. Teng(Sept. 1984)
29 C
30 C*****
31 C
32 C   IMPLICIT REAL*8(A-H,O-Z)
33 C   DIMENSION DX(21),DY(21),PERMX(21,21),PERMY(21,21),PHI(21,21),
34 C   +PO(21,21),PT(50),VT(50),ZT(50),TIME(100),Q(21,21),IPRINT(100)
35 C   +,PMZ(50),PG(21,21),A(21,21),B(21,21),C(21,21),D(21,21),E(21,21)
36 C   +,F(21,21),AA(441),BB(441),PGO(21,21)
37 C   +,XX(441),CC(441),DD(441),EE(441),FF(441),AAA(18501)
38 C   INTEGER KDR(441)
39 C***** open the file GPWOUT to accept p input
40 C   OPEN(UNIT=2,FILE='GPWOUT',ACCESS='SEQUENTIAL',STATUS='OLD')
41 C*****
42 C
43 C   Read in data from data file, detail explanation of each term can be
44 C   found in the user instructions
45 C
46 C   READ(5,*)IB
47 C   READ(5,*)JB
48 C   READ(5,*)H
49 C   READ(5,*)IX
50 C   READ(5,*)BX
51 C   DO 1 I1=1,21
52 C   DX(I1)=0.0
53 C   1 CONTINUE
54 C   DO 2 I2=1,IB
55 C   DX(I2)=BX
56 C   2 CONTINUE
57 C   IF(IX.EQ.0)GO TO 5
58 C   READ(5,*)IDX
59 C   DO 3 I3=1,IDX
60 C   READ(5,*)NOX,BX1
61 C   DX(NOX)=BX1
62 C   3 CONTINUE
63 C   5 CONTINUE
64 C   DO 6 I6=1,21

```

```
65      DY(I6)=0.0
66      6 CONTINUE
67      READ(5,*)IY
68      READ(5,*)BY
69      DO 7 I7=1,JB
70      DY(I7)=BY
71      7 CONTINUE
72      IF(IY.EQ.0)GO TO 10
73      READ(5,*)IDY
74      DO 8 I8=1,IDY
75      READ(5,*)NOY,BY1
76      DY(NOY)=BY1
77      8 CONTINUE
78      10 CONTINUE
79      DO 11 I11=1,21
80      DO 12 I12=1,21
81      PERMX(I11,I12)=0.0
82      PERMY(I11,I12)=0.0
83      12 CONTINUE
84      11 CONTINUE
85      READ(5,*)KXI
86      READ(5,*)BKX
87      BKX=BKX/1000.0
88      DO 13 I13=1,IB
89      DO 14 I14=1,JB
90      PERMX(I13,I14)=BKX
91      14 CONTINUE
92      13 CONTINUE
93      IF(KXI.EQ.0)GO TO 17
94      READ(5,*)NKX
95      DO 15 I15=1,NKX
96      READ(5,*)I,J,XK1
97      XK1=XK1/1000.0
98      PERMX(I,J)=XK1
99      15 CONTINUE
100     17 CONTINUE
101     READ(5,*)KYI
102     READ(5,*)BKY
103     BKY=BKY/1000.0
104     DO 18 I18=1,IB
105     DO 19 I19=1,JB
106     PERMY(I18,I19)=BKY
107     19 CONTINUE
108     18 CONTINUE
109     IF(KYI.EQ.0)GO TO 22
110     READ(5,*)NKY
111     DO 20 I20=1,NKY
112     READ(5,*)I,J,YK1
113     YK1=YK1/1000.0
114     PERMY(I,J)=YK1
115     20 CONTINUE
116     22 CONTINUE
117     READ(5,*)IPHI
118     READ(5,*)BPHI
119     DO 24 I24=1,21
120     DO 25 I25=1,21
121     PHI(I24,I25)=0.0
122     25 CONTINUE
123     24 CONTINUE
124     DO 26 I26=1,IB
125     DO 27 I27=1,JB
126     PHI(I26,I27)=BPHI
127     27 CONTINUE
128     26 CONTINUE
```

```
129      IF(I PHI.EQ.Ø)GO TO 3Ø
13Ø      READ(5,*)NPHI
131      DO 28 I28=1,NPHI
132      READ(5,*)I,J,PHI1
133      PHI(I,J)=PHI1
134      28 CONTINUE
135      3Ø CONTINUE
136      READ(5,*)IPOI
137      READ(5,*)BPOI
138      DO 31 I31=1,21
139      DO 32 I32=1,21
14Ø      PO(I31,I32)=Ø.Ø
141      32 CONTINUE
142      31 CONTINUE
143      DO 33 I33=1,IB
144      DO 34 I34=1,JB
145      PO(I33,I34)=BPOI
146      34 CONTINUE
147      33 CONTINUE
148      IF(IPOI.EQ.Ø)GO TO 38
149      READ(5,*)NPOI
15Ø      DO 35 I35=1,NPOI
151      READ(5,*)I,J,POI1
152      PO(I,J)=POI1
153      35 CONTINUE
154      38 CONTINUE
155      READ(5,*)SG
156      READ(5,*)TEMP
157      TEMP=TEMP+46Ø.Ø
158      READ(5,*)NPVT
159      DO 41 I41=1,NPVT
16Ø      READ(5,*)PT(I41),VT(I41),ZT(I41)
161      41 CONTINUE
162      READ(5,*)NTIME
163      READ(5,*)NTOT
164      DO 42 I42=1,NTOT
165      TIME(I42)=Ø.Ø
166      42 CONTINUE
167      IF(NTIME.EQ.1)GO TO 5Ø
168      READ(5,*)TIME1
169      TIME1=TIME1*864ØØ.Ø
17Ø      DO 43 I43=1,NTOT
171      TIME(I43)=TIME1
172      43 CONTINUE
173      5Ø CONTINUE
174      IF(NTIME.EQ.Ø)GO TO 6Ø
175      READ(5,*)NGT
176      IC=1
177      DO 51 I51=1,NGT
178      READ(5,*)TIME1,LAST
179      TIME1=TIME1*864ØØ.Ø
18Ø      DO 52 I52=1,LAST
181      TIME(IC)=TIME1
182      IC=IC+1
183      52 CONTINUE
184      51 CONTINUE
185      6Ø CONTINUE
186      READ(5,*)PSTD
187      READ(5,*)TSTD
188      TSTD=TSTD+46Ø.Ø
189      READ(5,*)NPOD
19Ø      DO 53 I53=1,21
191      DO 54 I54=1,21
192      Q(I53,I54)=Ø.Ø
```

```

193 54 CONTINUE
194 53 CONTINUE
195 IF(NPOD.EQ.0)GO TO 61
196 DEN=(28.97*SG*PSTD)/(10.73*TSTD)
197 DO 55 I55=1,NPOD
198 READ(5,*)I,J,Q1
199 Q1=(Q1/86400.0)*DEN
200 Q(I,J)=Q1
201 55 CONTINUE
202 61 CONTINUE
203 READ(5,*)MAXIN
204 READ(5,*)MAXEXE
205 READ(5,*)ICHECK
206 READ(5,*)CONVER
207 READ(5,*)IFORCE
208 IF(IFORCE.EQ.0)GO TO 500
209 READ(5,*)NFORIT
210 500 CONTINUE
211 DO 62 I62=1,NTOT
212 IPRINT(I62)=0
213 62 CONTINUE
214 READ(5,*)NPRINT
215 IF(NPRINT.EQ.0)GO TO 70
216 DO 63 I63=1,NPRINT
217 READ(5,*)NOPRT
218 IPRINT(NOPRT)=1
219 63 CONTINUE
220 GO TO 75
221 70 CONTINUE
222 DO 71 I71=1,MAXEXE
223 IPRINT(I71)=1
224 71 CONTINUE
225 75 CONTINUE
226 READ(5,*)ISKIPP
227 IF(ISKIPP.EQ.0)GO TO 510
228 READ(5,*)IBLPR,JBLPR
229 510 CONTINUE
230 READ(5,*)IBLPR2,JBLPR2

```

```

231 C
232 C*****
233 C The following part of the program perform the echo check of all
234 C read in data by writing them to the standard output
235 C*****
236 C

```

```

237 WRITE(6,99)
238 99 FORMAT(1X,' ')
239 WRITE(6,100)
240 100 FORMAT(/,1X,'*****',
241 + '*****',
242 + '*****')
243 WRITE(6,101)
244 101 FORMAT(1X,'*',118X,'*')
245 WRITE(6,102)
246 102 FORMAT(1X,'*',3X,'TWO DIMENSIONAL SINGLE PHASE AREAL',1X,
247 + 'HORIZONTAL GAS SIMULATOR',31X,'E.T.',6X,'MAY 84',8X,'*')
248 WRITE(6,103)
249 103 FORMAT(1X,'*',118X,'*')
250 WRITE(6,104)
251 104 FORMAT(1X,'*****',
252 + '*****',
253 + '*****')
254 WRITE(6,105)
255 105 FORMAT(/,50X,'-----')
256 WRITE(6,106)

```

```
257 106 FORMAT(53X,'INPUT DATA')
258 WRITE(6,107)
259 107 FORMAT(50X,'-----')
260 DO 108 I108=1,NPVT
261 PMZ(I108)=PT(I108)/VT(I108)*ZT(I108)
262 108 CONTINUE
263 IJB=IB*JB
264 WRITE(6,109)IJB
265 109 FORMAT(///,10X,'TOTAL NO. OF BLOCKS ASSIGNED = ',I3)
266 WRITE(6,110)IB
267 110 FORMAT(10X,'NO. OF BLOCKS IN X DIRECTION = ',I3)
268 WRITE(6,111)JB
269 111 FORMAT(10X,'NO. OF BLOCKS IN Y DIRECTION = ',I3)
270 WRITE(6,112)H
271 112 FORMAT(//,10X,'RESERVOIR THICKNESS = ',F9.4,1X,'(FT)')
272 WRITE(6,113)TEMP
273 113 FORMAT(10X,'RESERVOIR TEMPERATURE = ',F9.4,1X,'(R)')
274 WRITE(6,114)SG
275 114 FORMAT(//,10X,'GAS GRAVITY = ',F7.4)
276 WRITE(6,115)PSTD
277 115 FORMAT(10X,'STANDARD PRESSURE = ',F9.4,1X,'(PSIA)')
278 WRITE(6,116)TSTD
279 116 FORMAT(10X,'STANDARD TEMPERATURE = ',F9.4,1X,'(R)')
280 WRITE(6,117)
281 117 FORMAT(//,10X,'BLOCK ORDERING CONVENTION : ')
282 WRITE(6,118)
283 118 FORMAT(/,35X,'Y')
284 WRITE(6,119)
285 119 FORMAT(/,20X,'(1,1) (1,2) (1,3) . . . .')
286 WRITE(6,120)
287 120 FORMAT(15X,'X (2,1) (2,2) (2,3) . . . .')
288 WRITE(6,121)
289 121 FORMAT(20X,'(3,1) (3,2) (3,3) . . . .')
290 WRITE(6,122)
291 122 FORMAT(//,10X,'BLOCK LENGTH : ')
292 WRITE(6,123)
293 123 FORMAT(/,20X,'BLOCK NO.',15X,'DX(FT)',25X,'DY(FT)')
294 WRITE(6,124)
295 124 FORMAT(20X,'-----',15X,'-----',26X,'-----')
296 DO 125 I125=1,21
297 WRITE(6,126)I125,DX(I125),DY(I125)
298 126 FORMAT(/,23X,12,10X,F20.13,10X,F20.13)
299 125 CONTINUE
300 WRITE(6,127)
301 127 FORMAT(//,10X,'POROSITY MAP (FRACTION) :')
302 DO 128 L1=1,21
303 WRITE(6,129)PHI(L1,1),PHI(L1,2),PHI(L1,3),PHI(L1,4),PHI(L1,5),
304 +PHI(L1,6),PHI(L1,7),PHI(L1,8),PHI(L1,9),PHI(L1,10),PHI(L1,11),
305 +PHI(L1,12),PHI(L1,13),PHI(L1,14),PHI(L1,15),PHI(L1,16),
306 +PHI(L1,17),PHI(L1,18),PHI(L1,19),PHI(L1,20),PHI(L1,21)
307 129 FORMAT(/,2X,21F6.3)
308 128 CONTINUE
309 WRITE(6,130)
310 130 FORMAT(//,10X,'X DIR. PERMEABILITY MAP (DARCY) :')
311 DO 131 L2=1,21
312 WRITE(6,132)PERMX(L2,1),PERMX(L2,2),PERMX(L2,3),PERMX(L2,4),
313 +PERMX(L2,5),PERMX(L2,6),PERMX(L2,7),PERMX(L2,8),PERMX(L2,9),
314 +PERMX(L2,10),PERMX(L2,11),PERMX(L2,12),PERMX(L2,13),
315 +PERMX(L2,14),PERMX(L2,15),PERMX(L2,16),PERMX(L2,17),
316 +PERMX(L2,18),PERMX(L2,19),PERMX(L2,20),PERMX(L2,21)
317 132 FORMAT(/,2X,21F6.3)
318 131 CONTINUE
319 WRITE(6,133)
320 133 FORMAT(//,10X,'Y DIR. PERMEABILITY MAP (DARCY) :')
```

```
321      DO 134 L3=1,21
322      WRITE(6,132)PERMY(L3,1),PERMY(L3,2),PERMY(L3,3),PERMY(L3,4),
323      +PERMY(L3,5),PERMY(L3,6),PERMY(L3,7),PERMY(L3,8),PERMY(L3,9),
324      +PERMY(L3,10),PERMY(L3,11),PERMY(L3,12),PERMY(L3,13),
325      +PERMY(L3,14),PERMY(L3,15),PERMY(L3,16),PERMY(L3,17),
326      +PERMY(L3,18),PERMY(L3,19),PERMY(L3,20),PERMY(L3,21)
327 134 CONTINUE
328      WRITE(6,135)
329 135 FORMAT(/,10X,'ORIGINAL PRESSURE MAP (PSIA) :')
330      DO 136 L4=1,21
331      WRITE(6,137)PO(L4,1),PO(L4,2),PO(L4,3),PO(L4,4),PO(L4,5),PO
332      +(L4,6),PO(L4,7),PO(L4,8),PO(L4,9),PO(L4,10),PO(L4,11),PO(L4,12),
333      +PO(L4,13),PO(L4,14),PO(L4,15),PO(L4,16),PO(L4,17),
334      +PO(L4,18),PO(L4,19),PO(L4,20),PO(L4,21)
335 137 FORMAT(/,2X,21F6.0)
336 136 CONTINUE
337      WRITE(6,138)
338 138 FORMAT(/,10X,'FLOW RATE MAP (LBM/SEC)',1X,
339      + '(- FOR INJ. & + FOR PROD.) : ')
340      DO 139 L5=1,21
341      WRITE(6,140)Q(L5,1),Q(L5,2),Q(L5,3),Q(L5,4),Q(L5,5),Q(L5,6),
342      +Q(L5,7),Q(L5,8),Q(L5,9),Q(L5,10),Q(L5,11),Q(L5,12),Q(L5,13),
343      +Q(L5,14),Q(L5,15),Q(L5,16),Q(L5,17),Q(L5,18),Q(L5,19),
344      +Q(L5,20),Q(L5,21)
345 140 FORMAT(/,2X,21F6.2)
346 139 CONTINUE
347      WRITE(6,141)
348 141 FORMAT(/,50X,'-----')
349      WRITE(6,142)
350 142 FORMAT(51X,'GAS P.V.T. DATA')
351      WRITE(6,143)
352 143 FORMAT(50X,'-----')
353      WRITE(6,144)
354 144 FORMAT(/,3X,'PRESSURE',27X,'Z FACTOR',25X,'VISCOSITY',28X,
355      + 'P/(VIS.)(Z)')
356      WRITE(6,145)
357 145 FORMAT(3X,'(PSIA)',64X,'(CP)')
358      WRITE(6,146)
359 146 FORMAT(1X,'-----',
360      + '-----',
361      + '-----')
362      DO 147 I147=1,NPVT
363      WRITE(6,148)PT(I147),ZT(I147),VT(I147),PMZ(I147)
364 148 FORMAT(/,1X,F10.4,26X,F8.5,25X,F10.7,25X,F15.8)
365 147 CONTINUE
366      WRITE(6,146)
367      WRITE(6,150)
368 150 FORMAT(/,50X,'-----')
369      WRITE(6,151)
370 151 FORMAT(50X,'TIME STEP CONTROL')
371      WRITE(6,152)
372 152 FORMAT(50X,'-----')
373      WRITE(6,153)NTOT
374 153 FORMAT(/,1X,'TOTAL NO. OF TIME STEP ASSIGNED = ',I4)
375      WRITE(6,154)
376 154 FORMAT(/,20X,'TIME STEP NO.',20X,'TIME STEP SIZE (DAYS)')
377      WRITE(6,155)
378 155 FORMAT(20X,'-----',20X,'-----')
379      DO 156 I156=1,NTOT
380      TIMTEP=TIME(I156)/86400.0
381      WRITE(6,157)I156,TIMTEP
382 157 FORMAT(/,24X,I4,30X,F8.3)
383 156 CONTINUE
384      WRITE(6,158)
```



```

449      TMASS=TMASS+(DX(I200)*DY(I201)*PHI(I200,I201)*H)*
450      +((28.97*SG*PO(I200,I201))/(ZOMAS*10.73*TEMP))
451      201 CONTINUE
452      200 CONTINUE
453      TVOL=TMASS*((28.97*SG*PSTD)/(10.73*TSTD))
454      C set all block pressure to initial pressure
455      DO 205 I205=1,21
456      DO 206 I206=1,21
457      PG(I205,I206)=PO(I205,I206)
458      206 CONTINUE
459      205 CONTINUE
460      C start time step
461      DO 900 I900=1,MAXEXE
462      C set all block p to p of last time step
463      DO 300 I300=1,21
464      DO 301 I301=1,21
465      PO(I300,I301)=PG(I300,I301)
466      301 CONTINUE
467      300 CONTINUE
468      INNUB=0
469      801 CONTINUE
470      INNUB=INNUB+1
471      C set all pgo of current iteration to current p, pgo is the p of last
472      C iteration
473      DO 207 I207=1,21
474      DO 208 I208=1,21
475      PGO(I207,I208)=PG(I207,I208)
476      208 CONTINUE
477      207 CONTINUE
478      C initialize the 5-diagonal matrix to 0
479      DO 203 I203=1,441
480      AA(I203)=0.0
481      BB(I203)=0.0
482      CC(I203)=0.0
483      DD(I203)=0.0
484      EE(I203)=0.0
485      FF(I203)=0.0
486      203 CONTINUE
487      DO 211 I211=1,21
488      DO 210 I210=1,21
489      A(I211,I210)=0.0
490      B(I211,I210)=0.0
491      C(I211,I210)=0.0
492      D(I211,I210)=0.0
493      E(I211,I210)=0.0
494      F(I211,I210)=0.0
495      210 CONTINUE
496      211 CONTINUE
497      C calculate transmissibilities for all blocks
498      DO 800 J=1,21
499      DO 850 I=1,21
500      IF(I.EQ.1)PERMXM=0.0
501      IF(I.NE.1)PERMXM=(DX(I)+DX(I-1))/((DX(I-1)/PERMX(I-1,J))+
502      +(DX(I)/PERMX(I,J)))
503      IF(I.EQ.21)PERMXP=0.0
504      IF(I.NE.21)PERMXP=(DX(I)+DX(I+1))/((DX(I+1)/PERMX(I+1,J))+
505      +(DX(I)/PERMX(I,J)))
506      IF(J.EQ.1)PERMYM=0.0
507      IF(J.NE.1)PERMYM=(DY(J)+DY(J-1))/((DY(J-1)/PERMY(I,J-1))+
508      +(DY(J)/PERMY(I,J)))
509      IF(J.EQ.21)PERMYP=0.0
510      IF(J.NE.21)PERMYP=(DY(J)+DY(J+1))/((DY(J+1)/PERMY(I,J+1))+
511      +(DY(J)/PERMY(I,J)))
512      IF(I.EQ.1)DELXM=DX(I)

```

```
513 IF(I.NE.1)DELXM=(DX(I)+DX(I-1))*0.5
514 IF(I.EQ.21)DELXP=DX(I)
515 IF(I.NE.21)DELXP=(DX(I)+DX(I+1))*0.5
516 IF(J.EQ.1)DELYM=DY(J)
517 IF(J.NE.1)DELYM=(DY(J)+DY(J-1))*0.5
518 IF(J.EQ.21)DELYP=DY(J)
519 IF(J.NE.21)DELYP=(DY(J)+DY(J+1))*0.5
520 CALL SSCH(NPVT,PT,PMZ,PG(I,J),PVZ,NCODE,6)
521 CALL SSCH(NPVT,PT,ZT,PG(I,J),ZIJ,NCODE,6)
522 IF(I.NE.1)CALL SSCH(NPVT,PT,PMZ,PG(I-1,J),PVZIM1,NCODE,6)
523 IF(I.NE.21)CALL SSCH(NPVT,PT,PMZ,PG(I+1,J),PVZIP1,NCODE,6)
524 IF(J.NE.1)CALL SSCH(NPVT,PT,PMZ,PG(I,J-1),PVZJM1,NCODE,6)
525 IF(J.NE.21)CALL SSCH(NPVT,PT,PMZ,PG(I,J+1),PVZJP1,NCODE,6)
526 CALL SSCH(NPVT,PT,ZT,PO(I,J),ZOIJ,NCODE,6)
527 C set matrix elements to the calculated values
528 A(I,J)=(PERMYM*(PVZ+PVZJM1))/(DY(J)*DELYM)
529 B(I,J)=(PERMXM*(PVZIM1+PVZ))/(DX(I)*DELXM)
530 D(I,J)=(PERMXP*(PVZIP1+PVZ))/(DX(I)*DELXP)
531 E(I,J)=(PERMYP*(PVZJP1+PVZ))/(DY(J)*DELYP)
532 C(I,J)=(B(I,J)+D(I,J)+A(I,J)+E(I,J)+(PHI(I,J)/(3.6621907D-05*
533 +ZIJ*TIME(I900))))*(-1.0)
534 F(I,J)=((-1.0)*PHI(I,J)*PO(I,J))/(3.6621907D-05*ZOIJ
535 +*TIME(I900))+(10115.589*TEMP*Q(I,J))/(SG*H*DX(I)*DY(J))
536 850 CONTINUE
537 800 CONTINUE
538 C routine used to check matrix, it will print all elements out
539 IF(ICHECK.EQ.0)GO TO 1240
540 DO 1234 I1234=1,20
541 DO 1235 I1235=1,20
542 WRITE(6,1236)A(I1235,I1234),B(I1235,I1234),C(I1235,I1234)
543 +,D(I1235,I1234),E(I1235,I1234),F(I1235,I1234)
544 1236 FORMAT(6(2X,F15.8))
545 1235 CONTINUE
546 1234 CONTINUE
547 1240 CONTINUE
548 C align matrix element to go into GBAND matrix solver
549 DO 600 I600=1,21
550 AA(I600)=A(I600,1)
551 BB(I600)=B(I600,1)
552 CC(I600)=C(I600,1)
553 DD(I600)=D(I600,1)
554 EE(I600)=E(I600,1)
555 FF(I600)=F(I600,1)
556 600 CONTINUE
557 DO 601 I601=22,42
558 AA(I601)=A(I601-21,2)
559 BB(I601)=B(I601-21,2)
560 CC(I601)=C(I601-21,2)
561 DD(I601)=D(I601-21,2)
562 EE(I601)=E(I601-21,2)
563 FF(I601)=F(I601-21,2)
564 601 CONTINUE
565 DO 602 I602=43,63
566 AA(I602)=A(I602-42,3)
567 BB(I602)=B(I602-42,3)
568 CC(I602)=C(I602-42,3)
569 DD(I602)=D(I602-42,3)
570 EE(I602)=E(I602-42,3)
571 FF(I602)=F(I602-42,3)
572 602 CONTINUE
573 DO 603 I603=64,84
574 AA(I603)=A(I603-63,4)
575 BB(I603)=B(I603-63,4)
576 CC(I603)=C(I603-63,4)
```

577 DD(1603)=D(1603-63,4)
578 EE(1603)=E(1603-63,4)
579 FF(1603)=F(1603-63,4)
580 603 CONTINUE
581 DO 604 1604=85,105
582 AA(1604)=A(1604-84,5)
583 BB(1604)=B(1604-84,5)
584 CC(1604)=C(1604-84,5)
585 DD(1604)=D(1604-84,5)
586 EE(1604)=E(1604-84,5)
587 FF(1604)=F(1604-84,5)
588 604 CONTINUE
589 DO 605 1605=106,126
590 AA(1605)=A(1605-105,6)
591 BB(1605)=B(1605-105,6)
592 CC(1605)=C(1605-105,6)
593 DD(1605)=D(1605-105,6)
594 EE(1605)=E(1605-105,6)
595 FF(1605)=F(1605-105,6)
596 605 CONTINUE
597 DO 606 1606=127,147
598 AA(1606)=A(1606-126,7)
599 BB(1606)=B(1606-126,7)
600 CC(1606)=C(1606-126,7)
601 DD(1606)=D(1606-126,7)
602 EE(1606)=E(1606-126,7)
603 FF(1606)=F(1606-126,7)
604 606 CONTINUE
605 DO 607 1607=148,168
606 AA(1607)=A(1607-147,8)
607 BB(1607)=B(1607-147,8)
608 CC(1607)=C(1607-147,8)
609 DD(1607)=D(1607-147,8)
610 EE(1607)=E(1607-147,8)
611 FF(1607)=F(1607-147,8)
612 607 CONTINUE
613 DO 608 1608=169,189
614 AA(1608)=A(1608-168,9)
615 BB(1608)=B(1608-168,9)
616 CC(1608)=C(1608-168,9)
617 DD(1608)=D(1608-168,9)
618 EE(1608)=E(1608-168,9)
619 FF(1608)=F(1608-168,9)
620 608 CONTINUE
621 DO 609 1609=190,210
622 AA(1609)=A(1609-189,10)
623 BB(1609)=B(1609-189,10)
624 CC(1609)=C(1609-189,10)
625 DD(1609)=D(1609-189,10)
626 EE(1609)=E(1609-189,10)
627 FF(1609)=F(1609-189,10)
628 609 CONTINUE
629 DO 610 1610=211,231
630 AA(1610)=A(1610-210,11)
631 BB(1610)=B(1610-210,11)
632 CC(1610)=C(1610-210,11)
633 DD(1610)=D(1610-210,11)
634 EE(1610)=E(1610-210,11)
635 FF(1610)=F(1610-210,11)
636 610 CONTINUE
637 DO 611 1611=232,252
638 AA(1611)=A(1611-231,12)
639 BB(1611)=B(1611-231,12)
640 CC(1611)=C(1611-231,12)

641 DD(I611)=D(I611-231,12)
642 EE(I611)=E(I611-231,12)
643 FF(I611)=F(I611-231,12)
644 611 CONTINUE
645 DO 612 I612=253,273
646 AA(I612)=A(I612-252,13)
647 BB(I612)=B(I612-252,13)
648 CC(I612)=C(I612-252,13)
649 DD(I612)=D(I612-252,13)
650 EE(I612)=E(I612-252,13)
651 FF(I612)=F(I612-252,13)
652 612 CONTINUE
653 DO 613 I613=274,294
654 AA(I613)=A(I613-273,14)
655 BB(I613)=B(I613-273,14)
656 CC(I613)=C(I613-273,14)
657 DD(I613)=D(I613-273,14)
658 EE(I613)=E(I613-273,14)
659 FF(I613)=F(I613-273,14)
660 613 CONTINUE
661 DO 614 I614=295,315
662 AA(I614)=A(I614-294,15)
663 BB(I614)=B(I614-294,15)
664 CC(I614)=C(I614-294,15)
665 DD(I614)=D(I614-294,15)
666 EE(I614)=E(I614-294,15)
667 FF(I614)=F(I614-294,15)
668 614 CONTINUE
669 DO 615 I615=316,336
670 AA(I615)=A(I615-315,16)
671 BB(I615)=B(I615-315,16)
672 CC(I615)=C(I615-315,16)
673 DD(I615)=D(I615-315,16)
674 EE(I615)=E(I615-315,16)
675 FF(I615)=F(I615-315,16)
676 615 CONTINUE
677 DO 616 I616=337,357
678 AA(I616)=A(I616-336,17)
679 BB(I616)=B(I616-336,17)
680 CC(I616)=C(I616-336,17)
681 DD(I616)=D(I616-336,17)
682 EE(I616)=E(I616-336,17)
683 FF(I616)=F(I616-336,17)
684 616 CONTINUE
685 DO 617 I617=358,378
686 AA(I617)=A(I617-357,18)
687 BB(I617)=B(I617-357,18)
688 CC(I617)=C(I617-357,18)
689 DD(I617)=D(I617-357,18)
690 EE(I617)=E(I617-357,18)
691 FF(I617)=F(I617-357,18)
692 617 CONTINUE
693 DO 618 I618=379,399
694 AA(I618)=A(I618-378,19)
695 BB(I618)=B(I618-378,19)
696 CC(I618)=C(I618-378,19)
697 DD(I618)=D(I618-378,19)
698 EE(I618)=E(I618-378,19)
699 FF(I618)=F(I618-378,19)
700 618 CONTINUE
701 DO 619 I619=400,420
702 AA(I619)=A(I619-399,20)
703 BB(I619)=B(I619-399,20)
704 CC(I619)=C(I619-399,20)

```
705 DD(1619)=D(1619-399,20)
706 EE(1619)=E(1619-399,20)
707 FF(1619)=F(1619-399,20)
708 619 CONTINUE
709 DO 2000 12000=421,441
710 AA(12000)=A(12000-420,21)
711 BB(12000)=B(12000-420,21)
712 CC(12000)=C(12000-420,21)
713 DD(12000)=D(12000-420,21)
714 EE(12000)=E(12000-420,21)
715 FF(12000)=F(12000-420,21)
716 2000 CONTINUE
717 C routine used for debugging, will print matrix out
718 IF(ICHECK.EQ.0)GO TO 1241
719 DO 770 1770=1,441
720 WRITE(6,771)AA(1770),BB(1770),CC(1770),DD(1770),EE(1770)
721 +,FF(1770)
722 771 FORMAT(6(2X,F15.8))
723 770 CONTINUE
724 1241 CONTINUE
725 DO 544 1544=1,18501
726 AAA(1544)=0.0
727 544 CONTINUE
728 DO 540 1540=1,441
729 KDR(1540)=0
730 540 CONTINUE
731 KDR(1)=1
732 DO 541 1541=2,441
733 IF(L541.GT.21)GO TO 542
734 KDR(L541)=KDR(L541-1)+21+L541
735 GO TO 541
736 542 IF(L541.GT.420)GO TO 543
737 KDR(L541)=KDR(L541-1)+43
738 GO TO 541
739 543 KDR(L541)=KDR(L541-1)+441-L541+23
740 541 CONTINUE
741 DO 545 1545=1,441
742 AAA(KDR(1545))=CC(1545)
743 545 CONTINUE
744 AAA(2)=DD(1)
745 AAA(22)=EE(1)
746 DO 546 1546=2,21
747 AAA(KDR(1546)-1)=BB(1546)
748 AAA(KDR(1546)+1)=DD(1546)
749 AAA(KDR(1546)+21)=EE(1546)
750 546 CONTINUE
751 DO 547 1547=22,420
752 AAA(KDR(1547)-1)=BB(1547)
753 AAA(KDR(1547)-21)=AA(1547)
754 AAA(KDR(1547)+1)=DD(1547)
755 AAA(KDR(1547)+21)=EE(1547)
756 547 CONTINUE
757 DO 548 1548=421,440
758 AAA(KDR(1548)-21)=AA(1548)
759 AAA(KDR(1548)-1)=BB(1548)
760 AAA(KDR(1548)+1)=DD(1548)
761 548 CONTINUE
762 AAA(18500)=BB(441)
763 AAA(18480)=AA(441)
764 CALL GBAND(AAA,FF,XX,441,21,1.0,IERR,0)
765 C set pg to the calculated pressures
766 LLL=0
767 DO 752 1752=1,21
768 DO 753 1753=1,21
```

```
769     LLL=LLL+1
770     PG(I753,J752)=XX(LLL)
771     753 CONTINUE
772     752 CONTINUE
773 C calculate the difference, if converged, go to print out subroutine
774     DO 702 I702=1,21
775     DO 703 I703=1,21
776     DIFF=PG(I702,I703)-PGO(I702,I703)
777     DIFFA=DABS(DIFF)
778     IF(DIFFA.GT.CONVER.AND.INNUB.LT.MAXIN.AND.IFORCE.EQ.0)GO TO 801
779     703 CONTINUE
780     702 CONTINUE
781 C check if the force iteration option is engaged
782     IF(IFORCE.EQ.1.AND.INNUB.LT.NFORIT)GO TO 801
783     IF(I900.NE.1)CMASOLD=CURMAS
784     QTO=0.0
785     CURMAS=0.0
786 C calculate current mass in place
787     DO 710 I710=1,21
788     DO 711 I711=1,21
789     CALL SSCH(NPVT,PT,ZT,PG(I710,I711),ZRM,NCODE,6)
790     CURMAS=CURMAS+(DX(I710)*DY(I711)*PHI(I710,I711)*H)*
791     +((28.97*SG*PG(I710,I711))/(ZRM*10.73*TEMP))
792     QTO=QTO+Q(I710,I711)
793     711 CONTINUE
794     710 CONTINUE
795     PROMAS=TMASS-CURMAS
796     IF(I900.EQ.1)CMASP=TMASS-CURMAS
797     IF(I900.NE.1)CMASP=CMASOLD-CURMAS
798     TIMETO=0.0
799     DO 715 I715=1,I900
800     TIMETO=TIMETO+TIME(I715)
801     715 CONTINUE
802     PROD=TIMETO*QTO
803     GRTHEO=TMASS-PROD
804     PRODC=QTO*TIME(I900)
805     ERR=((GRTHEO-CURMAS)/GRTHEO)*100.0
806     IF(IPRINT(I900).NE.1)GO TO 950
807     CALL OUTPUT(PG,INNUB,I900,TIME(I900),
808     +PROMAS,TIMETO,PROD,PRODC,CMASS,CURMAS,ERR,CMASP,GRTHEO,
809     +ISKIPP,IBLPR,JBLPR,IBLPR2,JBLPR2)
810     950 CONTINUE
811     900 CONTINUE
812     STOP
813     END
814     SUBROUTINE OUTPUT(PG,INNUB,I900,TM,PROMAS,TIMETO,PROD,PRODC,
815     +TMASS,CURMAS,ERR,CMASP,GRTHEO,ISKIPP,IBLPR,JBLPR,IBLPR2,JBLPR2)
816     IMPLICIT REAL*8(A-H,O-Z)
817     DIMENSION PG(21,21)
818     WRITE(6,1)
819     WRITE(6,15)
820     1 FORMAT(1X,'*****',
821     + '*****',
822     + '*****')
823     WRITE(6,2)I900
824     2 FORMAT(///,2X,'TIME STEP NO. = ',I4)
825     WTM=TM/86400.0
826     WRITE(6,3)WTM
827     3 FORMAT(/,2X,'TIME STEP SIZE FOR THIS TIME STEP = ',F20.11,1X,
828     +'(DAYS)')
829     WTM2=TIMETO/86400.0
830     WRITE(6,4)WTM2
831     4 FORMAT(2X,'TOTAL TIME ELAPSED FROM START OF SIMULATION = ',
832     +F20.11,1X,'(DAYS)')
```

```
833 WRITE(6,5)TMASS
834 5 FORMAT(/,2X,'ORIGINAL GAS IN PLACE AT START OF SIMULATION = ',
835 +F26.11,1X,'(LBS)')
836 WRITE(6,30)CMASP
837 30 FORMAT(2X,'GAS PRODUCED FOR THE CURRENT TIME STEP',1X,
838 +'(CALCULATED) = ',F20.11,1X,'(LBS) - FOR INJ. & + FOR PROD.')
839 WRITE(6,6)PRODCT
840 6 FORMAT(2X,'GAS PRODUCED FOR THE CURRENT TIME STEP (THEO.) = ',
841 +F20.11,1X,'(LBS) - FOR INJ. & + FOR PROD.')
842 WRITE(6,7)PROMAS
843 7 FORMAT(2X,'TOTAL GAS PRODUCED FROM START OF SIMULATION',1X,
844 +'(CALCULATED) = ',F26.11,1X,'(LBS) - FOR INJ. & + FOR PROD.')
845 WRITE(6,8)PROD
846 8 FORMAT(2X,'TOTAL GAS PRODUCED FROM START OF SIMULATION',1X,
847 +'(THEO.) = ',F26.11,1X,'(LBS) - FOR INJ. & + FOR PROD.')
848 WRITE(6,9)CURMAS
849 9 FORMAT(2X,'GAS REMAIN (CALCULATED) = ',F26.11,1X,'(LBS)')
850 WRITE(6,31)GRTHEO
851 31 FORMAT(2X,'GAS REMAIN (THEO.) = ',F26.11,1X,'(LBS)')
852 WRITE(6,10)ERR
853 10 FORMAT(/,2X,'MATERIAL BALANCE ERROR = ',F20.11,1X,'(%)')
854 IF(ISKIPP.EQ.1)GO TO 520
855 WRITE(6,11)
856 11 FORMAT(/,2X,'PRESSURE MAP (LEFT HALF) :')
857 DO 12 I12=1,21
858 WRITE(6,13)PG(I12,1),PG(I12,2),PG(I12,3),PG(I12,4),PG(I12,5),
859 +PG(I12,6),PG(I12,7),PG(I12,8),PG(I12,9),PG(I12,10)
860 13 FORMAT(/,2X,10F12.5)
861 12 CONTINUE
862 WRITE(6,20)
863 20 FORMAT(/,2X,'PRESSURE MAP (RIGHT HALF) :')
864 DO 21 I21=1,21
865 WRITE(6,2001)PG(I21,11),PG(I21,12),PG(I21,13),PG(I21,14),
866 +PG(I21,15),PG(I21,16),PG(I21,17),PG(I21,18),PG(I21,19),
867 +PG(I21,20),PG(I21,21)
868 2001 FORMAT(/,1X,11F11.5)
869 21 CONTINUE
870 520 CONTINUE
871 IF(ISKIPP.EQ.1)WRITE(6,521)IBLPR,JBLPR,PG(1BLPR,JBLPR)
872 521 FORMAT(/,1X,'P(',I2,',',I2,') = ',F15.8,1X,'PSIA')
873 WRITE(6,14)INNUB
874 14 FORMAT(/,2X,'NO. OF ITERATION PERFORMED',1X,
875 +'FOR THIS TIME STEP = ',I4)
876 WRITE(6,1)
877 WRITE(6,15)
878 15 FORMAT(1X,' ')
879 C*****
880 WRITE(2,3000)WTM2,PG(1BLPR2,JBLPR2)
881 3000 FORMAT(2X,F20.11,5X,F20.11)
882 C*****
883 RETURN
884 END
885 SUBROUTINE SSCH(N,X,Y,XIN,YOUT,NCODE,IW)
886 IMPLICIT REAL*8(A-H,O-Z)
887 DIMENSION X(N),Y(N)
888 IF(XIN.LT.X(1))NCODE=88
889 IF(XIN.LT.X(1))YOUT=0.0
890 IF(XIN.LT.X(1))WRITE(6,10)
891 10 FORMAT(/,'INPUT DATA EXCEED LOWER LIMIT')
892 IF(XIN.GT.X(N))NCODE=99
893 IF(XIN.GT.X(N))YOUT=0.0
894 IF(XIN.GT.X(N))WRITE(6,11)
895 11 FORMAT(/,'INPUT DATA EXCEED UPPER LIMIT')
896 IF(XIN.LT.X(1).OR.XIN.GT.X(N))GO TO 9999
```

```
897      K=1
898      GO TO 1
899      2 K=K+1
900      1 CONTINUE
901      IF(XIN.EQ.X(K))YOUT=Y(K)
902      IF(XIN.EQ.X(K))GO TO 999
903      IF(XIN.GT.X(K))GO TO 2
904      YOUT=Y(K-1)+(Y(K)-Y(K-1))*(XIN-X(K-1))/(X(K)-X(K-1))
905      999 CONTINUE
906      NCODE=1
907      9999 CONTINUE
908      RETURN
909      END
910      SUBROUTINE GBAND(A,D,X,N,M,EPS,IERR,IFRST)
911      IMPLICIT REAL*8(A-H,O-Z)
912      DIMENSION A(18501),D(441),X(441)
913      IERR=0
914      J=1
915      DO 10 I=1,N
916      IE=M
917      IF(I+M-N)21,21,22
918      22 IE=N-I
919      21 IEAUX=M
920      IF(I-M)23,23,24
921      23 IEAUX=I
922      24 IE1=IE+IEAUX
923      MBIG=IE
924      J1=J+IE1
925      J2=J1
926      IF(IFRST.GT.0)GO TO 27
927      IF(DABS(A(J))-EPS)25,25,27
928      25 IERR=IERR+1
929      27 IF(MBIG)10,10,26
930      26 DO 20 J0=1,MBIG
931      S=A(J1)/A(J)
932      IF(IFRST.GT.0)GO TO 35
933      DO 30 K=1,MBIG
934      J1K=J1+K
935      JK=J+K
936      30 A(J1K)=A(J1K) -A(JK)*S
937      35 CONTINUE
938      IAUX=J0+I
939      D(IAUX)=D(IAUX)-D(I)*S
940      IE=M
941      IF(IAUX+M-N)31,31,32
942      32 IE=N-IAUX
943      31 IEAUX=M
944      IF(IAUX-M)33,33,34
945      33 IEAUX=IAUX
946      34 IE1=IE+IEAUX
947      20 J1=J1+IE1
948      10 J=J2+1
949      J=J-M-1
950      NP1=N+1
951      DO 40 IINV=1,N
952      I=NP1-IINV
953      IE=M
954      IF(I+M-N)41,41,42
955      42 IE=N-I
956      41 MBIG=IE
957      X(I)=D(I)
958      IF(MBIG)44,44,43
959      43 DO 50 K=1,MBIG
960      IK=I+K
```

```
961      JK=J+K
962      50 X(I)=X(I)-X(IK)*A(JK)
963      44 X(I)=X(I)/A(J)
964      IE=M
965      IF(I+M-NP1)51,51,52
966      52 IE=NP1-I
967      51 IEAUX=M
968      IF(I-1-M)53,53,54
969      53 IEAUX=I-1
970      54 IE1=IE+IEAUX
971      J=J-IE1-1
972      40 CONTINUE
973      RETURN
974      END
```

